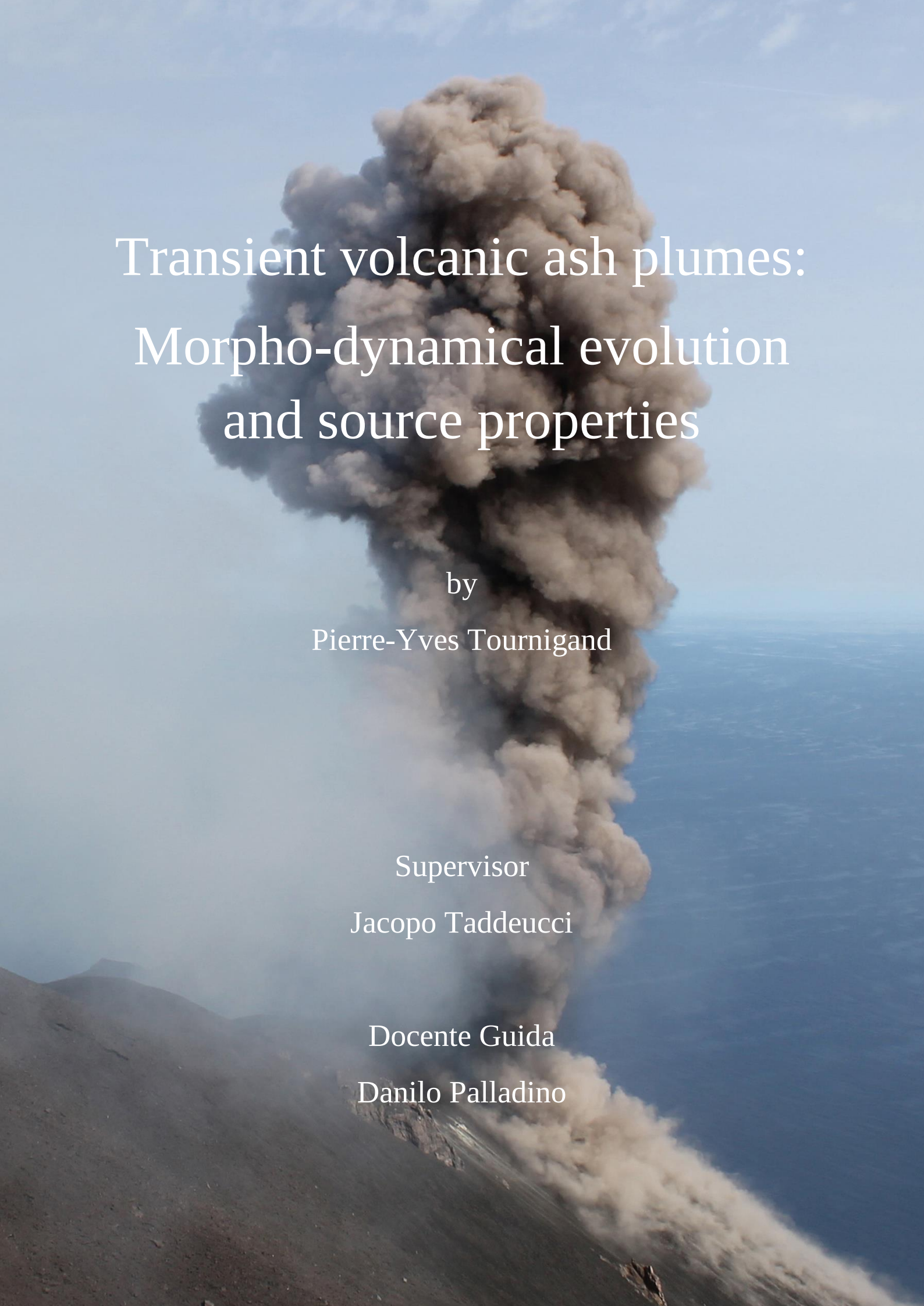

Transient volcanic ash plumes: Morpho-dynamical evolution and source properties

by

Pierre-Yves Tournigand

Supervisor

Jacopo Taddeucci

Docente Guida

Danilo Palladino

Index

Abstract

Transient volcanic plumes, typically generated by Strombolian and Vulcanian eruptions, are time-dependent features characterized by rise and development time scales similar to the eruption duration. Their morphological and dynamical properties are thus strongly related to the source conditions and evolution over time, i.e. (ejection duration, spatial spreading, ejection angle, time interval between pulses). In this study, the shape evolution and dynamics of initial transient volcanic plumes development, as well as their relation with discharge history, have been investigated using high-speed and high-resolution visible-light and thermal infrared videos.

Physical parameterization of the plumes has been performed by defining their front velocity, volume and apparent surface temperature. Optical flow computer vision tool and fractal dimension analysis were applied for the first time in order to extract plume velocity field and shape complexity evolution over time, respectively. The source conditions were characterized both qualitatively, in terms of number, location, duration, and frequency of individual ejection pulses, and quantitatively, in terms of time-resolved ash eruption rate and a newly-defined instability factor. The newly proposed, image-based method I developed to retrieve discharge rate provides results that are comparable with previous methods but with more than one order of magnitude increase in time resolution.

Results show that the connection between source properties and the dynamical and morphological features of transient plumes holds true for every one of our study cases, which encompass a variety of eruption styles and plume heights and shapes. In particular, plume front velocity, temperature decay, and plume complexity, as measured by fractal dimension, all follow complex evolutions which are intimately linked with the discharge history at the vent. Of the different factors that characterize vent discharge, lateral shifts in the ejection (from, e.g., vent shifts or changes in vent geometry or angle of the ejection) and temporal fluctuations, including the tempo and intensity of ejection pulses and other changes in the discharge rate, exert the strongest controls

on plume evolution. These lateral and temporal changes at the vent can be combined in a general source instability factor that, by controlling the formation of the vortexes at the base of the plume, eventually determines the modes of air entrainment and the overall evolution of the plume.

The connection between source instability and plume dynamics that I quantified in this study brings new understandings on the formation and initial development of unsteady volcanic plumes. Settings of new characterization tools such as fractal analysis and time-dependent discharge rate show promising results and potential for new monitoring resources.

Riassunto

Le nubi vulcaniche transienti, o transient plumes, generate da eruzioni Stromboliane e Vulcaniane, sono strutture dipendenti dal tempo e caratterizzate da durate di sviluppo simili a quelle dell'eruzione. Le loro morfologie e dinamiche sono collegate alle proprietà della bocca eruttiva e alla sua evoluzione nel tempo, i.e., durata dell'emissione, diffusione areale, angolo, intervallo di tempo tra le emissioni. In questo lavoro, l'evoluzione della forma e della dinamica iniziale delle nubi transienti, cosi come l'evoluzione dell'attività alla bocca, sono stati studiati attraverso l'impiego di telecamere ad alta risoluzione ed alta velocità.

La parametrizzazione dei plumes è stata effettuata definendo la loro velocità di ascesa, volume e temperatura. La tecnica di analisi d'immagine Optical flow e l'analisi della dimensione frattale sono stati utilizzati per estrarre il campo di velocità e l'evoluzione del grado di complessità dei plumes. Le condizioni all'origine sono state caratterizzate qualitativamente (quantità, durata e frequenza di emissione) e quantitativamente con la stima delle emissione di cenere e di un fattore di instabilità di nuova introduzione. Il nuovo metodo di stima del tasso eruttivo da me sviluppato fornisce stime in linea con i metodi precedenti, ma offre una risoluzione temporale decisamente maggiore.

I risultati mostrano che la connessione tra la dinamica e la morfologia dei plume e l'emissione, persiste per ogni plume analizzato . In particolare, la velocità, la temperature e la complessità, come misurate con l'evoluzione frattale, seguono un'evoluzione legata all'emissione alla bocca. Tra i diversi fattori che caratterizzano l'emissione, le variazioni laterali (e.g. spostamento del vent o cambiamento della geometria o del angolo dell'emissione) e le fluttuazioni temporali, compreso il tempo e l'intensità dell'emissione e altri cambiamenti nell'esplosione, esercitano i più forti controlli sull'evoluzione del plume. Questi cambiamenti laterali e temporali possono essere combinati in un fattore di instabilità generale che, controllando la formazione dei

vortici alla base del plume, determina la modalità di entrainment dell'aria e l'evoluzione generale del plume.

La connessione tra l'evoluzione dell'emissione e la dinamica che ho quantificato in questo lavoro portano ad una nuova comprensione della formazione e dello sviluppo iniziale dei transient plumes. La creazione di nuovi strumenti di caratterizzazione, come l'analisi frattale e del tasso delle emissione, mostrano risultati promettenti, potenzialmente utili per il monitoraggio futuro dei vulcani attivi.

1 Introduction

Volcanic eruptions are at the origin of numerous dynamical phenomena (e.g. ash plumes, lava flows, lahars, pyroclastic density currents, dome collapses) which can constitute hazards for people living in the close, intermediate and far-field regions from the volcano. Some of these hazards are directly or indirectly related to volcanic ash plumes dynamics (e.g. pyroclastic density currents and ash fallouts). Understanding volcanic plume's fundamental dynamics is then crucial in order to mitigate the associated hazards. Volcanic plumes have then been the object of many experimental, numerical and field studies over decades, trying to parameterize them in order to provide better understandings of their behavior.

In most studies, volcanic ash plumes have been subdivided in two end-members based on the time scales of explosion duration and plume development, respectively. The first end-member is the *thermal cloud*, a minutes- to tens of minutes-lasting, stand-alone plume that originates from seconds-lasting explosions and, in literature, is generally associated with Strombolian eruptions (Figure 1.1a). The second end-member is the *sustained plume*, an hours-lasting plume originating from quasi steady-state eruptions that may last several hours, such as plinian eruptions (Figure 1.1c). Most of plume parameterizations (e.g. plume height, volume, mass eruption rate) and of empirical plume models performed so far, rely on these source dynamics simplifications. Even though those two end members succeed to model the behavior of small thermal clouds and large plinian columns, none of them accurately describes the dynamics of *transient plumes*, i.e., those plumes which are characterized by explosion duration similar to the duration of plume development (Figure 1.1b). In other words, while for thermals and sustained plumes ejection properties at the vent, e.g., mass ejection rate and vent diameter or location, can be considered as invariant at the time scale of plume growth, in the case of transient volcanic plumes ejection properties vary at the same time scale as plume development, and thus have a significant impact on the overall plume dynamics. This impact has been recently demonstrated by experimental studies, together with the

need for further expand source and plume characterization in the field, since transient plumes are the most represented type of volcanic plumes on planet Earth [*Clarke et al.,* 2015, *Taddeucci et al.,* 2015].

The first objective of this study is thus to provide a detailed characterization of transient ash plumes recorded on the field using high-speed and high-resolution cameras. A selection of videos from three different volcanoes, Stromboli (Italy), Fuego (Guatemala) and Sakurajima (Japan), representative of Strombolian and Vulcanian activity, is accomplished. This study has been done using a dataset unique in the world, of more than 200 videos. Parameter extraction has then been performed on the selected plumes, including their front velocity, velocity field, apparent surface temperature, and volume.

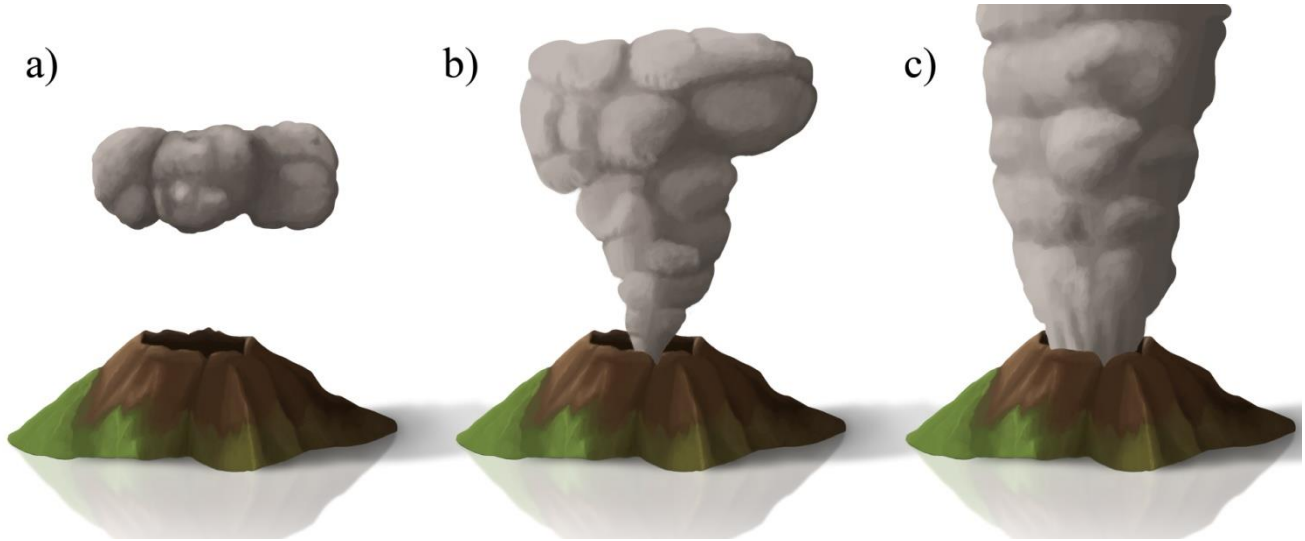

Figure 1.1: Illustration of the different volcanic plume types: a) Thermal cloud characterized by a quasi-instantaneous ejection phase, b) Transient plume characterized by ejection duration similar to the plume development, c) Steady-state plume characterized by a constant ejection of material over time.

The second objective of this study is to describe and quantify the discharge history at the vent, of our selected plumes. To do so, we created a new methodology in order to estimate the time-resolved discharge rate of the recorded explosions. This method merges field data and dynamical flow theory to retrieve the mass of ash present in the plume and the particles exit velocities

evolution over time. Implementation of flow dynamics theory in this method has been done during two secondments at the Institute of Fluid Dynamics and Technical Acoustics of Berlin (Germany) in collaboration with Dr. Juan José Peña Fernández and Prof. Joern Sesterhenn.

Discharge history estimations combined with qualitative morphological observations highlight the impact of the source on the plume's shape evolution. These findings encouraged us to develop better ways to quantify plume shape evolution, in order to establish an empirical relation with source properties.

Following this idea the third objective of this study is the fractal dimension measurements of the plumes, in collaboration with Prof. Diego Perugini, from the Petro-Volcanology Research Group (PVRG), University of Perugia (Italy). Fractal measurements applied to high speed imaging, as well as to numerical simulations provided by the Institute of Fluid Dynamics and Technical Acoustics of Berlin, allowed us to characterize and uniquely quantify the complexity of transient volcanic plumes and its changes over time. With this tool it became then possible to illuminate better the inter-connection between the main dynamical aspects governing plume development.

This thesis is a compilation of two manuscripts and is organized as follow: Section 2 corresponds to a published article about the impact of the discharge history at the vent on the initial development of transient volcanic plumes from Strombolian and Vulcanian eruptions. In this section, we use unique high speed videos to perform qualitative observations of plume development and quantifications of physical plume and source parameters (e.g. velocity, volume, temperature, ash eruption rate). In this part of the study, I was part of several field campaigns, and personally performed the video processing, parameter extraction, discharge rate methodology set up, data interpretation and writing of the manuscript. Dr. Elisabetta Del Bello, Dr. Piergiorgio Scarlato, Dr. Ulrich Kueppers, and Dr. Akihiko Yokoo were present during the field campaigns where videos were recorded. Dr. Jacopo Taddeucci and Dr. Damien Gaudin were part of every field campaign and provided technical support for video processing and data interpretations. Dr. Juan José Peña

Fernández and Prof. Joern Sesterhenn participated to some of the field campaigns and provided support in the implementation of flow dynamics theory in the ash eruption rate estimation method. All the co-authors also participated in manuscript preparation.

Section 3 corresponds to a manuscript in preparation about the characterization of transient plume shape evolution and its relation with the source behavior using fractal analysis. In this specific part of the study, I performed the manual plume outline, the fractal dimension analysis, the perimeters ratio analysis, the data interpretations and writing of the manuscript. Dr. Juan José Peña Fernández and Prof. Joern Sesterhenn provided the three numerical gas jet simulations. Dr. Diego Perugini contributed with his expertise in fractal analysis. Dr. Jacopo Taddeucci assisted the data interpretations. Dr. Danilo Palladino participated in the manuscript preparation.

Some modifications have been performed on the original manuscripts, such as the incorporation of the supporting information within the text, as well as a few additional figures for clarity. Section 4 brings a general conclusion on the impact of time-dependent ejection on transient plume's dynamical and morphological evolution, as well as implications for future studies.

As supporting information, this thesis comes with a CD containing a selection of eleven high-speed and high resolution videos in the visible and the thermal spectral range from our dataset, in order to enable readers to have access to dynamical features described in the thesis. Here every video has been set to play in real time at 25 fps. For each high-speed video a regular frame skip interval has been performed in order to have the appropriate frame rate. For each thermal record the gray scale correspond to the apparent temperature indicated in the color bar.

Data supporting this work is available in supporting information and at INGV Roma – Department of Seismology and Tectonophysics, HP-HT lab. This work is supported by the VERTIGO Marie Curie ITN, funded through the European Seventh Framework Programme (FP7 2007-2013) under Grant Agreement number 607905.

2 The initial development of transient volcanic plumes as a function of source conditions

Pierre-Yves Tournigand[1], *Jacopo Taddeucci*[1], *Damien Gaudin* [1,2], *Juan José Peña Fernández*[3], *Elisabetta Del Bello*[1], *Piergiorgio Scarlato*[1], *Ulrich Kueppers*[2], *Joern Sesterhenn*[3], *Akihiko Yokoo* [4]

[1] Istituto Nazionale di Geofisica e Vulcanologia, Sezione di Roma 1, Rome, Italy,

[2] Ludwig-Maximilians-Universität (LMU), Munich, Germany

[3] Institute of Fluid Dynamics and Technical Acoustics, Technische Universität Berlin, Germany

[4] Aso Volcanological Laboratory, Institute for Geothermal Science, Kyoto University, Kumamoto, Japan

Key words

transient plume, vulcanian, strombolian, vent, ejection pulse, ash eruption rate.

Key Points

1) Transient plumes from Strombolian to Vulcanian explosions are described via high-speed visible light and thermal imaging.

2) Parameterization includes plume front velocity, velocity field, volume, apparent surface temperature and ash eruption rate at vents.

3) Initial plume dynamic is controlled by number, source location, angle, duration, velocity and interval between ejection pulses at vents.

2.1 Abstract

Transient volcanic plumes, having similar eruption duration and rise time scales, characterize many unsteady Strombolian to Vulcanian eruptions. Despite being more common, such plumes are less studied than their steady state counterpart from stronger eruptions. Here, we investigate the initial dynamics of transient volcanic plumes using high-speed (visible light and thermal) and high-resolution (visible light) videos from Strombolian to Vulcanian eruptions of Stromboli (Italy), Fuego (Guatemala) and Sakurajima (Japan) volcanoes. Physical parameterization of the plumes has been performed by defining their front velocity, velocity field, volume, and apparent surface temperature. We also characterized the ejection of the gas-pyroclast mixture at the vent, in terms of number, location, duration and frequency of individual ejection pulses, and of time-resolved mass eruption rate of the ejecta's ash fraction. Front velocity evolves along two distinct trends related to the initial gas-thrust phase and later buoyant phase. Plumes' velocity field, obtained via optical flow analysis, highlights different features, including initial jets and the formation and/or merging of ring vortexes at different scales. Plume volume increases over time following a power law trend common to all volcanoes and affected by discharge history at the vent. Time-resolved ash eruption rates range between 10^2 and 10^7 kg/s and may vary up to two orders of magnitude within the first seconds of eruption. Our results help detailing how the number, location, angle, duration, velocity, and time interval between ejection pulses at the vents crucially control the initial (first tens of second), and possibly later, evolution of transient volcanic plumes.

2.2 Introduction

Transient volcanic plumes are a common outcome from a variety of explosive eruption styles, including Strombolian, violent Strombolian and Vulcanian, and can exhibit a variety of morphological features. The shape evolution of volcanic plumes holds key information on eruptive processes occurring at the vent, and has been investigated at several volcanoes. However, our understanding of the link between source conditions at the vent and plume morphology and evolution is still far from complete, and theoretical and experimental models still require validation

from field observations [*Chojnicki et al.,* 2015a]. In this study, we use imaging techniques to parameterize both source conditions and the initial growth stage of transient volcanic plumes from three different volcanoes showing a range of eruption styles.

Volcanic plumes consist in a mixture of ash, gas and entrained atmospheric air that rises and expands in a turbulent flow including multiple vortexes. Bigger particles (> 2 mm) can be part of this mixture in the early development stages. Volcanic plume dynamics have been theoretically divided into two end-members based on the ratio between the characteristic time scale of gas and ash injection (t_i) in the atmosphere and that required for the full rise and development of the plume (t_d) [*Wilson et al.,* 1978]. On one hand, steady-state plume dynamics result from plumes that are fed by a sustained, constant-rate source ($t_i >> t_d$) [*Morton et al.*, 1956]. Such dynamics and the associated theory are commonly used to model large volcanic plumes released by Plinian eruptions [*Woods*, 1988]. On the other hand, plumes formed by a quasi-instantaneous release of ash and gas ($t_i << t_d$), often termed "puffs" or "thermals", rise and grow following different dynamics [*Turner*, 1969]. However, these two end-members often may fail to describe plumes from, e.g., Strombolian to Vulcanian activity, in which the timescale of ash and gas release is of the same order of magnitude as that of plume development and rise. These intermediate plumes are generally named "transient" and their evolution is strongly dependent on the specific, often unsteady or fluctuating, discharge history at the vent [*Clarke et al.,* 2002].

Field observations have parameterized several aspects of transient plumes, including: i) plume rise velocity [*Patrick et al.*, 2007; *Patrick,* 2007; *Sahetapy-Engel and Harris*, 2009; *Zanon et al.*, 2009; *Webb et al.*, 2014], ii) volume [*Yamamoto et al.*, 2008; *Delle Donne and Ripepe*, 2012] and temperature [*Marchetti et al.*, 2009; *Harris et al.*, 2013], iii) air entrainment [*Yamamoto et al.*, 2008], and iv) exit velocities [*Suwa et al.*, 2014]. Two main dynamical stages are recognizable in most transient volcanic plumes [*Patrick,* 2007; *Patrick et al.*, 2007]. In the first stage, the evolution of the plume is dominated by the initial momentum of an eruptive vent (gas-thrust phase), while at a

later stage plume rise is dominated by buoyancy originating from the entrainment and heating of the surrounding atmosphere (buoyancy-driven phase). In eruptions with transient plumes, pulsating behavior of ejection at the vent has been observed repeatedly [*Harris et al.*, 2012; *Taddeucci et al.*, 2012; *Gaudin et al.*, 2014; *Scharff et al.*, 2015; *Capponi et al.*, 2016, *Gaudin et al.*, 2017]. Such unsteady vent discharge is expected to induce large changes on the resulting morphology and dynamics of plumes [*Clarke et al.*, 2002; *Chojnicki et al.*, 2014, 2015a, b; *Peña Fernández and Sesterhenn*, 2017]. However, the impact of specific discharge history on volcanic plume evolution has not yet been investigated in detail.

In order to provide new insights on the initial evolution of transient volcanic plumes in general, and on their link with vent dynamics in particular, here we focused on plumes from three different volcanoes: Stromboli (Italy), Fuego (Guatemala) and Sakurajima (Japan), covering a range of eruptive styles from Strombolian to Vulcanian. Eruptive plumes have been parameterized using a combination of high-speed visible light camera, thermal infrared camera, and high-definition visible light cameras. Videos were processed by classical and novel techniques, including Optical Flow analysis. Imaging the initial stages of plumes development provides a detailed characterization of the link between plume evolution and changes in eruptive vent dynamics.

2.3 Field sites

2.3.1 Stromboli

Stromboli volcano is a 924 m above sea level (a.s.l) stratovolcano located in the northeast part of the Aeolian Archipelago (Italy). The activity is characterized by intermittent explosions since at least the 10th century Common Era [*Harris and Ripepe*, 2007; *Patrick*, 2007; *Rosi et al.*, 2013]. During the period of recording in May 2013 [http://www.ov.ingv.it/ov/comunicati-stromboli/bollettino-2013-05-26.pdf]) and May 2016, 9 to 12 events took place per hour from several vents hosted in the 300 m long crater terrace at ~800 m a.s.l. This volcano serves as a reference for Strombolian activity due to its frequent explosions, accessibility, and vast literature on

multi-parametric investigations. Explosions from normal strombolian activity, generally assumed to result from the bursting of gas pockets close to the top of a mafic magma column inside the conduit, are divided into three main types: i) gas-dominated (Type 0), ii) ballistic-dominated (Type 1), and iii) ash-dominated (Type 2). The latter can be further subdivided into either ballistic-rich (Type 2a) or ballistic-poor (Type 2b) [*Francalanci et al.*, 1989; *Patrick et al.*, 2007; *Del Bello et al.*, 2012; *Barnie et al.*, 2015, *Leduc et al.*, 2015; *Taddeucci et al.*, 2015].

During two field campaigns in May 2013 and May 2016, twenty-one plume-forming ash-rich explosions (Types 2a and 2b), typically rising a few hundred meters above the vent, were filmed from three different locations (286, 370 and 542 m from the vent) (Figure 2.1, Table 1).

2.3.2 Fuego

Fuego is a basaltic-andesitic 3800 m a.s.l stratovolcano in the central Guatemalan arc. Its activity varies between discrete Subplinian phases and continuous Strombolian to Vulcanian eruptions [*Yuan et al.*, 1984; *Marchetti et al.*, 2009; *Lyons et al.*, 2010; *Lyons and Waite*, 2011]. Explosions, originating from two main active vents [*Lyons and Waite*, 2011], are described as an abrupt ejection combined with a vigorous degassing lasting for several tens of seconds, generating plumes typically rising up to 1500 m elevation above the source [*Johnson et al.*, 2004a]. At the time of our measurements the activity was characterized by several explosions per day forming ash plumes rising 400 to 1000 m above the crater [Global Volcanism Program, 2012].

Eight videos were recorded from 968 m distance from the vent in January 2012 (Figure 2.1, Table 1). The geometrical constraints of the field did not allow us to monitor the evolution of the largest plumes over a significant distance. Therefore, we focused this study only on the weakest plumes corresponding to the ones remaining within 200 m above the vent for the first 5s of the explosion. This selection represents the low-energy end-member of activity of the volcano at the time of recording.

2.3.3 Sakurajima

Sakurajima is an andesitic, 1117 m a.s.l. high stratovolcano in the southern rim of the Aira caldera (Kagoshima Bay, south Japan), composed of three different cones: Kitadake, Nakadake and Minamidake [*Ishihara*, 1985; *Iguchi et al.*, 2013]. During July 2013, Sakurajima produced about eighty Vulcanian explosions within the month, generating ash plumes, mostly from Showa crater, rising from 1000 to 4000 m elevation above the source [Japan Meteorological Agency, 2016]. Eruptions are driven by the accumulation of gas below a low-permeable or impermeable plug of degassed, crystalline magma until the failure of the plug initiates the eruption [*Iguchi et al., 2008*].

We used ten explosions from July 2013, occurring from the Showa crater, located at about 800 m elevation on the eastern flank of Minamidake, from two different observation points at 3.5 km distance from the vent (Figure 2.1, Table 1.1).

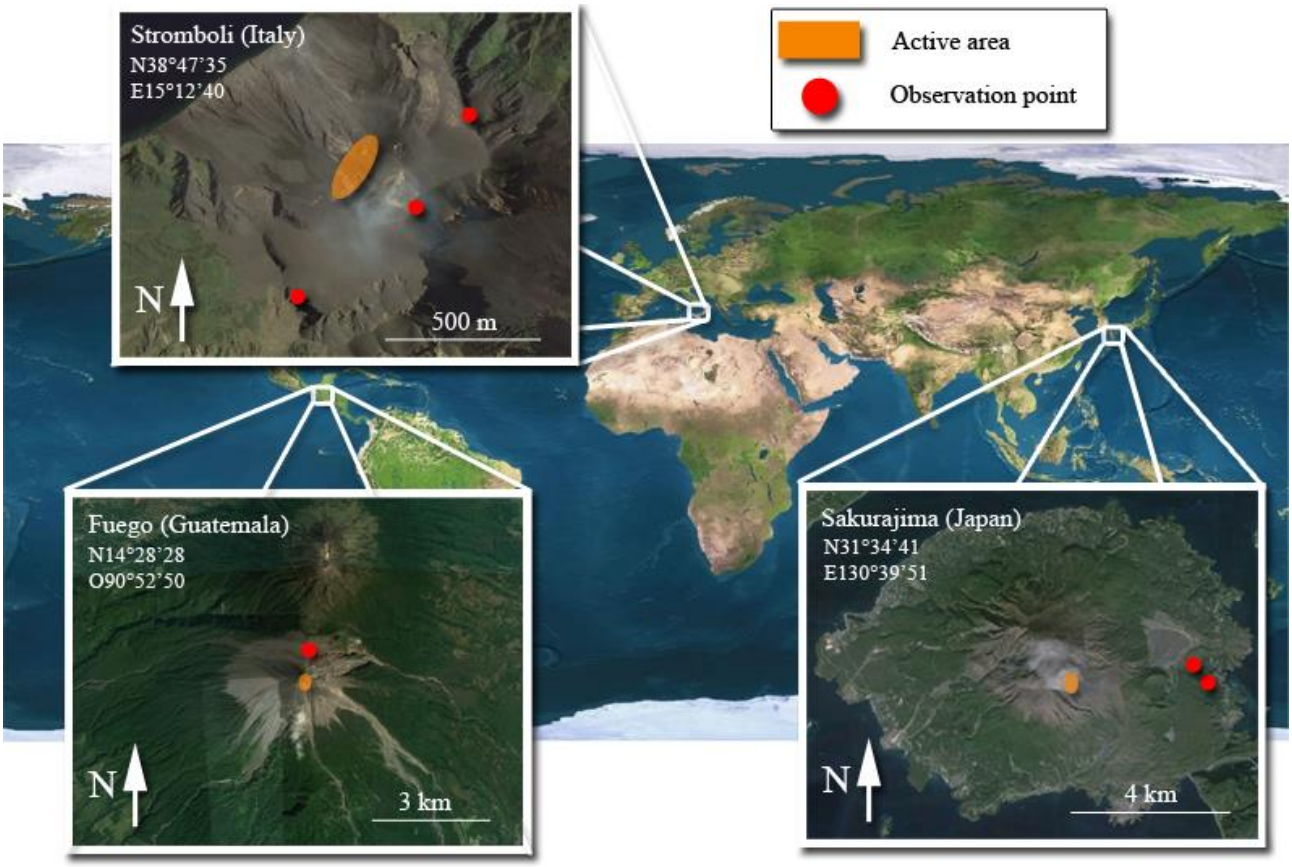

Figure 2.1: Map of the three different studied volcanoes, including the location of the active vent at the time of the field measurements (orange zone) and the locations of the cameras (red points). Coordinates refer to the vent area.

2.4 Methods

2.4.1 Recording setup

Videos were acquired using: 1) a visible-light high-speed camera (Optronis CamRecord CR600x2; 1024x1280 pixels definition, 500 frames per second (fps)), 2) a thermal infrared high-speed camera (FLIR SC655; 640x480 pixels definition, 50 fps frame rate, or 640x240 pixels, 100 fps), and 3) two wide-angle high-resolution visible-light Sony Handycam FDR-AX100 (3840x2160 pixels, 25 fps). FLIR and Optronis cameras were synchronized using a common trigger signal. Atmospheric correction of the thermal video was achieved using the FLIR ThermaCam software, taking into account the temperature and the humidity of the atmosphere and the distance from the camera to the plume. We did not correct for other effects such as sunlight intensity, angle of view, emissivity of the source, and absorption of radiations due to gas and aerosols [*Sawyer and Burton*,

2006; *Spampinato et al*., 2011; *Harris*, 2013b] and thus only relative, not absolute, values of temperature are reported in this study. From the original dataset of more than 200 videos, quantitative parameterization was performed on 43 (24 thermal, 12 high speed and 7 SONY) selected videos covering 29 explosions with the best visibility (Table 1.1).

Table 1.1: List of explosions presented in this study. [a]

Date and hour	Explosion #	Camera	fps	FOV (m)	v_{max} (m/s)	v_b (m/s)	ED (s)
16/07/2013 09:30:00	Sa_1	Opt	500	209x167	187.1	8.0	9.5
		FLIR	50	928x696	153.0	10.8	9.5
15/07/2013 06:01:50	Sa_2	Opt	500	209x167	65.3	9.5	n.a.
16/07/2013 01:24:10	Sa_3	Opt	500	209x167	149.1	11.4	n.a.
		FLIR	50	928x696	124.9	12.4	n.a.
19/07/2013	Sa_4	Opt	500	209x167	136.1	9.0	49.6
		FLIR	50	928x696	94.9	23.8	49.6
17/07/2013 22:29:00	Sa_5	Opt	500	209x167	134.8	-	n.a.
		FLIR	50	928x696	89.4	12.8	n.a.
17/07/2013 03:10:25	Sa_6	Opt	500	209x167	32.2	8.4	n.a.
16/07/2013 06:56:22	Sa_7	FLIR	50	928x696	52.0	12.5	36.1
16/07/2013 08:31:51	Sa_8	FLIR	50	928x696	117.5	14.3	12.3
15/07/2013 05:11:10	Sa_9	FLIR	50	928x696	121.8	21.0	21.3
19/07/2013	Sa_10	FLIR	50	928x696	227.0	n.a.	45.3
26/05/2013	St_1	Opt	500	37x30	51.2	10.9	n.a.
26/05/2013	St_2	Opt	500	37x30	112.9	n.a.	n.a.
26/05/2013 12:12:31	St_3	Opt	500	37x30	53.7	n.a.	5.6
		FLIR	50	307x230	54.7	10.2	5.6
26/05/2013 14:08:26	St_4	FLIR	50	307x230	68.7	14.4	3.0
26/05/2013 15:07:35	St_5	FLIR	50	307x230	52.3	10.0	1.5
26/05/2013 15:20:12	St_6	FLIR	50	307x230	62.9	15.0	2.0
26/05/2013 11:54:15	St_7	FLIR	50	307x230	77.7	12.9	3.5
26/05/2013 15:10:54	St_8	FLIR	50	307x230	33.2	9.4	4.2
22/05/2016 15:24:12	St_9	FLIR	50	307x230	25.3	6.7	23.5
25/05/2016	St_10	FLIR	50	450x338	24.8	8.4	5.6

13:44:00		Sony	25	370x657	22.0	8.2	5.6
25/05/2016 14:42:18	St_11	FLIR	50	450x338	29.7	7.4	13.0
		Sony	25	370x657	13.8	7.0	13.0
		Sony	25	370x657	15.7	8.5	13.0
26/05/2016 14:09:07	St_12	FLIR	50	450x338	22.9	7.3	17.0
		Sony	25	370x657	27.4	9.4	17.0
		Sony	25	370x657	29.2	7.2	17.0
26/05/2016 14:32:56	St_13	FLIR	50	450x338	58.4	7.3	25.2
		Sony	25	370x657	45.0	7.3	25.2
		Sony	25	370x657	55.0	8.0	25.2
14/01/2012 16:11:05	Fu_1	Opt	500	128x102	35.5	9.1	5.1
		FLIR	100	428x161	31.1	7.9	5.1
14/01/2012 18:36:14	Fu_2	Opt	500	128x102	26.5	8.8	11.4
		FLIR	100	161x428	21.4	7.3	11.4
14/01/2012 16:48:20	Fu_3	Opt	500	128x102	64.4	11.8	n.a.
13/01/2012 17:05:20	Fu_4	FLIR	100	96x255	48.0	14.2	4.7
14/01/2012	Fu_5	FLIR	100	161x428	22.4	10.1	3.3
14/01/2012 19:04:00	Fu_6	FLIR	100	161x428	70.4	n.a.	10.2

[a] Key. Explosion #: Sa=Sakurajima, Fu=Fuego, St=Stromboli. Camera: Opt=high-speed, visible light range Optronis CR600x2, FLIR= thermal infrared FLIR SC655, Sony= high definition Sony FDR-AX100. Fps=Recording frame rate. FOV= horizontal and vertical field of view. v_{max}= maximum plume front velocity. v_b= average buoyant rise velocity. ED= estimated ejection duration. Videos from multiple cameras are occasionally available for one explosion (shaded lines).

2.4.2 Plume parameterization

2.4.2.1 Plume motion

In order to track the motion of the plumes, we manually tracked the top part of individual vortexes, which represent clearly visible features, shifting to a new vortex when the tracked one started blurring with the plume. This method allows tracking the motion of the plume in all its different regions, although for most purposes we just refer to the front velocity, that is, the velocity of the uppermost part of the plume. Manual tracking was performed using the MtrackJ plug-in of the ImageJ software [*Abramoff et al.*, 2004].

To highlight individual structures (e.g. vortexes and bombs) and to detail the velocity field of the plume at specific development stages, we used the Optical Flow computer vision technique that compare to the widely used Particle Image Velocimetry (PIV) technique and allowed a

characterization of the flow. Following brightness constancy assumption over the measurement time, this method solves the optical flow equation based on pixel intensity [*Baker et al.*, 2011]. Couples of frames at ten frame intervals were selected from the thermal videos and pre-processed by extracting the thermal gradient of each frame combined with a temperature threshold visually adjusted for each explosion in order to remove the background (Figure 2.2a and 2.2b). Then we used the Optical flow Matlab toolbox [*Sun et al.*, 2010, 2014] to extract the direction and rate of plume motion in between these two frames using the "classic+nl–fast" method (Figure 2.2c). Velocity estimations from manual tracking and optical flow diverge by less than 4%. The results of the optical flow analysis are displayed using color encoding of flow vectors [*Baker et al.*, 2011].

In all cases, the reported velocities are two-dimensional, not accounting for motion towards or away from the camera. Considering the tilt angle of the camera at each location and the height reached by the plumes, our measurements may, in the case of a plume rising vertically, underestimate plume velocity by less than 10%, 22% and 25% for Stromboli, Fuego and Sakurajima, respectively (Figure 2.3). Deviations from the vertical in the rise direction of the plumes, due to local wind and oblique ejection at the vent, are not accounted for in our analysis.

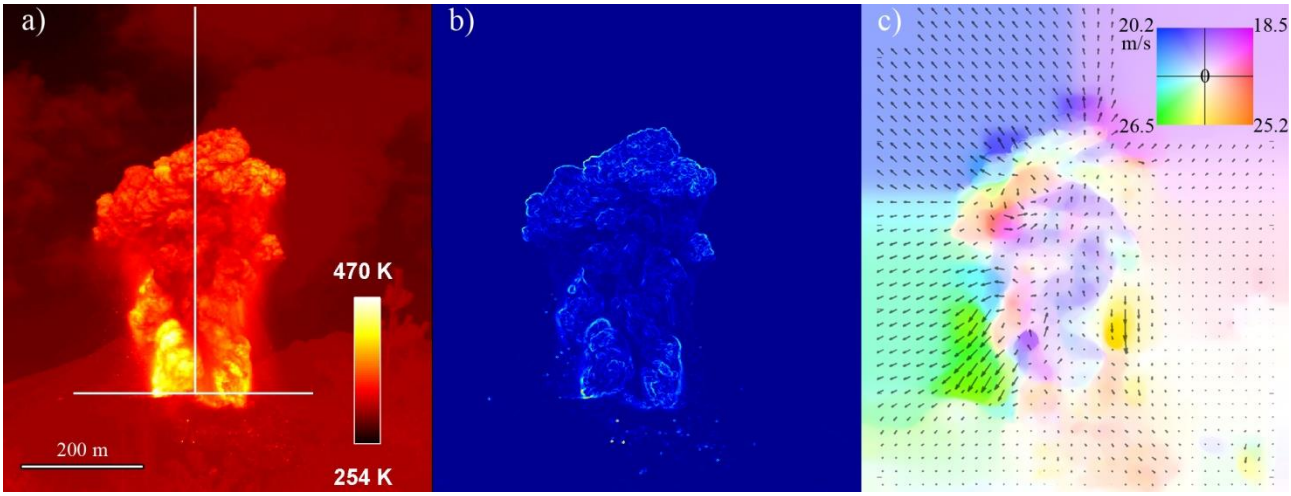

Figure 2.2: The Sa_7 explosion of Sakurajima. (a) The original, unprocessed thermal image (in color scale the apparent surface temperature). Horizontal and vertical temperature profiles along the white lines are plotted against time in Figure 5. (b) The same frame as in a) after pre-processing by thermal gradient and temperature threshold. (c) The Optical flow results illustrating the projected (bi-dimensional) motion of the plume in the 0.2 s before the current frame (in color scale the velocity magnitude). Direction and rate of the motion are represented by the hue and saturation of different

colors, respectively [*Baker et al.*, 2011]. For instance, the two blue/purple color-saturated areas at the plume front represent fast-rising bomb 'swarms' exiting the plume, green and yellow zones at the plume side denote diverging ash-bombs fallout areas, and orange to purple zones at the plume head mark large-scale vortex motion. Arrows also display the direction and the velocity of the plume, sub sampled every 16 pixels. Note the artifact propagation of the flow field away from the plume area.

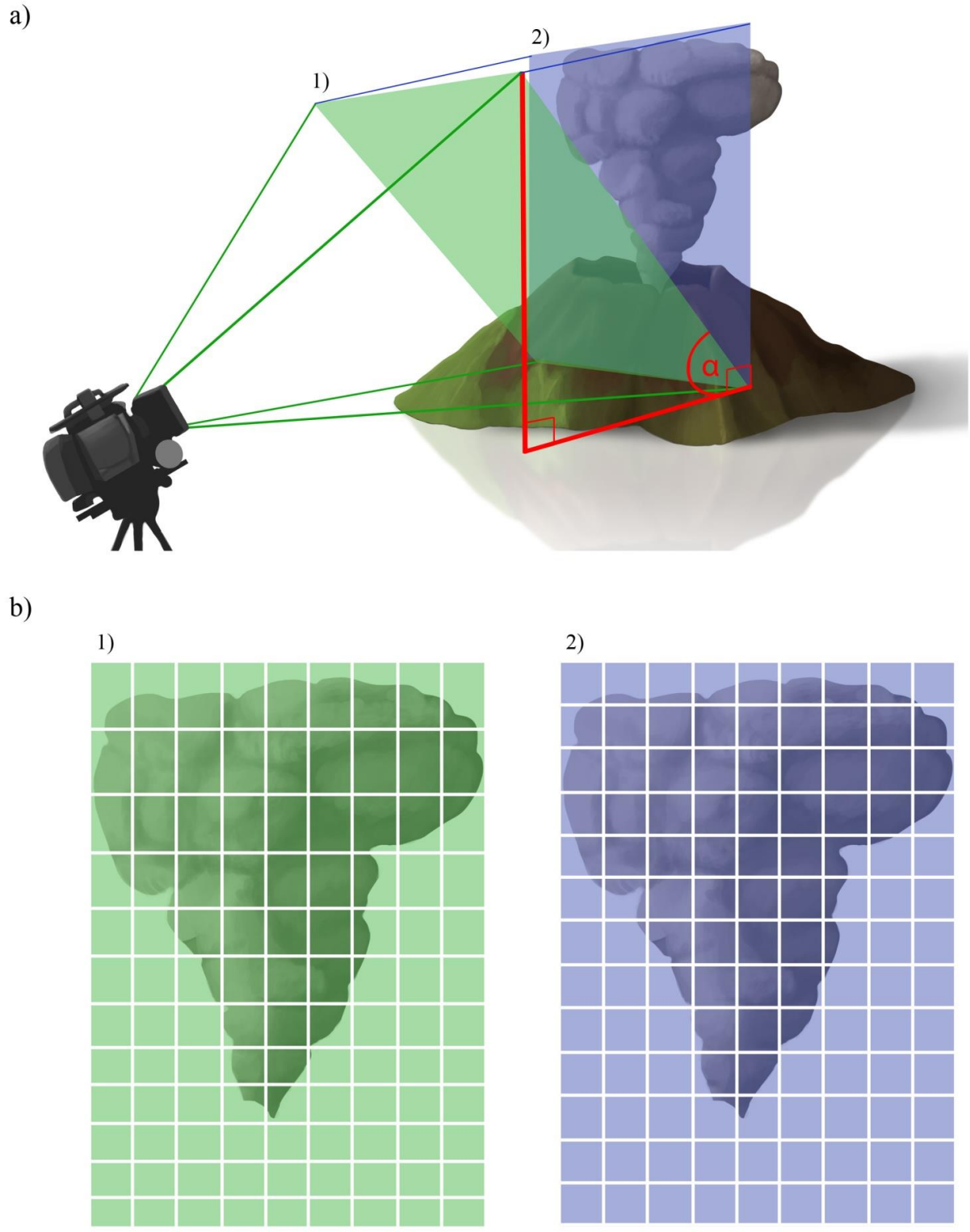

Figure 2.3: Illustration of the camera's tilt angle effect on the resulting plume's video: a) Recorded frame on the field with a tilt angle α (in green) compare to theoretical frame without tilt angle (in blue); b) resulting pixel distortion (in green) compare to the theoretical case (in blue).

2.4.2.2 Plume volume over time

The evolution of plume volume over time was estimated by manually contouring the plume area at a regular frame interval, individually defined for each video. Plume area was then converted into volume, assuming the plume to be axisymmetric [*Valade et al.*, 2014]. The plume is divided into horizontal slices, each one having volume equal to that of a cylinder one pixel in height and with the diameter corresponding to the width of the plume at that height. The sum of the volume of all slices provides an estimate of plume volume at any frame [*Valade et al.*, 2014]. Applying this method over several frames gives an estimation of the evolution of plume volume over time. Repeated measurements on the same explosion from different cameras located at the same place deviate by about 10 % on average. Uncertainties due to the axisymmetric plume assumption have been quantified on two explosions at Stromboli volcano using two cameras at different location with an angle of 90° between them and the plume and are about 46 % (Figure 2.4).

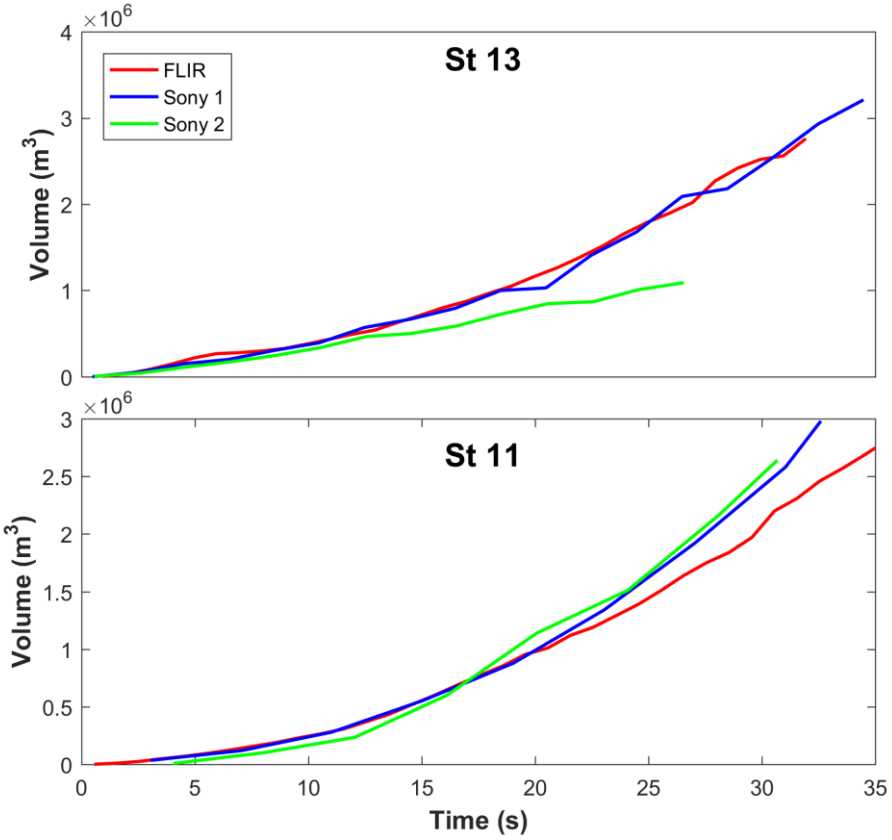

Figure 2.4: Plume volume evolution over time recorded by three different cameras (FLIR, Sony 1 and Sony 2). The FLIR and one Sony were at the same location, while the second Sony camera was at a

different location with a 90° angle between the plume and the two other cameras. The FLIR has a different resolution and recording rate than the two Sony, as detailed in section 2.4.1.

2.4.2.3 Ash eruption rate

An estimation of the ash mass in the plume as fraction of the total erupted mass, or ash eruption rate (AER), is provided following the principles described in *Morton et al.* [1956] and *Yamamoto et al.* [2008]. This estimation concerns only the solid fraction of the buoyant plume which, on the time scale of our observation, is coupled with the gas, while the mass of larger clasts and gas is not taken into account. Based on our calculations in order to obtain a Stokes number of 1 in the case of our transient plumes, the average particle diameter would range between 1.8 and 13 mm. Consequently, the solid fraction coupled with gas in our case includes only ash particles (i.e., smaller than 2 mm). To apply this method we selected explosions that fulfilled the following two criteria: 1) having a fully buoyant phase while the plume is still entirely in the field of view of the cameras; and 2) having a well-defined gas-thrust phase. In this study, the plume is assumed fully buoyant when its front velocity is not decreasing anymore with time. As an additional, conservative precaution, we also considered only rise velocities lower than 15 m/s, as used by *Patrick* [2007].

AER calculation requires the estimation of the concentration of ash C_{Ash0} and the volumetric flux at the vent. C_{Ash0} is derived from observation of the buoyant phase of the plume rise. In this phase, the vertical front velocity is determined by the plume buoyancy and can be linked to the plume density ρ_P at a given time [*Morton et al.*, 1956; *Yamamoto et al.*, 2008]:

$$\rho_P = \rho_a - \frac{3W^2}{zg}\,\rho_a \tag{2.1}$$

with ρ_P corresponding to plume density (kg/m^3), ρ_a being atmosphere density at the considered elevation (kg/m^3), W is the front velocity (m/s), z is the height of the plume front above the vent (m) and g is the acceleration due to gravity (m/s^2). This plume density is estimated at a given time t_b selected for each explosion and corresponding to a stage of front velocity trend stable and below 15

m/s. Assuming that the volumetric fraction of gas in the plume is close to 1 and that $\rho_P - \rho_{gas}$ is constant in the plume, we obtain the following equation [*Yamamoto et al.*, 2008]:

$$m_{ash} = (\rho_P - \rho_{gas})V \tag{2.2}$$

with *V* corresponding to the estimated plume volume and ρ_{gas} corresponding to the average density of gas present in the plume.

In this method, we estimate ρ_{gas} at a late development stage where plume rise buoyantly. Consequently, the gas present in the plume mainly results from entrainment of surrounding atmosphere and thus we chose to assume the density of the gas equivalent to the density of the atmosphere at the temperature of the plume head:

$$\rho_{gas} = \rho_{atm0} \frac{273.15}{T_{head}} \tag{2.3}$$

where ρ_{atm0} is the atmosphere density at 273.15 K. However, since we do not know the proportions of air and volcanic gases present in the plume over time, we performed a second estimation corresponding to the intermediate value between two end-members of volcanic gas mixtures at Stromboli volcano, the first including 64% H_2O, 33% CO_2 and 3% SO_2 and the second with 80% H_2O, 17% CO_2 and 3% SO_2 [*Burton et al.*, 2007; *Aiuppa et al.*, 2010]. Using volcanic gases instead of atmosphere decreases the gas density by about 11%.

Thus, we obtain m_{ash}, which represents the total mass of ash present in the plume, as measured during its buoyant phase. Starting with m_{ash}, and assuming it to be equal to the total mass of ash erupted during the explosion, we can then retrieve the concentration of ash at the vent during the gas-thrust phase, by using our high speed measurements of exit velocity. In fact, if we suppose that it remains constant with time, C_{Ash0} is obtained by dividing m_{ash} by the volume of the ash-gas mixture erupted at the vent (V_0):

$$C_{Ash0} = \frac{m_{ash}}{V_0} \tag{2.4}$$

The assumption of ash concentration constancy over time at the vent is commonly used in literature due to a lack of constrains on this parameter. This is particularly true for analogue experiments and numerical simulations where usually the ejected flow keeps the same properties all along the ejection phase (e.g. *Clarke et al.,* 2002; *Chojnicki et al.,* 2014). Assuming the vent diameter to be constant over time, V_0 can be retrieved using the exit velocity (v_{exit}) of the gas-ash mixture at the vent and the estimate of the vent surface (S):

$$V_0 = \int_{t0}^{tf} v_{exit} S \, dt \tag{2.5}$$

with t_0 and t_f corresponding to the beginning and the end of the ejection phase, respectively.

Finally, under the assumption that C_{Ash0} can be considered constant over time, the instantaneous AER (kg/s) is obtained by:

$$AER = v_{exit} S C_{Ash0} \tag{2.6}$$

which can be simplified in this case in:

$$AER = m_{ash} \frac{v_{exit}}{\int_{t0}^{tf} v_{exit\ dt}} \tag{2.7}$$

Note that this last simplification provides an AER equation which is independent from vent diameter.

Exit velocity at the vent is thus a crucial parameter for AER estimates, but it cannot be directly measured in our (and most other) case, because (i) the vent is not always in direct view of the cameras and (ii) we can only observe the exterior of the plume, where the velocity is lower than that at the centerline. In our case, we can only measure the ejection velocity of the plume (*vo*) at its

surface and as near as possible to the vent with a 0.4, 0.67 and 1.45 m maximum resolution for Stromboli, Fuego and Sakurajima, respectively. However, here the velocity of interest is the ejection velocity at the vent and on its axis (v_{exit}). *Turner* [1962] experimentally showed in the case of a steady-state plume that the front velocity (*vf*) corresponds to 0.6 times the mean velocity on the centerline (*vc*) of the plume at the same height. To apply this relation to our transient plumes we considered only the period 0.5-1 s after the beginning of explosions, using our front velocity data collected to infer the centerline velocity of the plume at that location. Here we make the assumption that exit velocity is homogeneous over the whole vent section.

$$vf = 0.6vc \tag{2.8}$$

This result is then compared to *vo* and a correction factor (*b*) is obtained.

$$b = \frac{vc}{vo} \tag{2.9}$$

b is then applied to *vo* for the whole gas-thrust phase duration.

v_{exit} is equal to *vc* only below a distance above the vent equivalent to about five to twelve vent diameters in the case of turbulent, round jets and then decreases for greater distances [*Bogusławski and Popiel*, 1979; *Panchapakesan and Lumley*, 1993; *Hussein et al.*, 1994; *Abdel-Rahman et al.*, 1997; *Freund et al.*, 2000; *Xu and Antonia*, 2002; *Quinn*, 2006; *Iqbal and Thomas*, 2007]. To ensure our cases fell into this five to twelve vent diameter cases we estimated vent size and depth. For Stromboli we used vent diameter estimations from *Chouet et al.* [1974] and *Gaudin et al.*, [2014] (2-3 m). For Sakurajima and Fuego we used estimations obtained tracking the trajectory of about fifty bomb-sized pyroclasts. These trajectories were then fitted with parabolic functions and prolonged inside the vent to estimate vent diameter and depth from the location and width of their crossing area [cf. *Dürig et al.*, 2015b]. For our case, the velocity measurements we performed at the base of the plume are always below or around seven vent diameters from the source and thus

representative of exit velocity after centerline correction. Vent shape can also play a role in the exit velocity evolution [*Cigala et al.*, 2017]. Such variation would fall within the measurement error and thus is not taken into account here.

The error propagation has been taken into account by calculating the mathematical uncertainty at each steps of the method. The associated error ranges between 40 and 154% of the calculated AER. Variations of this value are due to the relative error associated to each parameter involved in the calculation.

2.5 Results

2.5.1 Plume morphology and evolution

All observed events display an initial gas-thrust phase at the vent and a subsequent, slower rise of the ash-loaded plume (Figure 2.5) in agreement with previous observations [*Patrick*, 2007; *Patrick et al.*, 2007; *Marchetti et al.*, 2009].

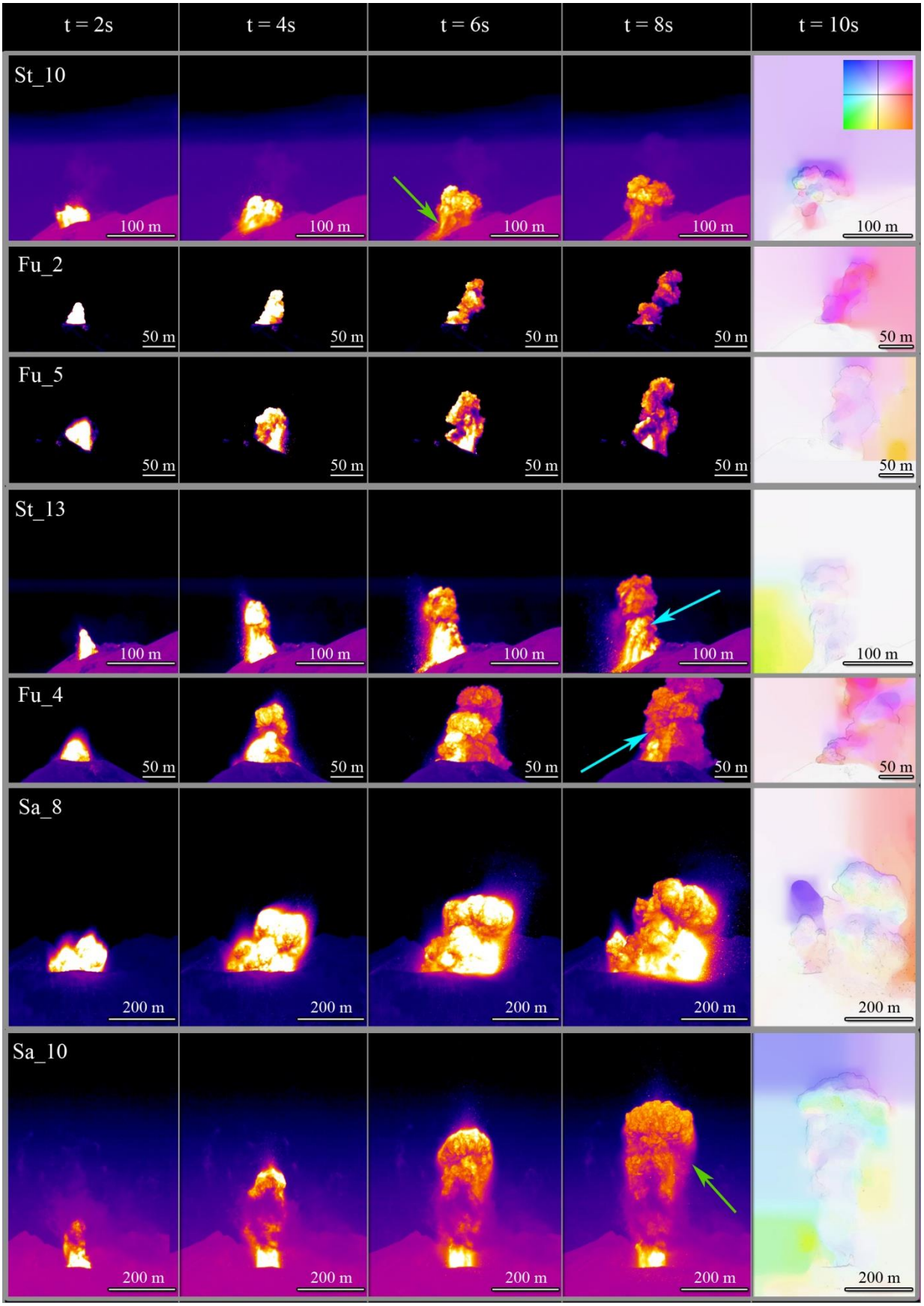

Figure 2.5: Still thermal frames showing the initial development of plumes from 7 explosions. In the right-hand column, the velocity field of the plume after 10 seconds. Velocity and temperature color

scales differ from case to case. Green and blue arrows correspond to ash downdrafts and helical motion of the plume, respectively.

The initial jet-like emission often has a spearhead morphology in the first few seconds and is always accompanied by the ejection of bomb-sized pyroclasts, occasionally simultaneously from multiple vents and at velocities up to hundreds of meters per second (supporting information video Fu_4 and Sa_1). The initial jets evolve into a slower rising structure through the development of vortexes at different scales, often combined and /or dominated by the formation of a large, toroidal, ring (or head) vortex (Figure 2.6). In the simplest case, one main vortex involves the largest part of the plume with a cylindrical body connecting it to the vent (e.g. supporting information video S4, explosion Sa_10). The rotation of this vortex involves absolute velocities in the order of tens of meters per second, in a flow field which is upward-divergent at the summit and downward-convergent at its base, below which displacement vectors point to a strong motion towards the vortex interior. In the cylindrical body velocity is slower, with motion towards plume interior also visible. In some cases, a pinch-off is observable [*Peña Fernández and Sesterhenn*, 2017], corresponding to successive ring vortexes formation, the new ones still developing while the previous ones start to detach from the plume through a neck, as experimentally observed by *Chojnicki et al.* [2014] (supporting information video Fu_4). In other cases, a first plume is developing before a second ejection phase, occurring with a different angle or from a different vent, which generates a secondary structure and impact the overall plume development (Figure 2.6 Sa_8, Figure 2.5 and supporting information video Sa_8).

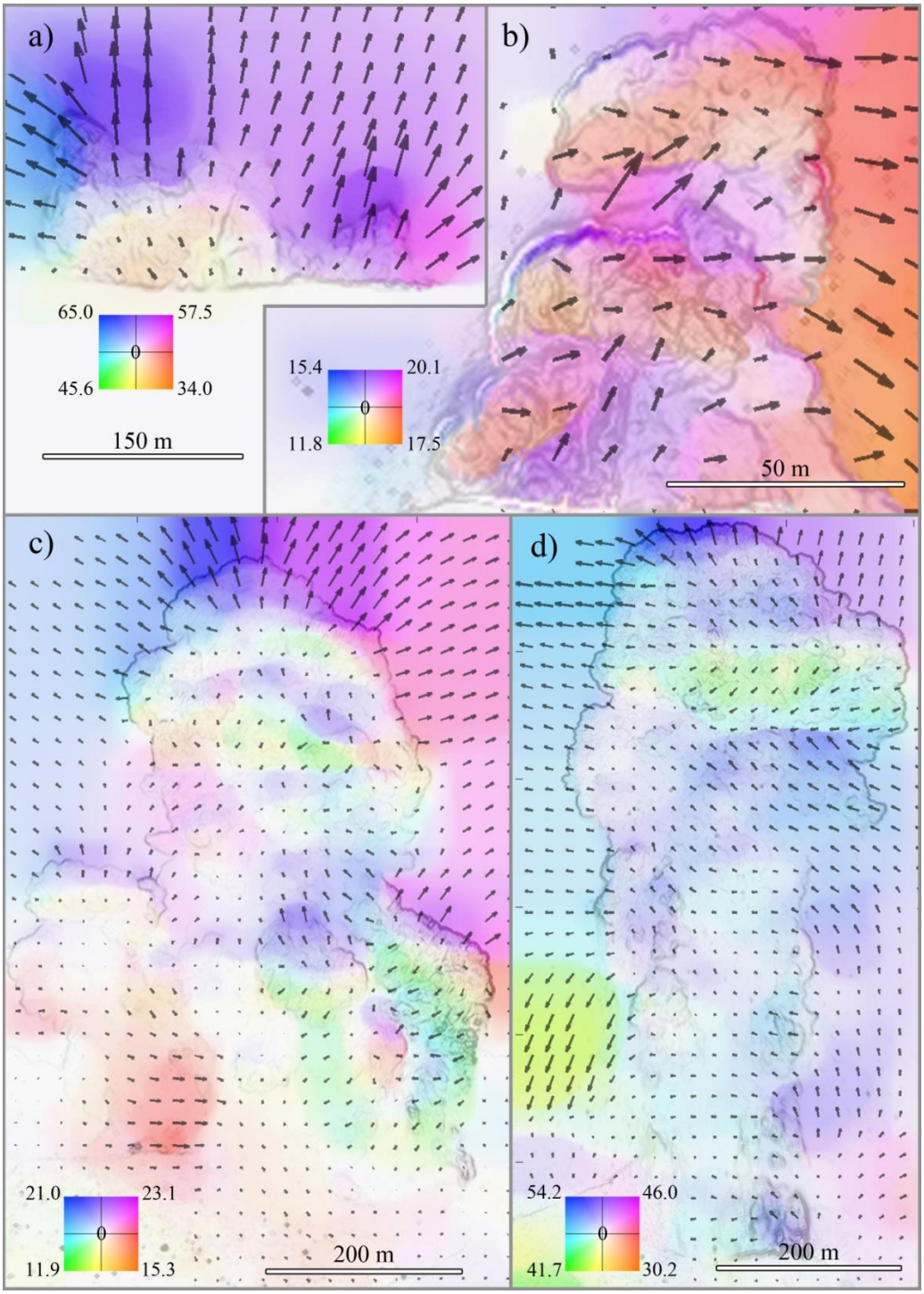

Figure 2.6: Flow field of volcanic plumes from the a) Sa_1, b) Fu_4, c) Sa_8 and d) Sa_10 explosions at 1.8, 4.5, 22.5 and 15.4 seconds after their beginning, respectively. Plume motion is displayed both using the color scale and sub-sampled arrows. a) Sa_1 features two jets with different angles from one or two different vents. Velocity is maximum (up to 65 m/s) at each jet front due to the ejection of bombs and ash in a radial pattern that heralds the formation of a ring vortex. Downward motion at the base of the jet on the left possibly marks the beginning of air entrainment. b) Fu_4 shows two similar, successive ring vortexes (marked by divergent velocity fields) and with upward air influx at their base (most developed for the upper one). Crosswind moves the entire plume from left to right, visible in the lack of leftward oriented (blue to green) velocity vectors. c) Sa_8 displays a complex plume formed by multiple ejection pulses from different vents. Several ring vortexes are present, marked by horizontal transitions of the flow field from upward- to downward-dominated motion. The uppermost and largest structure at the plume head displays two/three of these transitions, revealing several merging ring

vortexes. d) Sa_10, a plume almost sustained by multiple, fast-repeating pulses from the same vent, displays a large ring vortex, capped by overrunning bombs (high vertical velocities at plume's head), and followed by a strong (20 m/s ca.) area of air entrainment at the summit of a cylindrical body. Within the body, rising vortexes appear on the right-hand side (purple-bluish areas) and combine with a leftward oriented crosswind component.

The time evolution of plumes and respective source activities are best documented by changes in their apparent temperature. This was measured along a vertical profile located along the plume axis to track plume's rise and cooling, and along a horizontal profile located just above the vent to track changes in the activity and location of vents (Figure 2.2a). The temperature along these profiles is then plotted against time to provide a characteristic diagram (Figure 2.7). Finally, the integration of values of the horizontal profiles is plotted over time to qualitatively illustrate the discharge history at the vent for each corresponding plume.

Vertical changes highlight well the rise of the plume front, which often displays a sharp kink between two different rise velocities (Figure 2.7). The decrease with height of the apparent temperature of the plume surface is noticeable both at the plume front and in lower regions. Bombs appear as parabolic traces. Individual ejection pulses and vortexes are visible both in the vertical and horizontal evolution plots. Pulses inject new, hot material with a clear thermal signature visible close to the plume base. Vortexes cause hotter, inner parts of the plume to be first exposed at the surface and then cooled by conduction and convection, resulting in feather-like thermal features (Figure 2.7). Horizontal temperature evolution at the vent effectively traces lateral variations in the ejection source, which shifts position both sharply, and gradually, as the result of vent shifting and/or changes in the ejection angle of the gas-pyroclasts mixture. Finally, integrated horizontal temperature evolution at the vent reveals in most cases an asymmetric temperature anomaly, assumed to be somehow representative of the discharge history, with a short waxing phase, a peak – or plateau, and a longer waning phase. More than one peak phase may occur (e.g., St_12), and occasionally (e.g. Sa_10) an almost steady state supply seems to cover the whole duration of our videos.

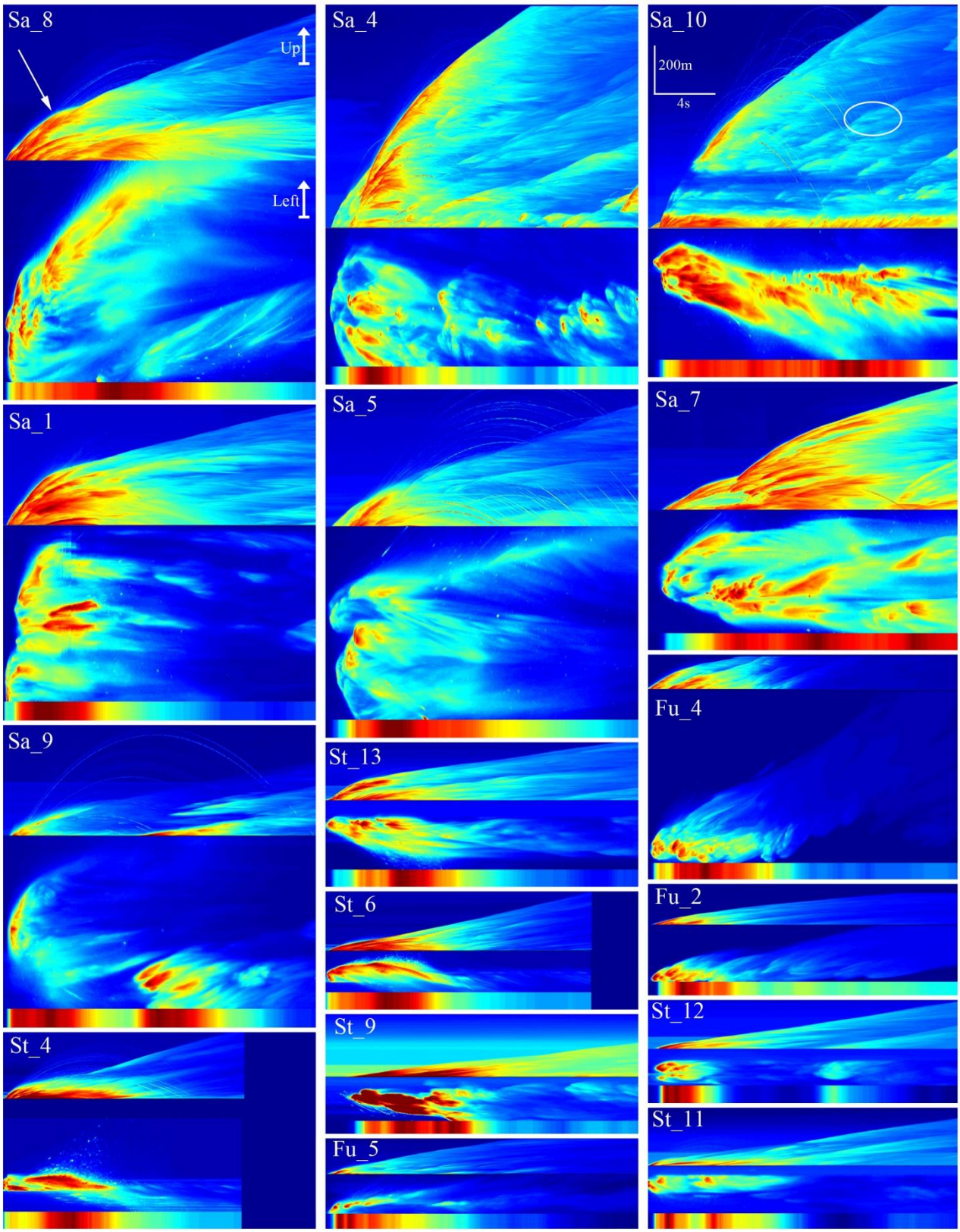

Figure 2.7: Vertical (top), horizontal (middle), and integrated (the average of horizontal values at any time, bottom) evolution of apparent plume surface temperature over the first 20 seconds of representative explosions (see Fig. 2 and section 3.2.1 for method description). Explosions are sorted downward in decreasing order of ejection duration and rightward in decreasing lateral span of ejection source. Vertical evolution tracks the rise and cooling of plume front (arrow in Sa_8 mark the kink in plume front rise velocity) and vortexes (circle in Sa_10), as well as the trajectory of ballistic

projectiles (Sa_5). Horizontal evolution illustrates well the number and duration of ejection pulses and their lateral variability. Integrated evolution is a proxy for the discharge history of each explosion. Space and time scales are the same for all explosions, while the apparent temperature scales (not shown) are normalized for each case.

The initial development of the observed plumes is essentially controlled by the source dynamics: occurrence of multiple ejection pulses, their number, intensity, duration, separation in time, and source vent (Figure 2.5, Figure 2.6, Figure 2.7). The jets and vortexes originated by these pulses interact and combine, giving rise to a wide spectrum of plumes morphologies and evolutions. Simple thermals are never present in our records; the shortest emission (St_10) still features a few ring vortexes from more than one ejection pulse. If ejection pulses are large and spaced by long time intervals, they may form multiple, distinguishable ring vortexes (e.g., Fu_4). Conversely, overlapping ejection pulses from one or a few close-by vents, if prolonged over tens of seconds, result in plumes with a large ring vortex at the head and a cylindrical body with smaller rising vortexes (e.g., Sa_10). These plumes are, among our cases, those whose morphology is closer to that of a sustained eruption column. Explosions involving ejection pulses with variable timing (from overlapping to a few seconds) and multiple vents (up to more than 100 m apart) produce complex plume morphologies, characterized by several independent large structures with merging and overlapping vortexes and jets (e.g., Sa_8).

Beside ejection pulses, other observed controls on plume morphology include: 1) crosswinds, affecting the interaction between jets from subsequent ejection pulses by laterally shifting the developing plume before initiation of secondary jets, like in the wind-bent plumes with well-separated vortexes of the Fuego cases (Figure 2.5, supporting information Fu_1); 2) the occurrence of ‘swarms’ of bomb-sized pyroclasts, dragging the ash, piercing the head of the plume from its front while rising and causing ash downdrafts at the plume margin while falling (Figure 2.5); and 3) partial collapses of the densest part of the plume to form small pyroclastic density currents, as observed at Fuego and Sakurajima volcanoes (Figure 2.6, Fu_4). Finally, we also report ash downdrafts developing from the lower corner of ring vortexes, and the wind affected outer part

of the plume rotating in helical motion (Figure 2.5, green and blue arrows, respectively) [*Patrick*, 2007].

Despite obvious differences in the intensity (index of eruption rate) and magnitude (index of erupted mass) of the activity at the three studied volcanoes, the abovementioned qualitative relationships between source variability and plume morphology holds true and no clear boundary divides them for plume morphology or evolution.

2.5.2 Plume parameterization

2.5.2.1 Rise velocity and volume

Depending on the magnitude of the event, plume heads reach heights between 100 and 800 meters within 40 seconds after ejection (Figure 2.8). Maximum plume rise velocities, always attained at explosion onset, are 113, 70 and 227 m/s, while average buoyant rise velocities are about 9, 10 and 13 m/s at Stromboli, Fuego and Sakurajima, respectively. Rise velocity of the plume head reflects the two phases previously described on the basis of the plume morphology. During the gas thrust phase, the rise velocity falls rapidly, due to the dissipation of the momentum, while during the buoyancy phase, the rise velocity remains fairly stable, with marked oscillations and in some cases late stage increases in rise velocity (e.g. Sa_1, St_10 and St_13). The transition between the two velocity phases is often abrupt and occurs two to fifteen seconds after the beginning of the explosion. Late stage velocity increases are less obvious at Fuego volcano, possibly because the field of view is small with respect to plume rise (Figure 2.8). The transition between the two rise velocity phases is strongly influenced by the number, duration, and time interval of ejection pulses that feed the plume: shorter, less and closer pulses result in earlier and more abrupt transitions, as exemplified by the Stromboli case (Figure 2.7 and Figure 2.8). On the contrary, at Sakurajima, longer-lasting ejection phases result in a slower decay of velocity in the first phase and a smoother transition to the second one. Fuego cases are in between these two. The velocity of individual

vortexes trailing behind the plume head, as measured by manual tracking and optical flow, ranges 5-22 m/s and decreases over time.

Within our limited time observation windows, plumes attain volumes ranging from about $4.2x10^4$ to $1.2x10^8$ m^3. In most cases, volume grows as a power law function of time with the Sakurajima explosions showing the largest volumes, and growth rates. Despite the very different initial and final volume attained by the plumes, all plumes display a similar expansion rate, as expressed by the power law coefficient, which shows an average value of 1.58 and ranges between 0.72 and 2.62. The average coefficient per volcano is 1.64, 1.47 and 1.56 for Stromboli, Fuego and Sakurajima, respectively. Higher coefficients, from 1.69 to 2.62, pertain to explosions with longer and more sustained ejection pulses such as Sa_4, Sa_7, Sa_10, St_9 and Fu_6, while events with shorter and more spaced pulses and wind and bombs interactions, such as Fu_1, St_4, St_7 and St_8, display lower coefficient in between 0.72 and 1.26.

Both velocity and volume results show a clear overlap of data in between Stromboli and Fuego cases, while most of Sakurajima's events appears to be larger and with higher rise velocities.

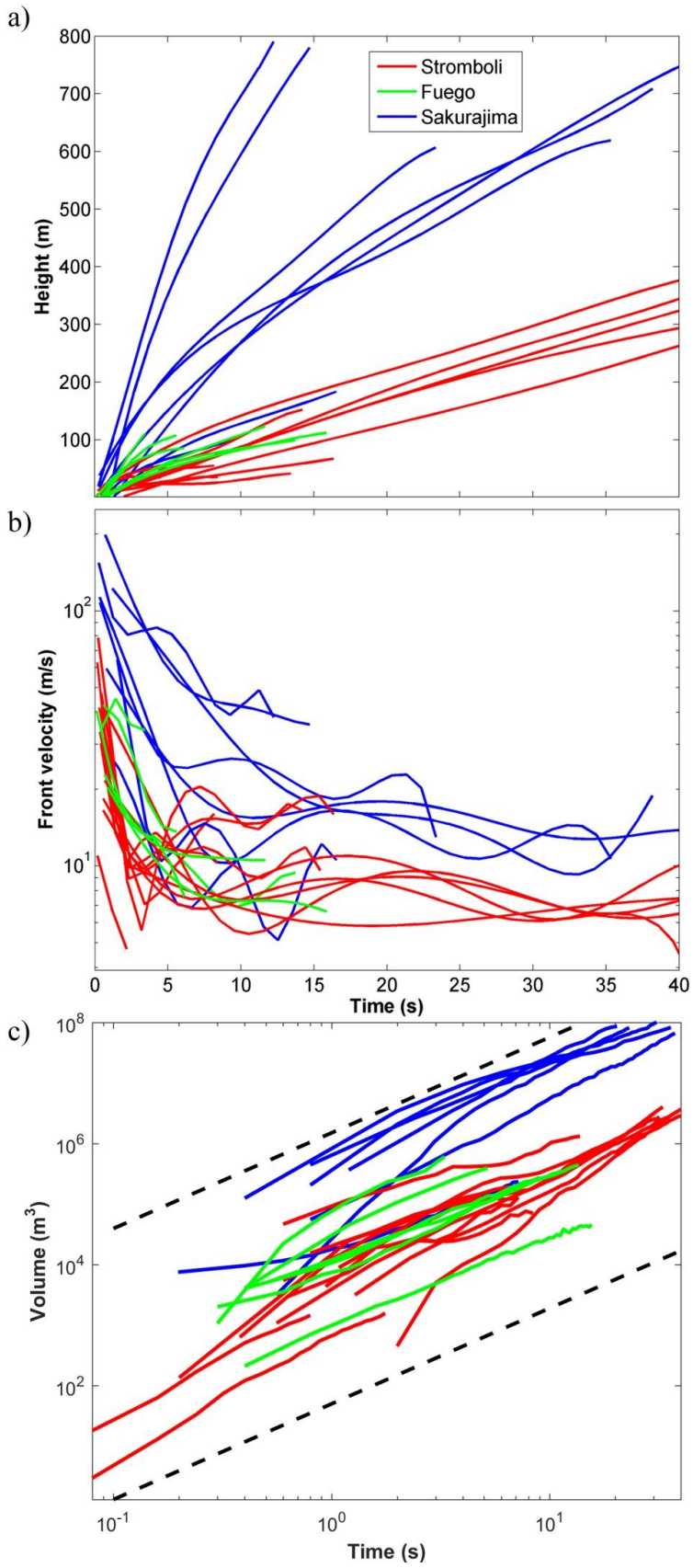

Figure 2.8: Evolution of (a) plume height, (b) front velocity and (c) volume measured until the time when the plume front exited the camera's FOV. For a better visualization, velocity curves were smoothed by a 4th order polynomial fit (cf. *Patrick et al.*, 2007). The black dashed lines in c) bound the

observed interval and have a slope corresponding to the average volume increase rate for all measured plumes. The corresponding average power law coefficient is 1.58.

2.5.2.2 Ash Eruption Rate

Estimation of ash eruption rate and its evolution over time was performed for six Stromboli, four Fuego and three Sakurajima explosions (Figure 2.9, Table 2.2), corresponding to the best cases from our dataset with respect to AER method requirements. Results show that the selected events cover a wide range of eruption intensities and magnitudes. Fuego and Stromboli display similar time-averaged AER values, in the order of 10^2-10^4 kg/s, while Sakurajima cases are about two order of magnitude higher, with time-averaged AER of about 10^5-10^6 kg/s. Using the average ash eruption rate and the ejection duration (estimated based on the videos) a cumulative erupted ash mass is obtained. Stromboli and Fuego cases, with similar AERs, eject 10^3-10^5 kg of ash in a few seconds, while the larger magnitude and more intense Sakurajima cases eject up to 10^7 kg of ash in up to 40 s (Table 2.2). In most cases, the time-resolved AER peaks at the beginning of the explosion, with subsequent increases occasionally being related to later ejection pulses. The initial AER peak, lasting about one second, can be up to two orders of magnitude higher than the final one and up to one order of magnitude higher than the time-averaged one.

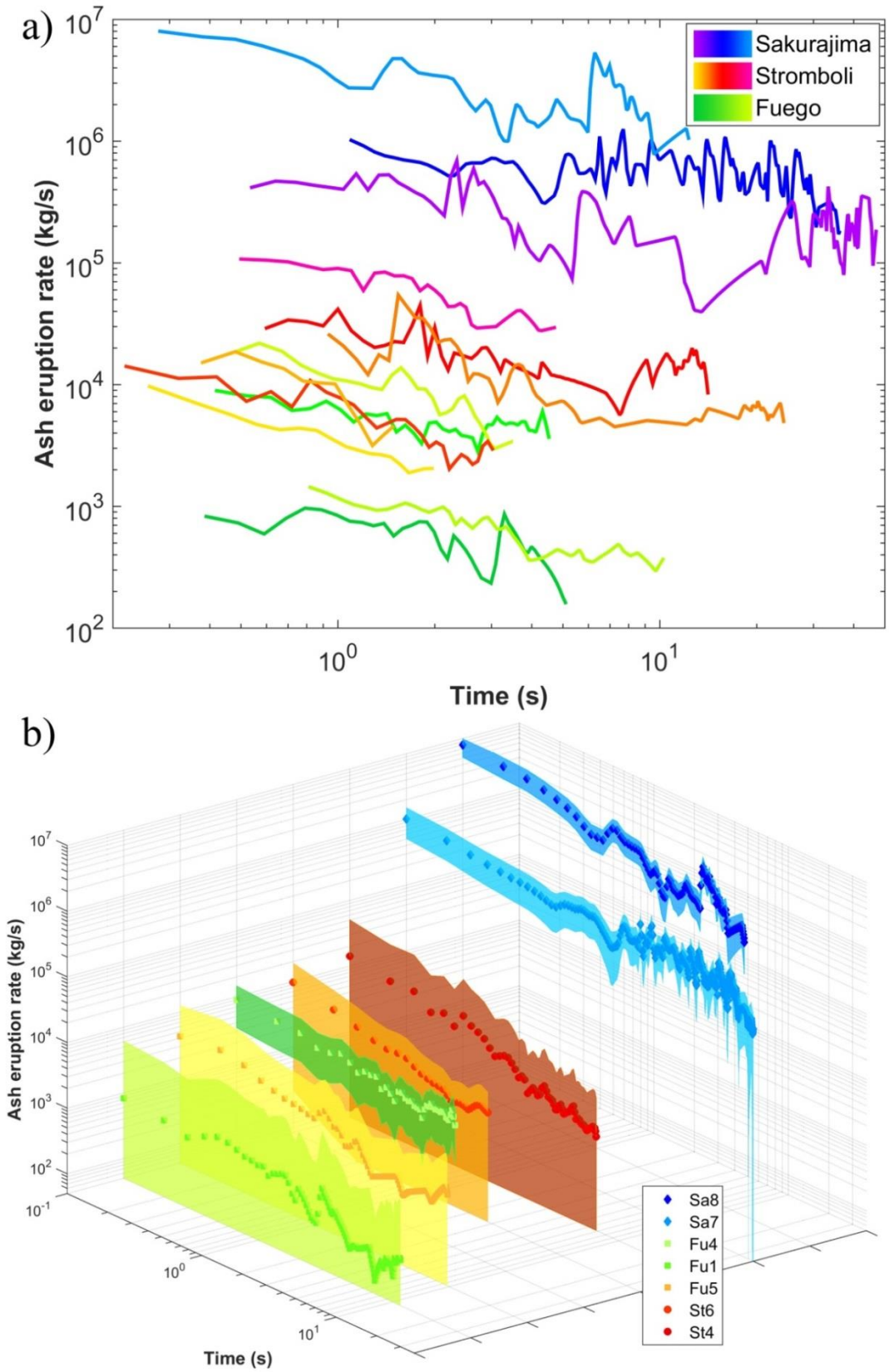

Figure 2.9: Ash eruption rate evolution over time, a) for all processed videos, and b) for selected explosions with their associated error (colored area). Note logarithmic axes scale.

Table 2.2: Summary of ash eruption rate (AER) results and parameters. [b]

Explosion	ρ^*_{Plume} (kg/m^3)	ρ^*_{Atm} (kg/m^3)	AER average (kg/s)	AER average error (%)	Cumulative ash mass (kg)	Ejection duration (s)	t_b (s)	v_{exit} correction factor	v_{front} buoyancy (m/s)	v_{front} max (m/s)	$v_{centerline}$ (m/s)	v_{exit} max (m/s)
Sa_5	1.195	1.117	1.85E+05	140	8.69E+06	46.94	33	1.0	13.4	72.5	120.8	116.5
Sa_7	1.237	0.836	6.63E+05	55	2.40E+07	36.12	33	1.3	10.0	54.2	90.3	70.6
Sa_8	1.267	0.910	2.87E+06	40	3.52E+07	12.28	23	1.6	6.4	131.2	218.7	138.7
St_4	0.881	0.855	2.47E+04	69	7.43E+04	3.01	10	1.7	11.6	111.5	185.8	111.5
St_5	1.138	1.083	9.73E+03	143	7,54E+03	1.52	13	1.7	7.3	56.0	93.3	54.3
St_6	0.593	0.540	7.76E+03	61	1.51E+04	1.95	6	1.4	13.4	46.0	76.7	57.0
St_10	1.236	1.165	5.25E+04	137	2.94E+05	5.6	30	1.5	6.3	21.3	35.5	23.5
St_12	1.235	1.138	1.48E+04	144	2.51E+05	17	33	1.3	6.3	19.6	32.6	26.1
St_13	1.190	1.093	7.42E+03	124	1.87E+05	25.16	25	1.5	8.5	59.1	98.5	65.0
Fu_1	1.096	1.083	4.86E+03	150	2.48E+04	5.09	10	1.0	7.7	24.7	41.2	47.2
Fu_2	1.253	1.135	5.36E+02	142	6.13E+03	11.43	14	1.7	3.7	26.8	44.7	26.6
Fu_4	0.939	0.777	7.55E+03	56	3.54E+04	4.69	6	1.5	11.6	49.4	82.3	55.4
Fu_5	1.016	0.949	5.33E+03	154	1.73E+04	3.25	8	1.0	4.5	24.8	41.4	43.5

[b] Plume and entrained air densities are marked as ρ^*_{Plume} and ρ^*_{Atm}, respectively and measured at the time t_b. ρ^*_{Atm} has been calculated using equation (2.3) based on plume head temperature at t_b. The cumulative ash mass corresponds to the integration of the average AER over the whole ejection duration. The v_{exit} correction factor is the correction applied to measured plume base velocities in order to retrieve exit velocities at the vent. The v_{front} buoyancy corresponds to the front velocity of the plume at t_b. The v_{front} max corresponds to the maximum front velocity measured on the plume. The $v_{centerline}$ is the calculated theoretical velocity at the plume centerline following *Turner* [1962]. The v_{exit} max corresponds to the maximum velocity manually measured at the plume base.

2.6 Discussion

Even though Vulcanian and Strombolian eruptive styles may differ in several aspects [*Clarke et al., 2015; Taddeucci et al., 2015*], our results show that initial plume dynamics from both styles share many common features. In both cases the impulsive, unsteady nature of the eruption mechanism strongly controls the features and evolution of the resulting transient plumes.

2.6.1 Diversity of plume morphology and evolution

Considering two theoretical end-members of plume morphology, i.e. impulsively-released thermals and steady-state plumes, the transient ones we describe fall in a broad, intermediate range. Some general features in morphology evolution are recognizable in almost every case. All explosions are characterized by the presence of a spear-head jet which evolves in a ring vortex and

then often transits in a more complex morphology during the buoyant phase, as already described in literature [*Patrick*, 2007; *Patrick et al.*, 2007; *Zanon et al.*, 2009; *Delle Donne and Ripepe*, 2012; *Webb et al.*, 2014] and as experimentally shown by *Kitamura and Sumita* [2011]. Complex plume morphologies originate from the occurrence of multiple ejection pulses, as visible in the thermal signature and velocity measurements (Figure 2.5, Figure 2.6), from one or more vents.

The morphology of transient plumes from unsteady sources has been investigated experimentally by *Chojnicki et al.* [2014], which injected finite volumes of water into water at constant temperature to get neutrally buoyant jets, following a "Gaussian-shaped history of flux over time". To visualize the flow field, a mixture of 10 microns diameter glass spherical particles was added to the jet and the recipient. The resulting experimental plumes varied in morphology over time along this Gaussian history: at the beginning, during the increase of momentum flux, a jet forms and then evolves into a rounded head, or ring vortex, followed by a cylindrical tail; during the decrease phase, after the peak flux, the ring vortex starts to overrun the body of the plume and a narrow neck forms in between. Finally, after the end of flux momentum, the body of the plume develops a new ring vortex at the head and a conical tail, both enlarging linearly while rising.

Comparing our observations with the experimental results of *Chojnicki et al.* [2014], we note that there is a general convergence of morphological features, but our study cases invariably display a higher degree of complexity, both in the variety of morphologies observed and in their evolution over time. The general convergence of features suggests that momentum is the dominating force of plume morphology in our observations of initial development, because buoyancy is entirely absent in the experiments of *Chojnicki et al.* [2014]. Buoyancy, while leaving a clear mark in the velocity trend of the plume head (Figure 2.8), does not significantly affect plume morphology in the region close to the vent which is the focus of our observations.

Besides the obvious differences between nature and a controlled laboratory environment, two main factors explain the increased complexity of our observations. First, our estimates of

ejection velocity, discharge history and ash eruption rates (Figure 2.7Figure 2.9) disagree with a Gaussian-shaped history of ejection flux at the vent, showing a maximum velocity at the very beginning of the ejection pulse, as already observed in several other cases [*Ripepe et al.*, 1993; *Taddeucci et al.*, 2012; *Gaudin et al.*, 2014]. This observation does not imply the absence of an acceleration phase at the beginning of the gas-thrust phase. A short acceleration exists but is not observed here due to geometrical constrains. Second and most relevant, almost all our explosions featured not one but multiple ejection pulses, also from more than one vent [*Taddeucci et al.*, 2012; *Gaudin et al.*, 2014; *Scharff et al.*, 2015; *Capponi et al.*, 2016]. Our observations focus on the initial development of plumes in a region which is relatively close to the vent area and it remains open to discussion how much of the complexity we observe is preserved in the morphology of plumes at later moments and higher elevations above the vent.

Of the several other factors influencing plume evolution, some have received more attention, like the presence of cross-wind [*Bonadonna et al.*, 2015] or the occurrence of partial collapses [*Neri et al.*, 2003]. Here we want to highlight that our observations suggest that large bomb 'swarms', both while descending and rising, can impact ash particles dynamics within the plume and cause premature ash falls.

Interestingly, we do not observe any clear difference of plume morphology and its evolution, even considering plumes with more than one order of magnitude differences in size and resulting from activity styles from Strombolian to Vulcanian. It appears that all those volcanic plumes belong to a continuous spectrum of eruption styles as first suggested by *Wilson et al.* [1978].

2.6.2 Plume parameterization

2.6.2.1 Velocity and volume

A twofold trend characterizes the rise velocity of the front of most of the observed plumes (Figure 2.8), i.e. first a sharp drop and then oscillations around a constant value. This trend has been

observed frequently for transient volcanic plumes and its two parts have been interpreted as the phases when gas-thrust and buoyancy drive the plume, respectively [*Blackburn et al.*, 1976; *Johnson et al.*, 2004b; *Patrick*, 2007; *Patrick et al.*, 2007; *Marchetti et al.*, 2009; *Sahetapy-Engel and Harris*, 2009; *Chojnicki et al.*, 2015a]. Front velocity fluctuations linked to multiple ejection pulses superimpose on the general trend, occasionally as sharp velocity changes but more often as smooth deviations from the trend.

Initial front velocities measured at Stromboli, Fuego and Sakurajima respectively range from 14 to 113 m/s, 21 to 70 m/s and 32 to 227 m/s at the very beginning of the explosion and values of average buoyant velocity converge to 9-13 m/s. Overall, the results match the one of *Patrick.* [2007] and *Patrick et al.* [2007] for initial front velocities at Stromboli volcano, ranging from 10 to 50 m/s and maximum buoyant rise of 10.9 m/s. As for the explosions closer to Vulcanian style, *Webb et al.* [2014] report initial front velocities between 6 and 60 m/s at Colima volcano (Mexico), *De Angelis et al.* [2016] measured a buoyant velocity of about 10 m/s at Santiaguito volcano (Guatemala), and *Suwa et al.* [2014] report initial rise velocities of about 34 m/s at Sakurajima. Their estimation of the velocity of trailing vortexes also matches well our measurements.

At Sakurajima, our estimated centerline exit velocities are maximum (90-292 m/s) in the first seconds of ejection, and later on average in the range of 39-121 m/s. These values are comparable with those estimated by *Suwa et al.* [2014] (40-50 m/s) in the same time interval. At Stromboli, maximum centerline values (76-186 m/s) are lower than maximum literature exit velocities (up to 400 m/s, [*Taddeucci et al.*, 2012]) which, however, were measured in ash-free explosions. Importantly, our data set enabled comparison of the front velocity of the same plume as measured with different camera setups. As expected, higher frame rate and higher magnifications results in higher measured velocities for the same plume, up to 50%.

Volumetric data show that plumes from Stromboli, Fuego and Sakurajima, follow a power law trend in their time-evolution (Figure 2.8):

$$V = Ct^{\alpha} \tag{2.10}$$

with t the time, C the proportionality coefficient and α the power coefficient. Theoretically, the radius of a thermal grows with the square root of time resulting in a time-volume power law dependency with slope 1.5 [*Turner*, 1979]. This value is remarkably similar to the 1.58 α average value of our plumes, which suggests that the air entrainment mechanism in our cases is similar to the one of individual thermals. However, our results also show that this coefficient deviates from the average value as a result of plume source properties, more 'sustained' conditions (i.e. more prolonged and closer in time ejection pulses) showing higher values, potentially reflecting the additional volume coming from the source (Table 2.3). The proportionality coefficient C defines the initial order of magnitude of the plume volume and thus can be considered as a proxy of the initial volume discharged during the ejection phase. It is interesting to notice that this coefficient displays a link with the average ash eruption rate (Figure 2.10). It appears that the AER increases with the coefficient C, following a power law trend. This observation suggests proportionality between the explosion magnitude (erupted mass) and intensity, at least for the ash fraction.

Sakurajima plume volumes range from 10^6 to 10^8 m^3 within the first 40s of explosions, in line with estimations for other Vulcanian plumes such as those of Santiaguito volcano (Guatemala), attaining volumes of $7x10^7$ and $2.2x10^5$ m^3 after 24 and 15s, respectively (*Yamamoto et al.* [2008] and *De Angelis et al.* [2016]). Results for Stromboli, 10^2-10^5 m^3 in 1 to 40s, are also comparable with the 10^2 - 10^4 m^3 in 10 to 12s of *Delle Donne and Ripepe*. [2012].

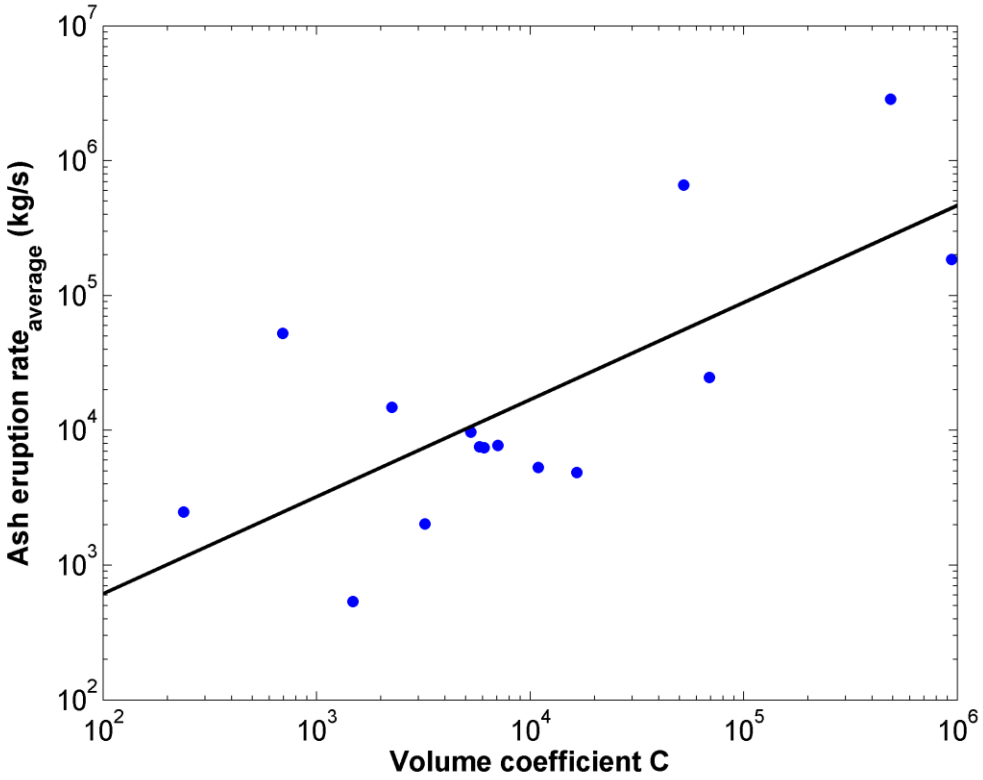

Figure 2.10: Average ash eruption rate (kg/s) in function of the proportionality coefficient C of the volume power law trends. The black line corresponds to the power law fit of the presented data with a R^2 of 0.52.

Table 2.3: Summary of coefficients from the power law evolution of volume over time ($V = C.t^{\alpha}$) [c]

Explosion	C	α	$C_{average}$	$\alpha_{average}$
Sa_1	1.72E+06	1.077		
Sa_2	6.89E+04	1.187		
Sa_3	n.a.	n.a.		
Sa_4	5.54E+05	1.694		
Sa_5	9.38E+05	1.358	4.98E+05	1.558
Sa_6	1.25E+04	1.489		
Sa_7	5.22E+04	1.970		
Sa_8	4.86E+05	1.626		
Sa_9	n.a.	n.a.		

Sa_10	1.45E+05	2.060		
St_1	6.36E+02	1.604		
St_2	2.11E+03	1.615		
St_3	2.50E+04	1.048		
St_4	6.90E+04	1.134		
St_5	5.28E+03	1.587		
St_6	7.07E+03	1.664		
St_7	3.45E+04	0.716	1.25E+04	1.636
St_8	6.02E+03	1.191		
St_9	2.38E+02	2.621		
St_10	6.92E+02	2.474		
St_11	3.22E+03	1.901		
St_12	2.25E+03	1.945		
St_13	6.08E+03	1.767		
Fu_1	1.65E+04	1.261		
Fu_2	1.48E+03	1.263		
Fu_3	4.23E+04	1.367	2.51E+04	1.469
Fu_4	5.79E+03	1.789		
Fu_5	1.09E+04	1.422		
Fu_6	7.39E+04	1.713		

[c] C and α respectively correspond to the proportionality and power coefficients of the volume trend evolutions of our transient plumes. $C_{average}$ and $\alpha_{average}$ provide the average coefficient per volcano.

2.6.2.2 Ash eruption rate

In literature, mass eruption rate (MER) can be inferred from observed volcanic plume height [e.g. *Sparks et al.*, 1997; *Mastin*, 2007] and theoretical/computational inversions [e.g., *Costa et al.*,2016]. Most applications of these methods assume steady-state plumes [*Morton et al.*, 1956] and concern Vulcanian to Plinian eruptions [*Mastin*, 2007]. MER can also be derived from tephra deposits and estimated eruption duration [e.g. *Andronico et al.*, 2013; *Pioli et al.*, 2014], but these methods neglect the erupted mass of gas and of tephra that are not mapped (e.g., large clasts that fall back into the vent) or not accounted by deposit extrapolation methods. In addition, most of the current MER estimates provide time-averaged values.

In this study, we use transient volcanic plumes to provide a first estimate of the eruption rate of ash from Strombolian and Vulcanian explosions, time-resolved at a sub-second scale. These two eruption styles typically generate different gas-ash-bombs proportions. Consequently, by focusing only on the ash mass of the plume, we underestimate the total erupted mass by different amounts in the different explosions. However, as mentioned in Section 2.4.2.3, all the transient plumes analysed in this study were specifically chosen to be notably ash-rich.

The methodology used in this study is, in principle, suitable to provide time-resolved AER from both steady and unsteady plumes without any *a priori* assumptions on vent diameter and particle density. Our AER method requires detailed observation on the rise velocity of the plume, an estimate/assumption of plume temperature, an estimation of gas species proportions inside the plume and is largely dependent on the exit velocity estimation at the vent. We also assume a homogeneous concentration of ash throughout the plume, which may not be the case [*Yamamoto et al.*, 2008].

Time-resolved data (Figure 2.9) reveal that AER may fluctuate as much as one order of magnitude in a matter of seconds. Instantaneous values for Sakurajima (Sa_8) even exceed literature reference for Plinian eruptions, but only in the first second of the explosions. The error

range we calculated reaches up to more than 150%. This relatively large error, however, must be viewed in the context of the order-of-magnitude variations that AER displays. Comparing our AER results with previous MER estimates of the same volcanoes, and keeping in mind the above assumptions and limitations, it appears that Sakurajima's explosions range in between Vulcanian and Plinian MER references, while Fuego and Stromboli show variations in between Strombolian and Violent Strombolian references, with higher values for Stromboli [*Pioli et al.*, 2008; *Mastin et al.*, 2009; *Cioni et al.*, 2015; *Clarke et al.*, 2015; *Taddeucci et al.*, 2015].

In *Iguchi.* [2016], a detailed overview of the mass of ash erupted by explosion at Sakurajima volcano between 2008 and 2013 is provided. From this study, we use the mass of ash from individual eruptions from December 2010 and the monthly mass of erupted ash from July 2013 (corresponding to our recording period). The minimum and maximum mass of ash from individual explosions from December 2010 is 0.5×10^6 kg and 2.7×10^7 kg, respectively. Dividing these values by the minimum and maximum ejection duration estimated from our videos (9.5 and 49.6s), we obtain an approximation of the range of time-averaged ash eruption rate of 1.0×10^4 to 2.8×10^6 kg/s. For July 2013, the monthly ash mass (1.07×10^9 kg) has been divided by the monthly number of explosions (80), obtaining an average mass of ash per explosion over this period. Then, we again estimated the range of time-averaged ash eruption rate using our minimum and maximum ejection durations and we obtained 2.7×10^5 and 1.4×10^6 kg/s. The time-averaged AER for Sakurajima volcano that we obtained integrating our time-resolved AER values range between 1.85×10^5 and 2.87×10^6 kg/s (Table 2.2), in good agreement with the December 2010 and July 2013 values obtained from *Iguchi.* [2016]. Our AER values are also in good agreement with MER estimates obtained via infrasound data at Sakurajima volcano during the same period [*Kim et al.,* 2015]. Using their volumetric flux and average plume density [*Ripepe et al.,* 2013], their estimated MER peaks at 6.1×10^6 kg/s. This results is logically higher than our estimation since it accounts for the total erupted mass.

Pioli et al. [2014] reported fallout masses of major events at Stromboli volcano ranging between 10^4 and 10^6 kg. These events, even though classified as "major explosions", displayed plumes rising only up to 200 m [Pioli et al., 2014], which corresponds to the plume height range observed in our records for Stromboli and Fuego volcanoes (Figure 2.8a). Our ash mass estimations per event range between 10^3 and 10^5 kg, which appears to be in good agreement with *Pioli et al.* [2014]. The authors of this study also provided estimations of mass discharge rates based on tephra mass load and neglecting the mass of gas and of unmapped bombs. Their results cluster around 10^4 kg/s, while our values range between 10^2 and 10^4 kg/s. Other studies, such as *Rosi et al.* [2013], showed that normal activity at Stromboli corresponds to fallout mass discharge rates of 10^2-10^3 kg/s. Our AER estimations for Stromboli and Fuego volcanoes seem to be in good agreement with previous studies on Strombolian activity. It is important to keep in mind that explosions from Stromboli volcano studied here, correspond to ash rich type 2 explosions. It is thus logic to obtain AER ranging in the uppermost MER values of normal Strombolian events, since a significant part of the total erupted mass is composed of ash.

Once again, values obtained at Sakurjima, Stromboli and Fuego are comparable with *Clarke et al.* [2015] and *Taddeucci et al.* [2015] for Vulcanian and Strombolian eruptions. When compared with other Ash Eruption Rate estimations at Sakurajima and Stromboli volcanoes [e.g. *Rosi et al.,* 2013; *Pioli et al.,* 2014; *Iguchi,* 2016], our AER values appear to be in good agreement with it, with the advantage of being time-resolved.

Considering the final height reached by the respective plumes, some of the values of AER we show are relatively high, exceeding, over few tenth of seconds, values for Subplinian and Plinian explosions [*Mastin et al.*, 2009]. This observation highlights the role of both ejection duration and MER fluctuations on the rise of transient volcanic plumes. For example, our Sakurajima values (duration about 30s, AER up to 10^6 kg/s with peaks up to 10^7 kg/s, and final plume height up to 4000 m), which agree with those of *Iguchi* [2016], contrast with those from the June 1992 eruption

of Mont Spurr, where a similar MER of $2x10^6$ kg/s, but sustained over much longer duration of more than 4h, resulted in an ash plume with a final height of 11.3 km [*Mastin et al.*, 2009].

It is also interesting to note that our AER estimations combined with MER values from literature can provide information about the respective ash to gas/bombs proportions during Strombolian and Vulcanian explosions. These kind of comparisons would provide useful information which could allow new understanding of transient plume dynamics, and will be the object of future work.

2.7 Conclusions

By the use of high-speed, thermal, and high resolution videos we parameterized the initial evolution of Strombolian- to Vulcanian-style eruptive plumes for their morphology, rise velocity, velocity field, volume, and apparent surface temperature.

It appears that the initial evolution of such plumes is fundamentally controlled by the time-space features of individual ejection pulses at the eruptive vent (i.e. their number, duration, frequency, intensity, angle, and source vent). The connection between ejection pulses and plume features seems to hold true for all our study cases, which encompass a variety of eruption styles and plume heights and morphologies. It remains open to question how much these observations can be extended to sustained eruptions, for which the occurrence of pulses is less documented, and how much our observations on the initial development of plumes may be expanded to later stages. However, these results stress the need for new experimental and numerical studies applying different and complex discharge histories in order to: i) predict the time evolution of transient plumes and associated hazards, and ii) retrieve eruptive parameters at the vent from plume measurements.

Future perspectives opened by this study also include: 1) quantification of other controlling factors on plume evolution (including the presence of bomb 'swarms'); 2) time-resolved ash

eruption rate measurements; 3) applicability of optical flow for plume parameterization; and 4) refined measurements of air entrainment.

Transient plume morphological observations and dynamical parameterization combined with ejection characterization at the vent allow a better understanding of the development and evolution of such flows. It is clear here that the fundamental dynamics and shape evolution of transient volcanic ash plumes is driven by their source behavior. The question raised by these findings is: can we quantify such shape evolutions ? To answer this question, fractal analysis of our plume's shape evolution has been performed and is presented in the following chapter.

3 Fractal analysis: A new tool in transient volcanic ash plume characterization

Pierre-Yves Tournigand[1], Juan José Peña Fernández[2], Jacopo Taddeucci[1], Diego Perugini[3], Jörn Sesterhenn[2], Danilo M. Palladino[4]

[1] Istituto Nazionale di Geofisica e Vulcanologia, Laboratory of Experimental Volcanology and Geophysics, via di Vigna Murata 605, Rome, Italy.

[2] Department of Fluid Mechanics and Technical Acoustics, Berlin University of Technology, Müller-Breslau-Str. 15, Berlin, Germany.

[3] Petro-Volcanology Research Group (PVRG), University of Perugia, Department of Physics and Geology, Piazza Università, Perugia, Italy.

[4] Dipartimento di Scienze della Terra, Sapienza Università di Roma, P.le Aldo Moro, 5 00185, Italy.

Key words

fractal analysis, transient plumes, Strombolian, Vulcanian, source properties

Key points

1) Fractal dimension analysis of high-speed and of high resolution videos of transient plumes is performed.

2) Fractal dimension is combined with other physical plume parameters (ash eruption rate and temperature).

3) An inter-connection is shown between the morphological evolution of the plume, its dynamics and the ejection properties at its source.

Abstract

Transient volcanic plumes are time-dependent features generated by unsteady eruptive sources. Their morphological evolution reflects both the discharge history at the vent and air entrainment, crucial parameters controlling volcanic ash dispersal and impact on the environment and human activities. However, transient plume's morphology has been so far scarcely quantified, due to both observational and analytical hindrances. In this study, we quantify the initial morphological evolution of transient volcanic plumes by applying fractal analysis to thermal high-speed and visible-light high-resolution videos of eruptions. Eruptive plumes from Sakurajima (Japan), Stromboli (Italy), and Fuego (Guatemala) volcanoes were recorded during several field campaigns in 2012 - 2016. The eruption dataset has been complemented by the fractal analysis of three numerical gas-jet simulations at different Reynolds number ($2x10^3$, $5x10^3$ and $10x10^3$) in order to provide reference cases to compare with the natural ones.

Results show different methods sensitivities, with the perimeter ratio method being more perceptive of punctual dynamical variations, while fractal analysis reflects the overall plume evolution. Both methods highlight the plume shape complexity increase over time related to the formation and development of smaller scale vortexes. Characteristic fractal increase rate (α_D) display a wide range of variability revealing different air entrainment abilities between plumes. Characterization of discharge history properties is performed via source instability factor (β) and ash eruption rate (AER) estimations. α_D and β happen to be anti-correlated, while high AER seem to decrease α_D values.

This study shows that discharge history and intensity at the vent are the first order control on plume's shape evolution and air entrainment ability.

3.1 Introduction

The morphological evolution of volcanic plumes is a decisive parameter to be monitored to understand their dynamics and the potential of ash dispersal in the environment.

In the past years, the dynamics of volcanic plumes have been studied mostly using physical models [e.g. *Wilson et al.*, 1978; *Mastin et al.*, 2009; *Cerminara et al.*, 2014; *Mastin*, 2014], mainly based on fluid dynamics theory developed in *Morton et al*, [1956], *Morton*, [1959] and *Turner*, [1962]. These models can describe accurately small thermal plumes generated by almost instantaneous sources (e.g. Strombolian explosions; e.g. [*Patrick et al*., 2007; *Patrick*, 2007]) and sustained eruptive columns generated by relatively steady-state sources (e.g. Subplinian and Plinian eruptions; e.g. [*Mastin*, 2014]). However, this theory fails in describing accurately transient volcanic plumes, which are characterized by unsteady source behavior and ejection durations comparable to the durations of plume's development.

The parameterization of transient volcanic plumes, typically from Strombolian and Vulcanian eruptions, has been attempted through different approaches, such as observational [*Patrick et al.*, 2007; *Patrick*, 2007; *Yamamoto et al.*, 2008; *Dürig et al.*, 2015; Section 2], experimental [*Kitamura and Sumita*, 2011; *Chojnicki et al.*, 2014, 2015a,b] and numerical ones [*Clarke et al.*, 2002]. These studies revealed how the morphology of plumes and its evolution over time can display a great variability, function of multiple parameters. In particular, the number, position and geometry of the erupting vents, and the discharge history at the vent in terms of number, location, angle and time of occurrence of successive pulses, are the prime control factors of the initial development of transient volcanic plumes [*Chojnicki et al.*, 2014; Section 2]. However, it is still unclear how these initial factors affect air entrainment and the later-stage development of plumes and ash transport and emplacement.

Air entrainment is linked to the development of vortexes at different scales, but turbulence measurement of dynamic transient plumes can be challenging. Concerning plume imaging, for

instance, vortex observations require both high spatial and temporal resolution and sophisticated image processing techniques like, for instance, Optical Flow or Particle Image Velocimetry [*Chojnicki et al.*, 2014; Section 2].

One viable alternative to characterize turbulence is the fractal analysis [*Mandelbrot*., 1982; *Lovejoy*., 1982; *Rys and Waldvogel*., 1986]. Following *Richardson,* [1922] and Kolmogorov, [1941, 1962] the local structure of a turbulence consist in a scale hierarchy of eddies, with eddies of a given order getting progressively destabilized and forming smaller ones to which energy is transmitted [*Sreenivasan and Meneveau,* 1986]. This hierarchy implies that turbulent flows are self-similar over a wide range of scales and are thus fractal objects. Fractal analysis has been applied in studies on experimental turbulent jets and buoyant plumes e.g. [*Sreenivasan and Meneveau,* 1986; *Prasad and Sreenivasan,* 1990; *Sreenivasan,* 1991; *Lane-Serff,* 1993; *Catrakis and Dimotakis,* 1998], as well as on atmospheric clouds e.g. [*Lovejoy,* 1982; *Lovejoy and Mandelbrot,* 1985; *Rys and Waldvogel,* 1986]. Fractal analysis, however, to the best of our knowledge has never been applied to transient volcanic plumes.

Fractal analysis is applied here for the first time to high-speed and on high-resolution videos of transient volcanic plumes. Our test case is a data set of Strombolian to Vulcanian ash-rich plumes whose morphology and source dynamics have been already parameterized [Section 2]. Our objectives are: 1) to test the suitability of fractal analysis to characterize efficiently the temporal evolution of transient volcanic plumes, and 2) to link suitable fractal parameters to the relevant volcanological factors, e.g., plume rise velocity, volume, temperature and discharge rate at the source.

3.2 Materials and Methods

We applied fractal analysis to thermal infrared, high-speed videos and visible light, high definition videos of initial transient volcanic plumes development from three different volcanoes: Sakurajima (Japan), Stromboli (Italy) and Fuego (Guatemala). Those three volcanoes have been selected for their diversity of eruptive styles, covering plumes generated by both Strombolian and Vulcanian activity. The videos, recorded during several field campaigns between 2012 and 2016, have been the object of a previous study where plume's dynamical evolution and discharge history at the vent were parametrized [Section 2]. In addition, videos from three numerical gas-jet simulations at different Reynolds number (Re) have been used in order to set reference values for the natural cases. Appendix 1 describes the methods we used to: 1) calculate Re of the plumes, 2) perform the numerical simulations, and 3) compare the plumes with the simulations.

3.2.1 Studied Volcanoes

Sakurajima volcano, located in Kagoshima Bay in south Japan, is a 1117 m above sea level (a.s.l) high andesitic stratovolcano in the southern rim of the Aira caldera, composed of three different cones, Kitadake, Nakadake and Minamidake [*Ishihara*, 1985; *Iguchi et al.*, 2013]. Current Vulcanian eruptions are driven by the accumulation of gas below a low-permeable or impermeable plug of degassed, crystalline magma until the failure of the plug initiates the eruption [*Iguchi et al.*, 2008]. During the recording period in July 2013, Sakurajima volcano produced about eighty Vulcanian explosions from the Showa crater, located at about 800 m a.s.l elevation on the eastern flank of Minamidake. Resulting ash plumes rose up to 4000 m elevation above the source [Japan Meteorological Agency, 2016]. Here we used four explosions from July 2013, recorded from two different observation points at 3.5 km distance from the vent (Table 1).

Stromboli volcano is located in the NE part of the Aeolian Islands of Italy. This 924 m a.s.l mafic stratovolcano is characterized by intermittent explosions at intervals from seconds to hours [*Taddeucci et al.*, 2013], occurring within a 300 m long crater terrace at ~800 m a.s.l [*Harris and*

Ripepe, 2007; *Patrick,* 2007]. This volcano serves as a reference for Strombolian activity due to its relatively high explosion frequency, its accessibility, and the vast literature investigating its activity. Stromboli's normal activity is subdivided in several types based on the ash-gas-bombs proportions of the ejecta [*Patrick et al.,* 2007; *Leduc et al.,* 2015; *Taddeucci et al.,* 2015]. Here we focus on ash rich explosions with and without the presence of bombs, corresponding to type 2 of *Patrick et al,* [2007]. Videos were taken from three different observation points around the crater terrace (286, 370 and 542 m away from the vent) during two field campaigns in May 2013 and May 2016. Plumes reached a height of about 400 m above the crater terrace before being pushed laterally and dispersed by local winds.

Fuego volcano is a basaltic-andesitic, 3800 m a.s.l high stratovolcano and the southernmost eruptive center of the Fuego-Acatenango massif in Guatemala. Its activity ranges from discrete Subplinian phases to persistent low Strombolian eruptions [*Yuan et al.,* 1984; *Marchetti et al.,* 2009; *Lyons et al.,* 2010; *Lyons and Waite,* 2011]. The style of activity of Fuego, from Strombolian to Vulcanian, potentially bridges the activity of Sakurajima and Stromboli volcanoes. The videos were recorded from a 968 m distance observation point in January 2012. During the measurement period, multiple explosions per day were generating up to 1000 m high ash plumes above the source [Global volcanism program, 2012]. However, due to the constraints in the local camera setting, here we focus on explosions that fall in the low range of intensity for the volcano.

3.2.2 Data acquisition setup

The cameras used to record transient plumes development are 1) a FLIR SC655 (640x480 pixels definition, 50 frame per second (fps), or 640x240 pixels definition, 100 fps), recording in the thermal infrared wavelength range; and 2) two high definition Sony Handycam FDR-AX100 (3840x2160 pixels, 25 fps) in the visible light spectral range.

Atmospheric correction of the thermal video takes into account the distance between the plume and the camera using the ThermaCam software. However, no further corrections have been

performed for other effects, such as sunlight intensity, angle of view, source emissivity and radiations absorption from gas and aerosols [*Sawyer and Burton,* 2006]. For the purpose of this study the absolute temperature of the plume is not relevant and thus it is not documented here.

From the 43 videos covering 29 explosions present in the original dataset of Section 2, fractal analysis has been performed on 24 selected videos (17 thermal and 7 high definition) covering 17 explosions. One new explosion from Fuego volcano (Fu_7) has been added to this dataset (Table 3.1). Each explosion was selected following several criteria including a clear visibility of the plume and the presence of both gas-thrust and buoyancy phases within the camera's field of view.

Table 3.1: List of recording parameters for the explosions presented in this study. [a]

Date and hour	Explosion #	Camera	fps	FOV (m)	v_{max} (m/s)	v_b (m/s)	ED (s)
17/07/2013 22:29:00	Sa_5	FLIR	50	928x696	89.4	12.8	48.7
16/07/2013 06:56:22	Sa_7	FLIR	50	928x696	52.0	12.5	36.1
16/07/2013 08:31:51	Sa_8	FLIR	50	928x696	117.5	14.3	12.3
19/07/2013	Sa_10	FLIR	50	928x696	227.0	n.a.	45.3
26/05/2013 14:08:26	St_4	FLIR	50	307x230	68.7	14.4	3.0
26/05/2013 15:07:35	St_5	FLIR	50	307x230	52.3	10.0	1.5
26/05/2013 15:20:12	St_6	FLIR	50	307x230	62.9	15.0	2.0
26/05/2013 15:10:54	St_8	FLIR	50	307x230	33.2	9.4	4.2
22/05/2016 15:24:12	St_9	FLIR	50	307x230	25.3	6.7	23.5
25/05/2016 13:44:00	St_10	FLIR Sony	50 25	450x338 370x657	24.8 22.0	8.4 8.2	5.6
25/05/2016 14:42:18	St_11	FLIR Sony Sony	50 25 25	450x338 370x657 370x657	29.7 13.8 15.7	7.4 7.0 8.5	13.0
26/05/2016 14:09:07	St_12	FLIR Sony Sony	50 25 25	450x338 370x657 370x657	22.9 27.4 29.2	7.3 9.4 7.2	17.0
26/05/2016 14:32:56	St_13	FLIR Sony Sony	50 25 25	450x338 370x657 370x657	58.4 45.0 55.0	7.3 7.3 8.0	25.2
14/01/2012 16:11:05	Fu_1	FLIR	100	428x161	31.1	7.9	5.1
14/01/2012 18:36:14	Fu_2	FLIR	100	161x428	21.4	7.3	11.4
13/01/2012 17:05:20	Fu_4	FLIR	100	96x255	48.0	14.2	4.7
14/01/2012	Fu_5	FLIR	100	161x428	22.4	10.1	3.3
13/01/2012 14:45:00	Fu_7	FLIR	100	96x255	34.4	11.5	13.0

[a] Key. Fps= frame per second. FOV= horizontal and vertical field of view. v_{max}= maximum plume front velocity. v_b= average buoyant rise velocity. ED= estimated ejection duration.

3.2.3 Fractal analysis

The mathematical concept of fractals is not recent [*Hausdorff* 1919, *Besicovitch* 1929], but its application as a tool to quantify complex shapes is [*Mandelbrot,* 1982]. One of the main issues when it comes to fractals is to bring a clear definition of it. An intuitive and applicable definition in our case is that a fractal is an object displaying a self-similarity over a wide range of scales [*Sreenivasan*, 1991; *Sreenivasan and Meneveau*, 1986].

To represent this notion we refer here to the same self-similarity example as in *Sreenivasan*, [1991], the Koch curve (Figure 3.1). In order to build the Koch curve an initial object, called the initiator (Figure 3.1, n=0), is needed. From the initiator, in this case a segment, a new shape is made out of lines. This new shape is called the generator (Figure 3.1, n=1). Each successive steps (from n=2 to n=+∞) is then built by replacing the segments of the previous stage by a scaled version of the generator. The resulting shape displays then a self-similarity, being made out of smaller versions of itself.

As mentioned in *Sreenivasan*, [1991], when studying a given object we often do not have the iterative process of construction but only the final resulting shape, as in our study. In this case, another parameter than the building process is necessary in order to characterize our object. Fractal objects can then be described by their fractal dimension. The fractal dimension correspond to the space-filling ability of the studied object, one would say its convolutedness [*Sreenivasan*, 1991], or its complexity, and is the parameter that will be used to characterize transient plumes here.

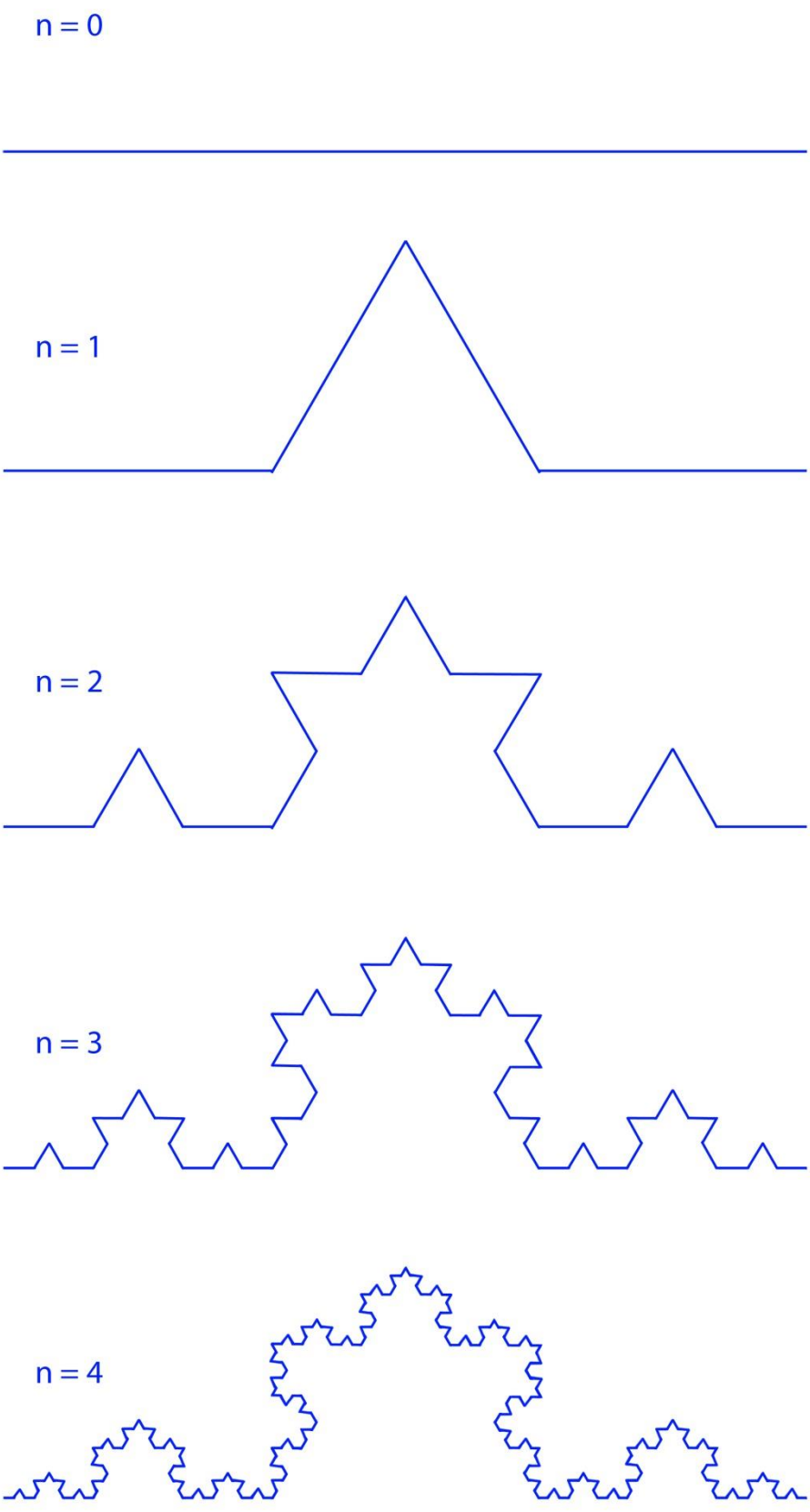

Figure 3.1: First iterations in the building process of the Koch curve.

Several methods of fractal analysis exist, but each of them relies on our ability to accurately determine the boundary of the transient volcanic plumes in the video frames.

3.2.3.1 Boundary detection

On thermal infrared images, the pixel intensity of the plume is significantly higher than that of the background atmosphere. These videos were processed by the extraction of the temperature gradient combined with a temperature threshold (Figure 3.2b), following the methodology of *Prasad and Sreenivasan*, [1989]. Visible light videos were not processed. On both thermal and visible videos we attempted different approaches to boundary detection, both automatic and manual. To detect automatically plume's boundary Plume Tracker, Particle Image Velocimetry and Optical Flow routines have been tested [*Sun et al*., 2010; *Valade et al*., 2014]. Manual boundary detection of plumes was performed, using a custom Matlab routine. The plume's contour was outlined every one second as a reasonable trade between temporal resolution and processing time. For each analyzed frame, we manually tracked the plume boundary, zooming into the image to carefully detail plume features down to the single pixel scale. Despite the longer processing time and the lower number of frames processed, we found that, for the videos of volcanic plumes, the results of manual boundary detection were systematically more accurate than those from automatic detection. Results comparison between the different automatic procedures and manual one showed higher scattering of data for automatic approaches due to an inaccuracy in isolating the plume from the background. For the synthetic videos of the numerical simulations, however, it appeared that manual and automatic boundary detection were providing identical results. For this reason, manual and automatic boundary detection methods have been applied to volcanic plume and numerical simulation videos, respectively.

3.2.3.2 Perimeter ratio method

The first shape complexity measurement we performed is the ratio between the length of the plume boundary (PP) and the length of the minimum box bounding the boundary (PB) (Figure

3.2c). The PP/PB ratio increases as the degree of convolution of the plume boundary increases, and the measurement is performed for each one-second-apart video frame. The advantage of this method is that the result is dependent on the shape complexity and independent of plume size. This is particularly important in our case because it allows one to discern the morphological effects due to changing plume turbulence over time from those due to plume rise and expansion.

3.2.3.3 Fractal analysis

A more complex measurement of plume complexity is the fractal analysis. We measured the fractal dimension of the plume boundary, or outline, using the box-counting (or Minkowski-Bouligand) method, particularly adapted to low-dimensional systems such as the analysis of 2D images [*Liebovitch and Toth*, 1989; *Sreenivasan*, 1991] (Figure 3.2). This method consists in covering the image with successive square meshes, or boxes, of decreasing box size, and each time counting the number of boxes that are required to cover the plume outline. Square box side here ranges in size from a minimum size of two pixels (corresponding to 2.9 m for Sakurajima, from 1.41 to 0.82 m for Stromboli depending on filming location and used lens, and 1.34 m for Fuego), to a maximum corresponding to the number of pixels in the longest side of the image. Each increment corresponds to the previous square size multiplied by two. *Mandelbrot* [1982] showed that a fractal object satisfies the relation:

$$N = r^{-D} \tag{3.1}$$

with N the number of boxes required to cover the object boundary, r the side length of the boxes and D the fractal dimension of the object. The negative slope of the number of boxes in function of their size in a log-log plot provides the fractal dimension of the object and is a measure of its complexity. In our case, D can be viewed as a measure of plume complexity at a given time (Figure 3.2e). Combining the fractal dimensions obtained at each time step for a given explosion provides an access to the time-evolution of shape complexity of the plume over the whole recorded period.

Fractal measurements in this study are performed on 2D projection of 3D objects, which can be compared to the extraction of a thin plane at the plume's centerline and parallel to it. Several studies tried to address the issue of linking the 2D fractal dimension obtained to the original object e.g. [Sreenivasan and Meneveau, 1986; Sreenivasan, 1991]. These studies concluded that if a 3D object is intersected by a thin plane (or line), then the dimension of the intersecting surface (or line) will be the one of the original object minus one (or two). This conclusion holds true if the intersecting plane (or line) is as thin as the finest scale of observation and the result is independent of the plane (or line) orientation.

In order to identify any dependency of the fractal analysis results from pixel resolution and the angle of view and frame rate of the camera, fractal measurements have been performed on three videos of the same explosion of Stromboli volcano (St_13) recorded with different cameras and from different positions. Two videos shared the same point of view but differed in type of camera (FLIR and Sony), resolution and frame rate, while the third one was recorded with a Sony camera but from a different observation point, located at about 90° from the other two videos (see below for results).

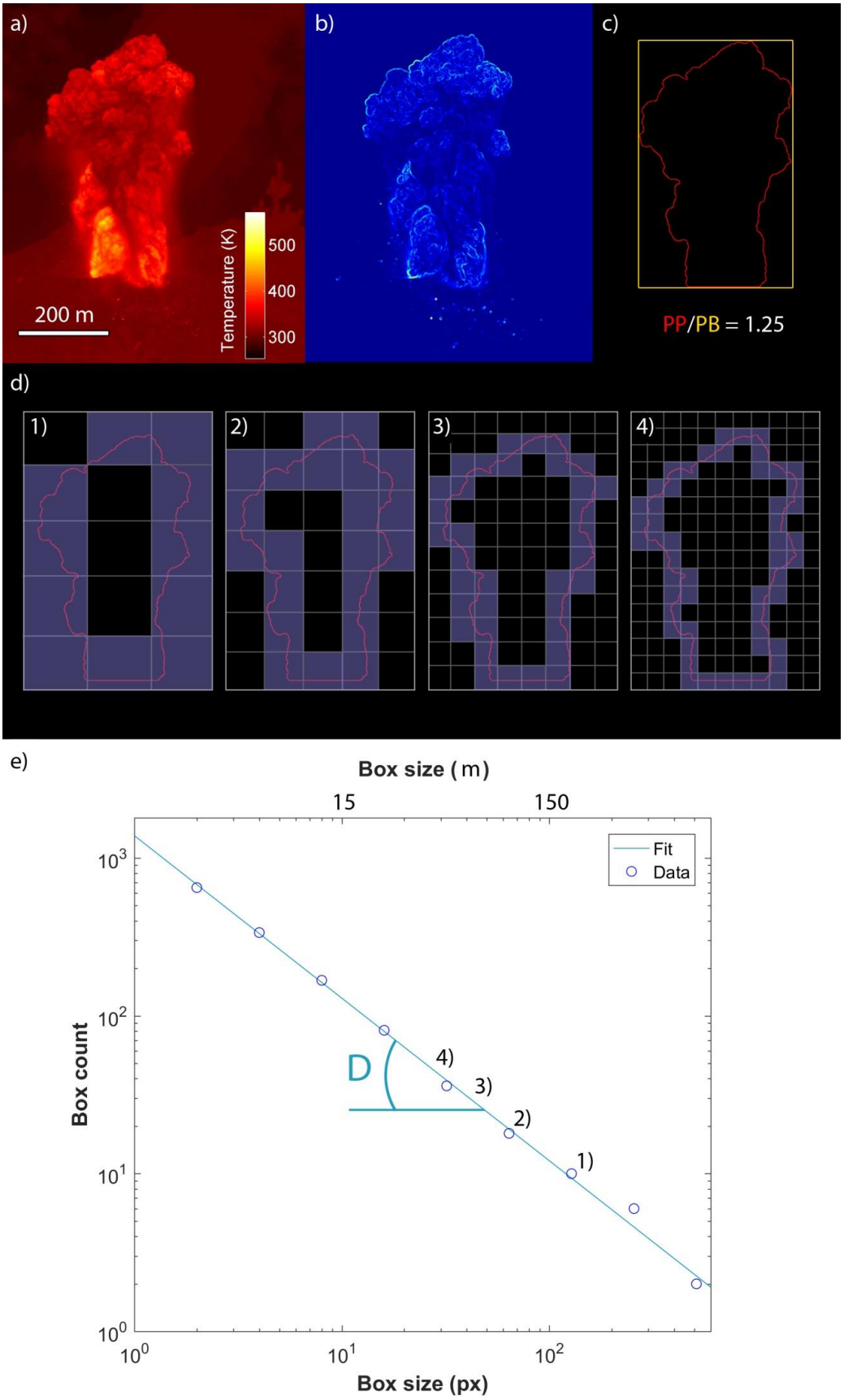

Figure 3.2: Image analysis methods: a) A thermal infrared video frame from a Sakurajima's explosion. b) Same image as a) after processing via temperature gradient extraction combined with a temperature threshold. c) Perimeter ratio measurement. The Result of the manual plume contouring

(in red) and the bounding box (in yellow). PP is the perimeter of the plume outline, PB is the perimeter of the bounding box. d) The box-counting method. The number of boxes required to cover the plume outline (in magenta) increases with decreasing box size (numbers from 1 to 4). e) Results of the box-counting method applied on the frame shown in (a). The points numbered from 1 to 4 correspond to the box size and the number of boxes of the corresponding image in (d). D, the slope of the power-law best fitting all the points, is the fractal dimension of the plume at the specific time of the given frame.

3.3 Results

3.3.1 The fractal dimension of transient volcanic plumes

The initial development of the transient volcanic plumes we analyze display a variety of morphologies over time (Figure 3.3). These encompass shapes that range from tall, narrow plumes capped by a well-defined ring vortex, similar to sustained eruption columns (Sa_7), to smaller, isolated ring vortexes similar to thermal clouds (St_10), but also remarkably convoluted shapes, resulting from the merging of several jets and vortex structures (Sa_8) and occasionally displaying unusual low height over width aspect ratios (Sa_5) (see also Section 2.5.1). Despite this variety, all analyzed plume boundaries consistently satisfy the fractal dimension requirements (Eq. 3.1) and can be characterized by a fractal dimension D. In all measured images, D ranges between 0.85 and 1.16. D increases systematically over time in all cases, and plumes that visually appear to be more complex (e.g., Sa_5 and Sa_8) display slightly higher values of D.

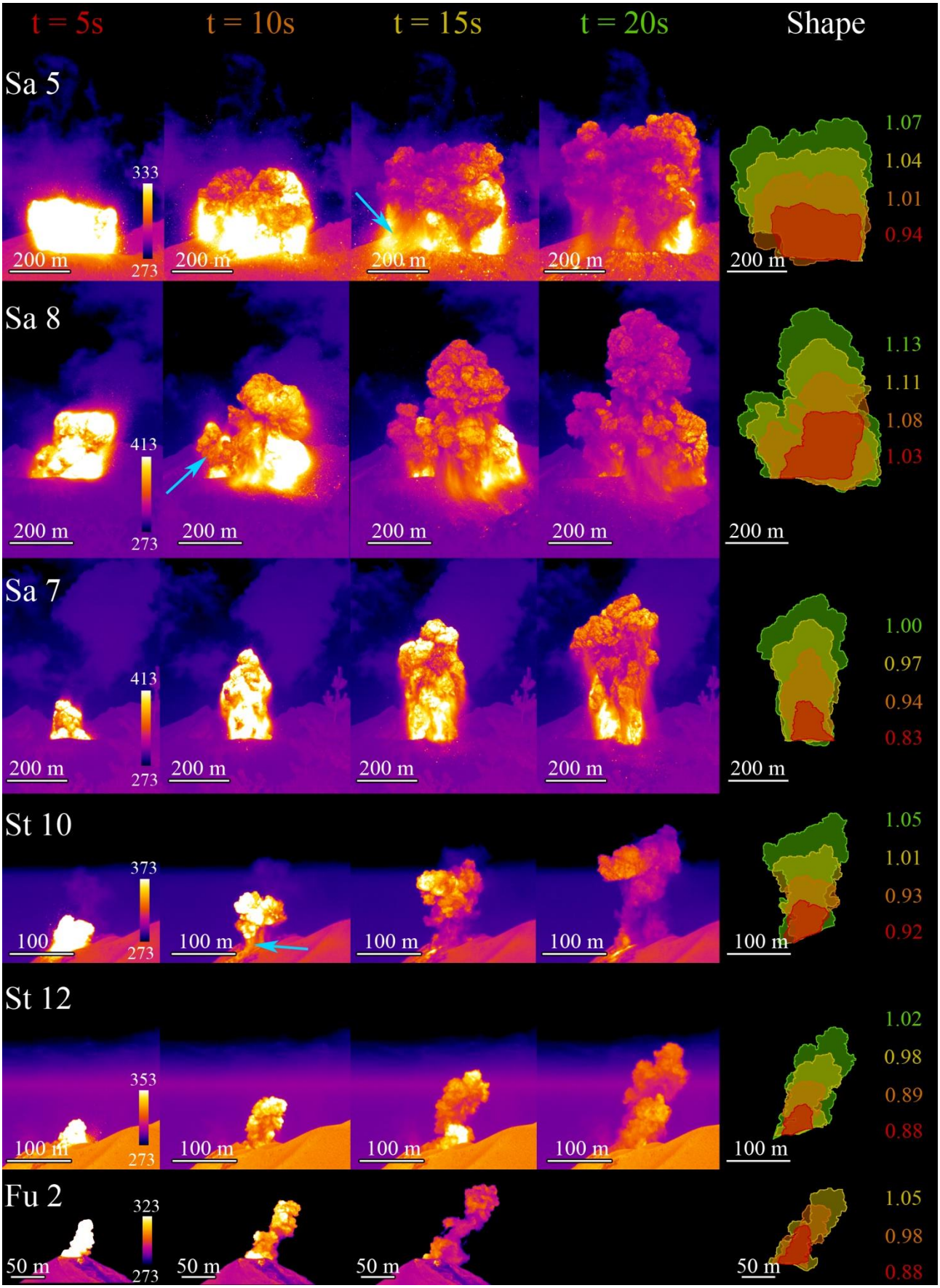

Figure 3.3: Transient plume morphology evolution over time. Still frames from thermal videos of 6 explosions from Sakurajima (Sa), Stromboli (St) and Fuego (Fu) volcanoes. For each explosion, frames

at 5, 10, 15 and 20 s after explosion onset are shown (Fu_2 frame at 20 s is not displayed since part of the plume is already outside of the field of view). The last panel on the right displays the plume outline at the four frames (red, 5s, orange, 10s, yellow, 15s, and green, 20s) and the corresponding value of the fractal dimension D. Note the consistent increase of D over time and the slightly higher value of D for more convoluted plumes (e.g., Sa_8).

3.3.2 Fractal evolution of plume morphology

The ratio of the plume perimeter over the bounding box (PP/PB) ranges 0.9-1.3, and, similarly to D, increases systematically over time (Figure 3.4). The trend describing the increase of PP/PB during plume growth ranges from an almost linear one (e.g., Sa_7 and Fu_1) to a downward-bended one with or without one sharp kink (e.g., Sa_8, Sa_5, St_10, and St_11). Interestingly, the occurrence of such bending and kinks is often related to some specific event occurring in the videos, like, e.g., the ejection of a new jet from the vent or the onset of ash fallout from the plume. As an example, the Sa_8 explosion displays a 4s deviation from the general trend about 8s after the explosion onset. This deviation coincides with the ejection of a second jet from a vent located on the left side of the previously developed plume (Figure 3.3 and Figure 3.4 Sa_8, arrow). The St_10 explosion also shows a significant deviation, which occurs at the end of an ash-fallout phase from the base of the ring vortex (Figure 3.4 St_10, arrow).

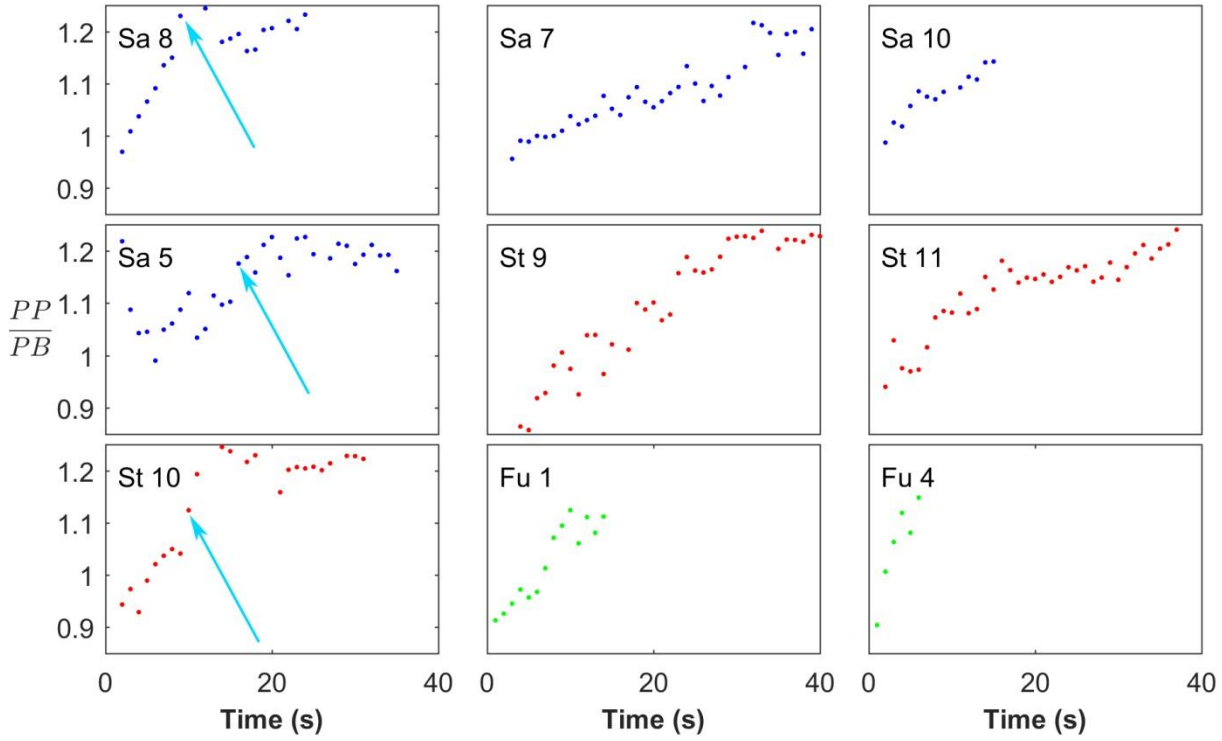

Figure 3.4: Time evolution of the plume perimeter over bounding box perimeter (PP/PB) ratio for nine explosions (thermal video frames, each point corresponding to one frame). Sakurajima, Stromboli and Fuego are respectively represented in blue, red and green. Blue arrows correspond to the specific features identified in figure 3.3 and described in the text.

In contrast to the variable increase of PP/PB over time, the increase of D over time is well approximated by a power-law trend for all studied explosions (Figure 3.6, Table 3.2). In particular, the power coefficient from this power-law trend, hereafter referred as $\alpha_{D,}$ seems to be an effective descriptor of plume evolution. For instance, the analysis of three videos of the same explosion, captured by different cameras and viewpoints, provided very similar values of α_D (0.085, 0.093 and 0.083), despite different individual values of D at the same time (Figure 3.5). These values cover a small range when compared with the measured α_D values from all explosions, ranging from 0.074 to 0.200 (Figure 3.6a, Table 3.2). When plotted together, the power-law fits to the D values of all examined explosions reveal no obvious difference in terms of D or α_D values, despite the different explosion style and intensity (Figure 3.6, Table 3.2). Given this apparent universality, we propose α_D as a suitable parameter to characterize the rate at which plume morphology becomes increasingly convoluted over time.

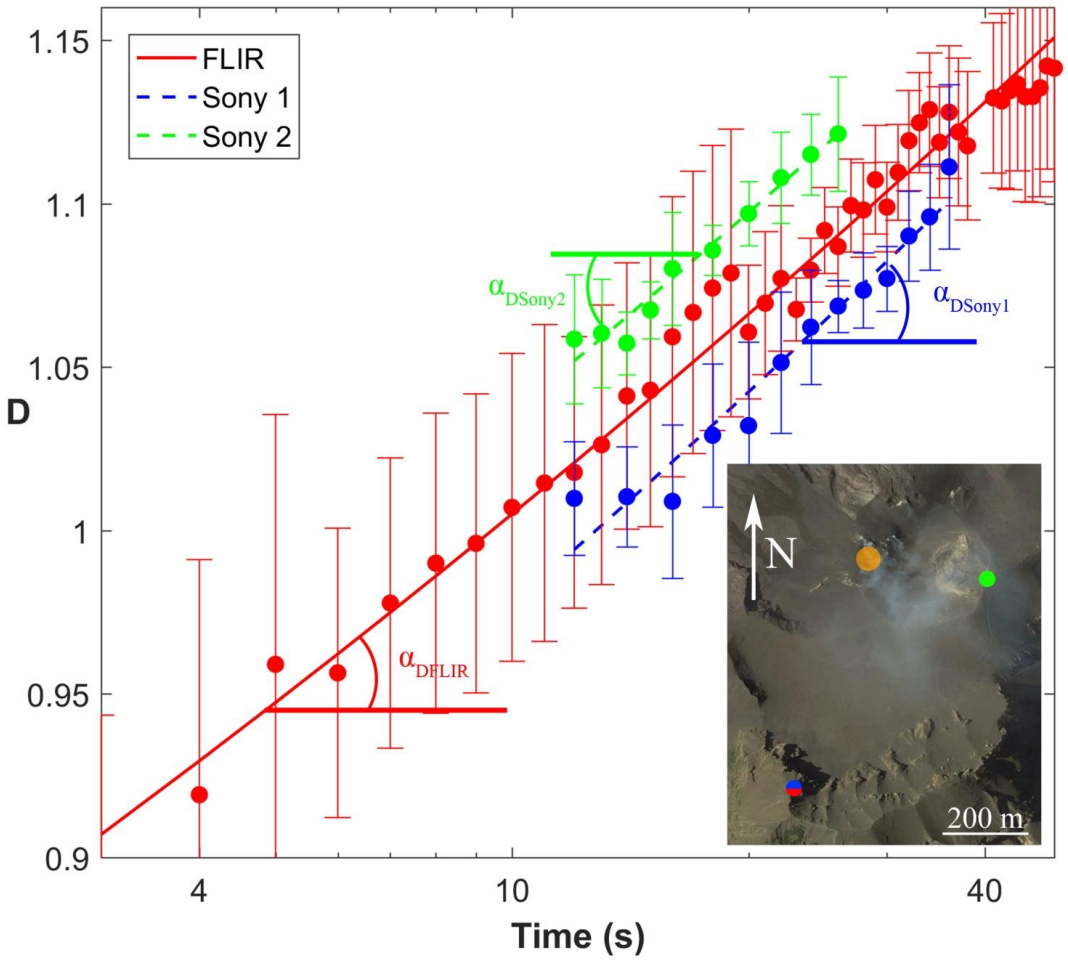

Figure 3.5: Fractal dimension D evolution over time: the case of the transient plume St_13 at Stromboli volcano. Red, blue and green points are D values obtained from the FLIR and the Sony 1 and Sony 2 videos, respectively, filmed from different positions (shown in the inset, orange dot corresponds to the vent location, see also Table 3.1 for video shooting settings). Despite the different D values at a given time, the power coefficient α_D of the power-law best fit to the points (solid and dashed lines) for the three cases is almost identical (α_DFLIR = 0.085, α_DSony1 = 0.093, and α_DSony2 = 0.083).

The increase in plume convolution could be related to more turbulent conditions in the plume. To test this hypothesis we attempt to relate α_D to Reynolds number (Re). Our data only allowed for an averaged, first-order estimation of Re for the studied transient volcanic plumes, calculated on the base of an interval of temperature and gas-composition. The obtained Re values range between 8.7×10^7 and 7×10^6 (Appendix 1). Since we were not able to compare the α_D and Re for our individual explosions, we attempted such a comparison using synthetic videos from numerical simulations of gas-jets. The simulated jets cover a limited range of Re, i.e., 2×10^3, 5×10^3 and 10×10^3, with values always much smaller than the explosions. In order to compare the explosions to the simulations, it was first necessary to non-dimensionalize the time using the

method described in Appendix 1. The results of this comparison show that: 1) simulations with higher Re have higher α_D, with Reynolds numbers of $2x10^3$, $5x10^3$ and $10x10^3$ corresponding to α_D of 0.09, 0.10 and 0.11, respectively; and 2) despite up to four orders of magnitude difference in Re, the explosions and the simulations overlap in terms of D and α_D (Figure 3.6b).

Table 3.2: Power law coefficient of plume fractal evolution over time. [b]

Explosion #	Power law coefficient						AER Average (kg/s)
	α_D	R^2	$\alpha_{D/PB}$	R^2	$\alpha_{D/PP}$	R^2	
Sa_5	0.081	0.94	0.484	0.99	0.535	0.99	1.85E+05
Sa_7	0.126	0.94	0.592	0.99	0.679	1.00	6.63E+05
Sa_8	0.074	0.96	0.427	1.00	0.517	0.99	2.87E+06
Sa_10	0.116	0.99	0.707	0.99	0.773	1.00	-
St_4	0.108	0.97	0.429	0.93	0.568	0.96	2.47E+04
St_5	0.112	0.97	0.485	0.99	0.614	0.97	4.96E+03
St_6	0.112	0.91	0.585	0.98	0.733	0.99	7.76E+03
St_8	0.145	0.89	0.488	0.95	0.579	0.94	-
St_9	0.134	0.96	0.751	0.99	0.931	0.99	2.48E+03
St_10	0.102	0.93	0.591	0.98	0.713	0.99	5.25E+04
St_11	0.108	0.95	0.599	0.99	0.699	0.99	2.03E+03
St_12	0.133	0.95	0.658	0.99	0.789	0.99	1.48E+04
St_13	0.086	0.98	0.5	0.99	0.632	0.99	7.42E+03
Fu_1	0.112	0.99	0.452	1.00	0.539	1.00	4.86E+03
Fu_2	0.200	0.97	0.601	1.00	0.722	1.00	5.36E+02
Fu_4	0.138	0.99	0.665	0.99	0.791	0.99	7.55E+03
Fu_5	0.132	0.98	0.508	0.99	0.602	1.00	3.27E+03
Fu_7	0.1669	0.97	0.673	0.99	0.775	0.99	3.17E+02

[b] Explosion#: Sa=Sakurajima, St=Stromboli and Fu=Fuego volcanoes. α_D=Power law coefficient of the plume's fractal dimension evolution. $\alpha_{D/PB}$=Power law coefficient of the evolution of the ratio between the fractal value of the plume and the perimeter of its bounding box. $\alpha_{D/PP}$=Power law coefficient of the evolution of the ratio between the fractal value of the plume and the perimeter of the plume. AER is the average Ash Eruption Rate [Section 2].

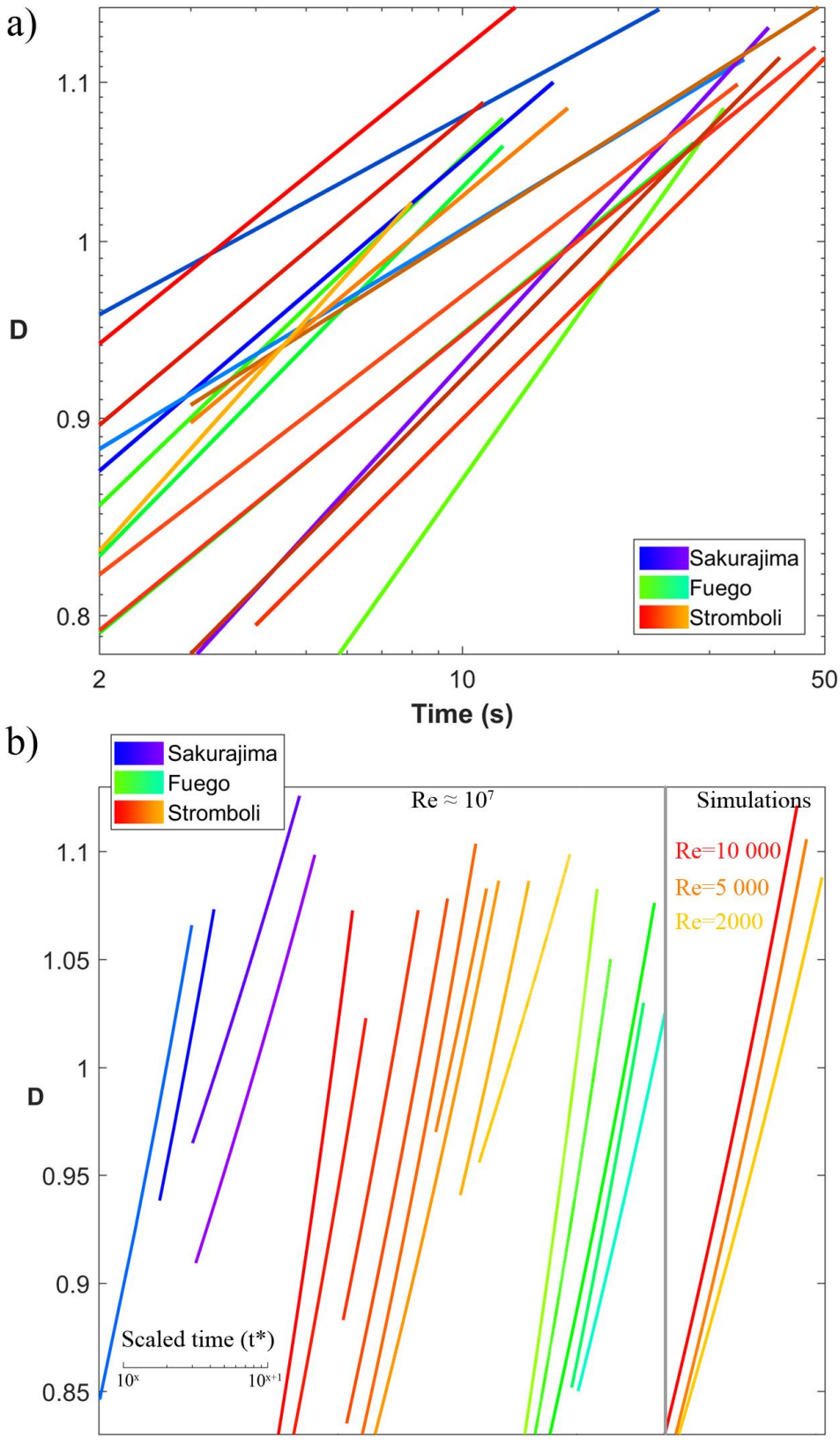

Figure 3.6: Fractal dimension (D) evolution in function of time (a) and of scaled time with numerical simulations (b). The different lines have been arbitrarily offset in b) for clarity and the x-axis is represented by the scale on the bottom left part of the graphic. Power-law fitted data are shown for better visualization (fit parameters are in Table 3.2).

3.3.3 Plume fractal evolution and explosion source parameters

Having explored the relationships between α_D and Re, we now explore how source parameters at the eruptive vents affect α_D and plume convolution. The evolution of vent activity during one explosion can be efficiently represented plotting over time the apparent surface temperature evolution (from FLIR videos) at the base of the plume [Section 2]. Such plots highlight the duration, discontinuities, and lateral shifts in gas-pyroclast ejection from one or multiple vents in the course of a single explosion (Figure 3.7). For instance, the relatively simple St_10 explosion (Figure 3.3), shows one single, laterally well-focused ejection phase lasting less than 6 s. In comparison, the more prolonged Sa_7 explosion is characterized by a succession of pulses very close in time but ejected with a limited lateral spreading. More complex plumes such as the Sa_5 and Sa_8, display more spatially spread sources (in one case up to 300 m) with great intensity variations over time. Weaker St_12 and Fu_2 plumes are both characterized by short and focused ejection phases (Figure 3.7). Another key source parameter of volcanic explosions is the rate of pyroclasts ejection at the vent. For the investigated explosions, this parameter is approximated by the instantaneous Ash Eruption Rate (AER), representative of the ejection rate of ash at any time [Section 2], and its time-averaged value (Table 3.2).

In order to quantify the variability of the explosion source parameters, a source instability factor (β) has been implemented. This factor combines the lateral spreading of the source, function of vent migration and changes in ejection angle, and the variability of the eruption rate, function of pressure fluctuations at the vent and linked to the pulsating nature of the ejection. Dimensionless source spreading is obtained dividing the base width of the plume by the plume height, as measured 10s after the explosion onset. This 10s choice is balancing between plumes development and camera's field of view, but tests with different choices did not result in significant changes in β. Dimensionless variability in the eruption rate is obtained dividing the difference between the maximum and minimum AER of an explosion by the average AER. The product of the two

dimensionless numbers is the instability factor (β), which is then scaled from 0 to 1 by dividing for the highest β value present in our dataset. Visually, it appears that the factor β and the increase rate α_D are related to the variability of the eruptive source (Figure 3.7). For instance, relatively steady sources, such as the Sa_7, St_10, St_12 and Fu_2 cases (Figure 3.3), display the highest α_D, the lowest β, the lowest fractal dimension values (D). Conversely, more unsteady sources, such as the Sa_5 and Sa_8 cases, display lower α_D, the highest β, and the highest fractal dimension values (D) (Figure 3.7).

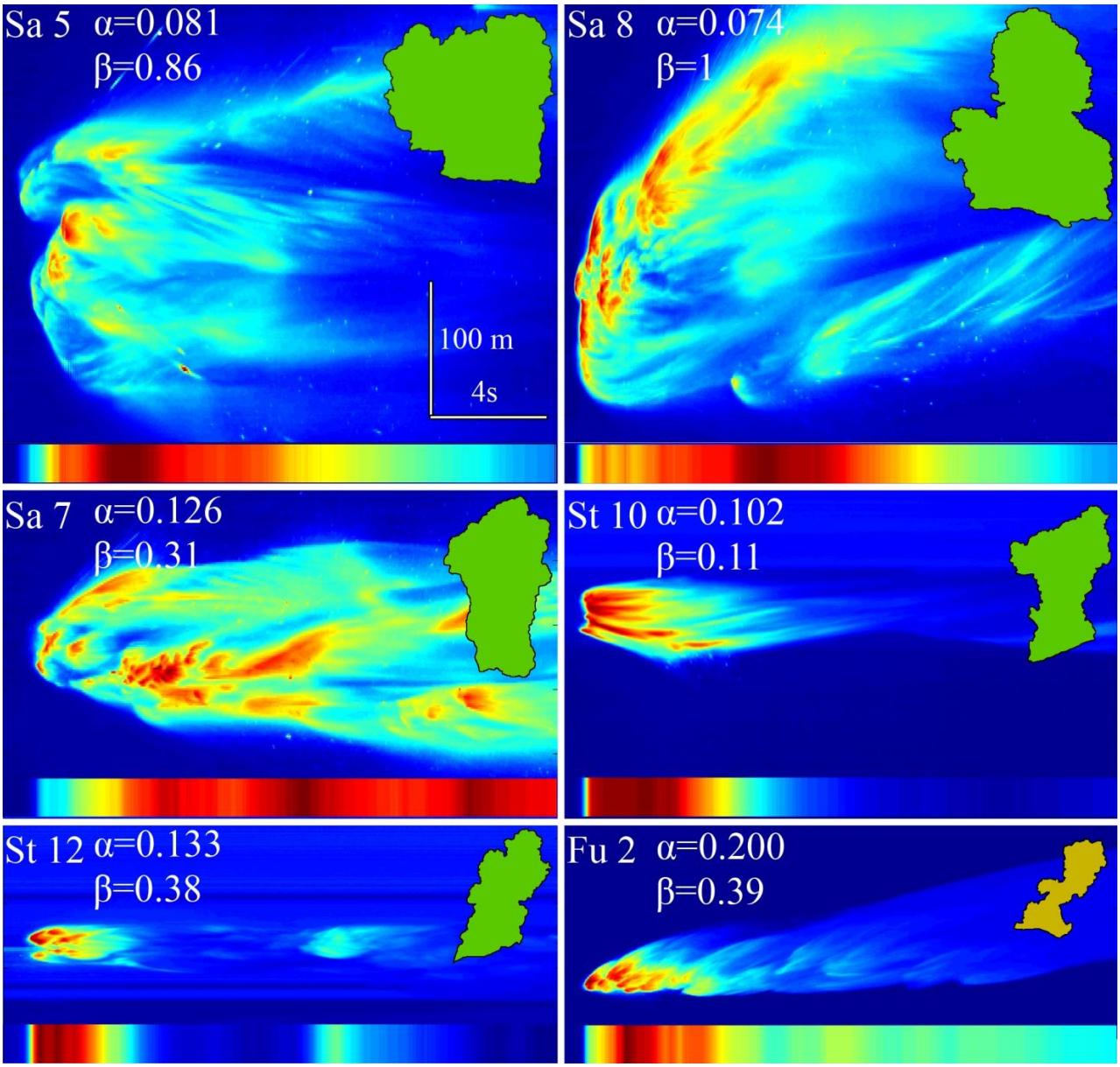

Figure 3.7: The evolution of the apparent surface temperature along a horizontal line crossing the base of the plume during the first 20 seconds after the explosion onset. On the vertical axis is the horizontal

position along the line, on the horizontal axis is time, and the color scale is apparent temperature. The colored band at the bottom is the temperature integration along the whole horizontal line over time and provides a proxy of the discharge history at the vent. Space and time scales are the same for all explosions, while the apparent surface temperature scale is normalized to the maximum temperature of each explosion. On the upper right corner of each plot is the plume outline 20s after the explosion's onset (in green), except for the Fu_2 case (15s in yellow). In white, the values of the plume fractal increase rate α_D and of the vent instability factor β (see text for parameter description) for each of the explosions.

Despite the limited number of explosions within our dataset (the only ones for which AER could be estimated) it appears that plumes generated by explosions with higher average AERs display lower values of α_D, following an approximated power-law trend (Figure 3.8a). Explosions at Sakurajima volcano display the highest AER (10^5-10^6 kg/s) and some of the lowest α_D (<0.081) values, while those at Stromboli and Fuego volcanoes mostly cluster together both in AER (10^3-10^5 kg/s) and α_D (0.1-0.14) values, while Fuego volcano also displays the two smallest AER $5.36x10^2$ and $3.17x10^2$ kg/s, and the two highest α_D at about 0.2 and 0.17, respectively for explosions Fu_2 and Fu_7.

Concerning the source instability coefficient β, explosions from all three volcanoes largely overlap, each volcano covering at least 60% of the total β range. The lowest β values belong to the previously identified cluster of explosions from Stromboli and Fuego volcanoes, while the highest β values are associated with the lowest α_D ones (Figure 3.8a, b). Interestingly, α_D increases with β exponentially until some optimum value is reached (Figure 3.8b). Further β increases show a drop of the α_D value. Intermediate AER values do not seem to have a first order impact on the α_D evolution, but only extremes values.

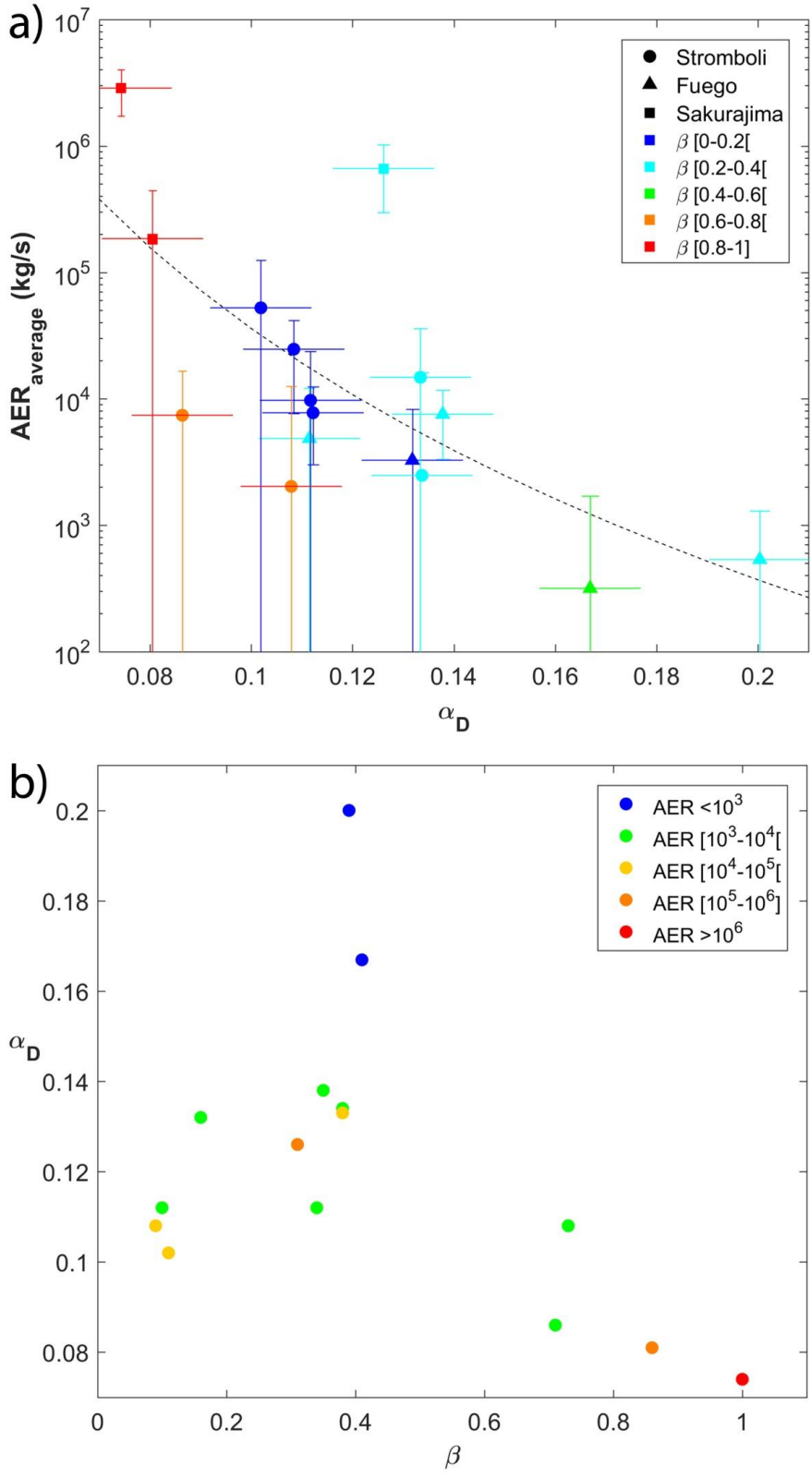

Figure 3.8 a) Average Ash Eruption Rate (AER) in function of the fractal increase rate power law coefficient (α_D). Color groups are referring to the source instability factor (β). Dashed line correspond to the power-law fit of the data ($AER=0.009\alpha_D^{-6.602}$, $R^2=0.48$). b) α_D evolution in function of β, the color groups referring this time to the AER (kg/s).

3.4 Discussion

3.4.1 Application of fractal analysis to volcanic plumes

Fractal analysis allows an efficient shape characterization and has already been used in numerous studies of experimental and natural fully developed flows e.g. [*Lovejoy,* 1982; *Lovejoy and Mandelbrot,* 1985; *Rys and Waldvogel,* 1986; *Sreenivasan and Meneveau,* 1986; *Prasad and Sreenivasan,* 1990; *Sreenivasan,* 1991; *Lane-Serff,* 1993; *Catrakis and Dimotakis,* 1998], but it has never been applied to study transient volcanic plumes. Our results show that the morphology of such plumes fully satisfies the requisites of a fractal object, as expected for multi-scale eddies in turbulent flows. In addition, we found that the fractal dimension D of the plume boundary always increases in time following a power-law trend.

Concerning the absolute values of D that we found, some plume outlines at the very beginning of the explosions have D values lower than one, while the D value of a convoluted fractal curve should fall in between 1 and 2. This discrepancy results from the chosen contouring method. The pixels of our contour lines are often connected by a corner instead of a side, decreasing the overall line length and continuity and thus leading to an underestimate of D. Also the pixel size in the video affects the D values that we found. Of the three videos that we analyzed of plume (St_13), the one providing the highest D values is the Sony 2 one, which also has the highest resolution (Figure 3.5). Although the different D in the three videos could also mirror differences in the angle of view, an increase of D with increasing pixel resolution is already known [*Lovejoy*, 1982].

Despite the discrepancies in their values at any time, D increases along a power-law trend in all the three cases of plume (St_13), and with remarkably similar power coefficient α_D (0.085, 0.093 and 0.083), in good agreement with previous experimental studies [*Sreenivasan et al.*,1989]. Based on the above findings and reasoning, in the rest of this discussion we will not focus on the D value but rather on the α_D one, which appears to be more suited for the fractal characterization on the evolution of transient plume morphology over time. We suggest that the difference in the three

measurements of α_D of plume (St_13), which is about 0.01, could be used as a rough estimate of the error in our measurement of that parameter.

In parallel to D, also the perimeter of the plume to the bounding box perimeter ratio (PP/PB) increases over time (Figure 3.4). PP/PB is a measure of plume convolution which is independent of plume size, thus demonstrating that the observed increase in D over time (expressed by the parameter α_D) is not exclusively a size effect.

With respect to $\alpha_{D,}$ the size independent PP/PB parameter appears to be more affected by sudden variations in plume morphology linked to, e.g. ejection pulses. The fact that PP/PB systematically increases at a lower rate after such variation suggest that, at the early stages of plume development, vent processes have the potential to rejuvenate the morphological evolution of transient plumes. To conclude this comparison of α_D versus PP/PB, we remark that the former is a more precise and accurate metric of plume evolution over time, while the latter may provide a quicker overview of plume-modifier events.

The fractal absolute values will not be interpreted here due to some underestimations related to the method. However, it is still interesting to note that our trend evolutions are power laws that seem to converge towards a specific value. Comparing with studies on natural atmospheric clouds e.g. [*Lovejoy*, 1982; *Lovejoy and Mandelbrot*, 1985; *Rys and Waldvogel*, 1986; *Prasad and Sreenivasan*, 1990] but also on experimentally generated turbulent flows e.g. [*Prasad and Sreenivasan*, 1990; *Sreenivasan*, 1991], the fractal dimension (D) of such structures, when fully developed, reaches about 1.36. We can thus make the assumption that fully turbulent flows reach a stable D value which corresponds to a maximum shape complexity. Considering this, transient volcanic plumes studied here are not fully developed while they are still within the camera's field of view and might reach such D value later in their evolution.

3.4.2 Implications for transient plume characterization

The systematic increase of fractal dimension over time (Figure 3.6) indicates an increase of plume convolution, which we associate, partially, to the formation and development of smaller scale vortexes that accompanies an increase in turbulence. In fact a higher turbulence and mixing (higher Reynolds number) implies a greater shape convolution, as suggested by *Sreenivasan et al*., [1989] and *Dimotakis and Catrakis* [1999]. This hypothesis is supported by the fractal analysis of the three simulated plumes, which are similar in all but for their respective Reynolds number ($2x10^3$, $5x10^3$ and $10x10^3$). Simulations with higher Re have not been achieved due to the excessive computational requirements. In these three simulations, α_D increases with higher Re. These findings support the notion that α_D is related to the vortex formation efficiency and thus could be a proxy of the air entrainment ability of the plume.

Our calculations of Re for the eruption plumes display results ranging between $8.7x10^7$ and $7x10^6$, in good agreement with the $2x10^7$ estimated by *Kitamura and Sumita,* [2011] for a Strombolian plume. However, the fractal results show that transient plumes from Sakurajima, Stromboli and Fuego display increase rates α_D belonging to the same range as the simulation's ones. Considering that there are 3 to 4 orders of magnitude differences of Re between the volcanic plumes (10^7) and the simulations (10^3-10^4), we conclude that Re cannot be the only parameter to impact α_D.

It is also important to notice that α_D is not affected by the transition between the gas-thrust and the buoyancy phases, as already experimentally observed by *Lane-Serff.* [1993]. It suggests that this fundamental change of dynamics do not impact the overall shape evolution of the plume, as already qualitatively observed in Section 2.6.1.

We found that α_D is mostly controlled by the discharge history at the erupting vent, and especially by its temporal and spatial variations. These variations are quantified by the Ash Eruption Rate (AER) and the instability source factor (β).

The results of Figure 3.8 suggest that lower values of AER at the vent result in plumes that develop turbulence faster (higher α_D). In our study cases, explosions at Sakurajima and Fuego volcanoes represent the two extremes having respectively the highest AERs and lowest α_D, and vice versa. The spreading of the data around the general trend, however, suggests that the ejection rate is not the only parameter impacting α_D. The time and space instability factor (β) provide supplementary information on the impact of other source parameters. The cluster of low β values at about 10^4 kg/s and 0.12, respectively for the mean AER and α_D, suggests that explosions of intermediate intensity, stable over time and space will produce plumes developing with similar dynamics. On one hand, increasing slightly the factor β increases the α_D and thus the plume complexity evolution. On the other hand, β factor values higher than 0.6 result in α_D dropping rapidly.

The three parameters we compare may be thought of as a measure of: 1) the rate at which convolution and turbulence increase in growing transient plumes (α_D); 2) the stability, over space and time, of ejection at the vent (β); and 3) rate of ejection, proxy for eruption intensity (AER). These parameters are not mutually independent, and yet their relationships seem to illuminate some so far poorly known aspects of transient plume dynamics. In general, low-intensity explosions release plumes that evolve faster, possibly as a result of a lower mass-to-surface ratio. Such plumes may also be expected to have entrainment coefficients that increase more rapidly with time, with respect to plumes from higher intensity explosions. The role of source stability on the rate at which plumes evolve is more complex. It seem like there is a threshold (with β around 0.5) over which an increase in source instability reverts from increasing the plume evolution rate to decreasing it. While for low β values an increase in source instability may again increase the mass-to-surface ratio, at higher values we speculate that multiple ejection phases from moving sources may disrupt the motion and evolution of existing eddies by the arrival of an external source momentum.

Sreenivasan et al., [1989] suggested that the increase in mixing of a turbulent flow goes hand to hand with a shape complexity increase of iso-concentration surfaces, while *Chojnicki et al.*, [2014] experimentally showed that entrainment estimation method applied for steady state dynamics do not effectively characterize the entrainment under unsteady source conditions. Clearly, the parameter α_D hold promises to become an efficient and relatively rapid proxy for air entrainment in transient volcanic plumes. However, an experimental validation of its robustness is required. Also, an extension of this fractal analysis to the later stage of plume development is desirable, to allow one to estimate the extent to which the near-vent dynamics that we inferred can be extended to the final dispersal area of a plume.

3.5 Conclusions

Fractal analysis has been applied for the first time to quantify the time-dependent morphology of transient volcanic plumes in their initial development stage. The studied plumes include ash-rich volcanic plumes originated from Strombolian to Vulcanian eruption styles and filmed in high-speed and high-definition in the visible and thermal infrared radiation, and three synthetic plumes with different Reynolds numbers (Re) generated by numerical simulations. The plumes, both volcanic and synthetic, were characterized by using two different shape analysis approaches: the fractal dimension (D, and its increase rate over time α_D) and the perimeter ratio (PP/PB). Both independent methods, despite their different assumptions, consistently reveal an increase in the degree of convolution of the plume boundary over time. In particular, the PP/PB method is more sensitive to changes in plume morphology reflecting changes in vent ejection dynamics, while the α_D method provides a robust metric of the rate at which plume convolution increases.

We explored the different factors that control the increase of plume convolution during its initial growth. Despite their limited range (order of 10), the different Re of the three synthetic plumes is captured by changes in the corresponding α_D. However, the synthetic and the volcanic plumes, despite a much larger difference in Re (order of 10^4) have similar α_D, suggesting the

presence of other controlling factors. In between the volcanic plumes, those originated by higher discharge rates at the vent display lower values of α_D, pointing to a slower rate of increase of plume convolution. The same rate is also affected by the spatial and temporal variability of ejection at the vent, which is captured by using the source instability factor (β), function of jumps in the ejection rate and shifts in vent position. The dominant trend in our data suggests that α_D may be maximum for intermediate values of β, i.e., both very unstable and very stable ejection sources reduce the rate at which plume convolution increases.

The convolution of plume boundary mirrors the presence of eddies at several spatial and temporal scales, and its increase over time is due to eddies evolution. Such eddies are a key factor in the entrainment of external air into the turbulent plume. We believe that the α_D parameter, effectively recording the rate at which the plume boundary increases its convolution, hold promises as a proxy for measuring the efficiency of air entrainment by volcanic plumes. In this case, it would appear that air entrainment increases non-linearly in the initial stages of development of transient volcanic plumes. Moreover, our results suggest that a faster increase of entrainment is favored by lower discharge rates and moderately variable ejection conditions at the vent.

Fractal analysis appears to be a powerful tool to characterize the initial evolution of transient volcanic plumes, being relatively fast and efficient in capturing, by design, complex morphologies. Future investigations will move in two directions: i) the application to laboratory experiment, to quantitatively link α_D and entrainment; and ii) the application of fractal analysis to late stages of plume development and dispersal.

3.6 Appendix 1. Plume Reynolds number, numerical simulations and time scaling

Reynolds number (Re) is a fundamental descriptor of flow turbulence. We therefore estimated and averaged order of magnitude of Re for our transient volcanic plumes as follows:

$$Re = \frac{\rho u D}{\mu} \tag{3.2}$$

with ρ the gas density, u the characteristic sound speed, D the characteristic length and μ the gas viscosity. The characteristic length used here is the vent diameter that we assumed between 2 and 15 m based on literature [*Chouet et al.,* 1974; *Gaudin et al.*, 2014 a, b] and estimations obtained by tracking the trajectory of bomb-sized pyroclasts on our videos following *Dürig et al.*, [2015].

The gas density has been calculated based on the ideal gas law:

$$\rho = \frac{MP}{RT} \tag{3.3}$$

with M the molar mass (kg/mol), P the atmospheric pressure (Pa), R the universal gas constant (8.314 $J^{-1}mol^{-1}$ K^{-1}) and T the plume temperature (K). The gas temperature range at the exit of the vent used here is between 1023 and 1273 K. We assume three different gas compositions. Two compositions correspond to gas measurements at Stromboli volcano [*Aiuppa et al.*, 2010; *Burton et al.*, 2007], with 64% H_2O, 33% CO_2 and 3% SO_2 for the first one, and 80% H_2O, 17% CO_2 and 3% SO_2 for the second one. The last composition used corresponds to the surrounding atmosphere. The characteristic sound speed is obtained with:

$$u = \sqrt{\frac{\gamma RT}{M}} \tag{3.4}$$

with γ the adiabatic index (γ =1.4). The gas viscosity has been calculated based on the Sutherland's law:

$$\frac{\mu_{(T)}}{\mu_{ref}} = \left(\frac{T}{T_{ref}}\right)^{\frac{3}{2}} \frac{T_{ref} + S}{T + S} \tag{3.5}$$

with subscript *ref* corresponding to the considered parameter at a reference temperature and *S* corresponds to the Sutherland constant at the reference temperature.

This Re's order of magnitude of natural volcanic plumes, was further investigated using numerical gas-jet simulations at different Reynolds number ($2x10^3$, $5x10^3$ an $10x10^3$) and constant ejection rate by comparing their respective fractal dimension evolution over time.

The simulations solved the compressible Navier-Stokes equations, modelling numerically the behaviour of a fluid with friction and heat transfer. The flow was considered to be two-dimensional, with a domain size of 30D x 15D, being D the vent diameter. The resolution of the numerical grid was 4608 x 2304 elements, where the spatial discretization was performed using sixth-order finite differences following the scheme of *Lele,* [1992]. For the time integration, a classical fourth-order Runge-Kutta method was used. The main input parameters of the simulations are the governing parameters of the compressible starting jet: (i) the Reynolds number, (ii) the total reservoir to ambient pressure ratio, (iii) the non-dimensional mass supply and (iv) the total reservoir to ambient temperature ratio. The initial condition was chosen to be quiescence. Instead of simulating the reservoir, the inlet condition was modeled as in *Peña Fernández and Sesterhenn* [2017].

In order to compare the results of fractal dimension analysis from gas-jet simulation with transient volcanic plumes, durations of jet and plume development had to be scaled. To do so, the non-dimensionalization of time was performed using:

$$t^* = \frac{tu}{D}\alpha \tag{3.6}$$

with t the time (s), u the characteristic speed of sound (m/s), D the vent diameter (m) and α a correction factor based on plume/jet front height evolution over time. Not only the time but also the space scale is different between the gas-jet simulations and the transient plumes on our videos. We thus took this space scale difference into account via the α correction factor obtained by calculating the following time ratio:

$$\alpha = \frac{t2_{expl} - t1_{expl}}{t2_{Re_{5000}} - t1_{Re_{5000}}} \tag{3.7}$$

with *expl* referring to the considered explosion and Re_{5000} to the gas-jet simulation at Reynolds number 5000. Times *t2* and *t1* indicate the non-dimensionalized time at which both front flows reached the same given distance L from the vent.

4 General conclusions

The use of unique high-speed, thermal and high-resolution videos in this study provides data about a large panel of transient plumes from Strombolian- to Vulcanian-style activity and from Sakurajima, Stromboli and Fuego volcanoes.

Innovative methods have been used to characterize the morphology and dynamics of the plumes presented in this study. Fractal analysis was applied for the first time to quantify plumes' shape complexity evolution during their development. Optical flow computer vision technique has been used in order to detail the plume's velocity field.

In our attempt to quantify source unsteadiness, a new kind of eruption rate estimation method has been designed, providing a time-resolved ash eruption rate (AER). This new resource, beside giving important information on ejection intensity, gives access to ejection amplitude variations at the vent. When combined with the source instability factor (β), taking into account the spatial spreading of the source and its AER variability, we obtain a global quantification of the ejection properties.

Results show that transient plume development can display great variability of shape complexity, dynamical evolution, and discharge rate at the source in function of time. Dynamical fluctuations, such as late front velocity peaks, multiple simultaneous jets and successive ring vortex formations are systematically related to changes in ejection phase properties at the vent.

The shape evolution characterization reveals that the formation of smaller scale vortexes during plume's development depends on the source properties. Source instability factor (β) and ash discharge rate (AER) show that successive pulses at the erupting vent, depending on their time-space features (e.g., location, angle, velocity and time of occurrence), have the potential to interact in complex ways with the already emplaced plume and impact its dynamics. Late ejections can

disrupt the rotary motion of vortexes, as well as their formation and development, which result in a modification of dynamics, shape and air entrainment ability of the plume over time.

In this study, a clear link between source unsteadiness and plume's dynamics and morphology has been established. Discharge history has a crucial impact on the initial and possibly late evolution of transient plumes, and leaves information held in their shape evolution. These new field data allow a better understanding of this type of eruptive events and a better constrain on their behavior (Figure 4.1).

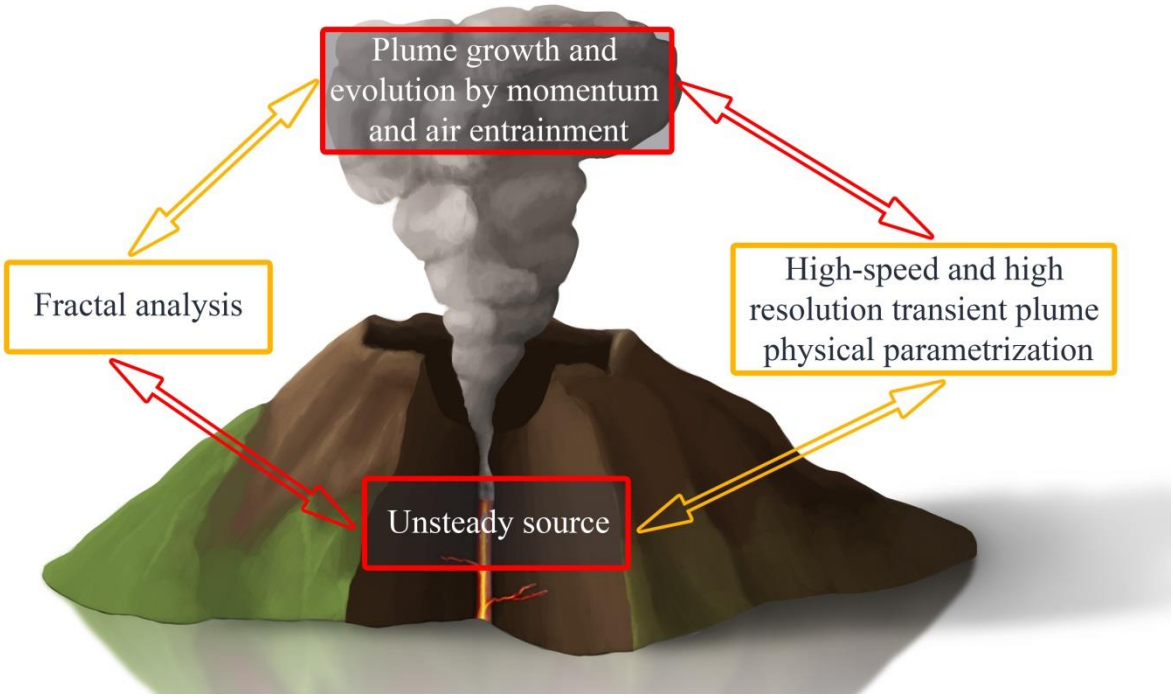

Figure 4.1: Sum up sketch of the highlighted interactions between plume's morphology, dynamics and source evolution.

There is now a strong requirement for new numerical and experimental studies taking unsteady discharge rates into account, both in time and space. Videos used in this study allowed the observation of the initial transient plume's development. However, the impact of the observed unsteady sources on plumes' dynamical and morphological evolution still needs to be described at later stages.

Based on the results from this study, second order impact parameters will also need further investigations in order to quantify their potential of enhancement or disruption of plume's dynamics. Among these parameters are two categories, the inner and the outer parameters. Inner parameters, including e.g. bombs swarms and ash fallouts, have an impact visible in our data, particularly through the PP/PB method. Bombs size particles, via their momentum, can drag upward while rising or downward while falling the ash present in the plume and thus change its dynamics. Outer parameters including e.g. wind, humidity and surrounding atmosphere temperature, also display a control on the developing plume, as particularly visible on our Fuego explosions.

Finally, the fractal dimension analysis does show potential in plume characterization. This method can be applied to all types of plume and provides a fast shape characterization which can then be related to ejection properties at the vent. This tool could become a strong asset in volcano monitoring techniques. It becomes clear here that future studies on transient volcanic plumes will need to account for source unsteadiness and will be able to use plume shape evolution to characterize it.

5 Acknowledgements

This work is supported by the VERTIGO Marie Curie ITN, funded through the European Seventh Framework Programme (FP7 2007–2013) under grant agreement 607905.

Thank you to my supervisor Jacopo Taddeucci for his presence, patience and will to always make me do better. Jacopo taught me a lot during these three years and I am really grateful for this opportunity he gave me.

I would also like to thank Damien Gaudin (and his matlab addiction) for his patience and technical support in coding.

I would like to thank the INGV Volcanology team of Rome, especially Tullio Ricci, Elisabetta Del Bello and Piergiorgio Scarlato for their support at work and in my new life in a foreign country which with the help of everybody rapidly became home.

Thank you to my wife Ines for enduring my moods, stress and craziness during these three years of intense work, travelling and networking.

Thank you to my mom Liliane for her constant support all these years of study and moving around.

Thank you to my most devoted friend Lucky.

6 References

Abdel-Rahman, A. A., W. Chakroun, and S. F. Al-Fahed (1997), LDA measurements in the turbulent round jet, *Mech. Res. Commun.*, *24*(3), 277–288, doi:10.1016/S0093-6413(97)00025-6.

Abramoff, M. D., P. J. Magalhães, and S. J. Ram (2004), Image processing with ImageJ, *Biophotonics Int.* Available from: http://dspace.library.uu.nl/handle/1874/204900 (Accessed 26 September 2016)

Aiuppa, A., A. Bertagnini, N. Métrich, R. Moretti, A. Di Muro, M. Liuzzo, and G. Tamburello (2010), A model of degassing for Stromboli volcano, *Earth Planet. Sci. Lett.*, *295*(1–2), 195–204, doi:10.1016/j.epsl.2010.03.040.

Andronico, D., J. Taddeucci, A. Cristaldi, L. Miraglia, P. Scarlato, and M. Gaeta (2013), The 15 March 2007 paroxysm of Stromboli: video-image analysis, and textural and compositional features of the erupted deposit, *Bull. Volcanol.*, *75*(7), 733, doi:10.1007/s00445-013-0733-2.

Baker, S., D. Scharstein, J. P. Lewis, S. Roth, M. J. Black, and R. Szeliski (2011), A Database and Evaluation Methodology for Optical Flow, *Int. J. Comput. Vis.*, *92*(1), 1–31, doi:10.1007/s11263-010-0390-2.

Barnie, T., M. Bombrun, M. R. Burton, A. Harris, and G. Sawyer (2015), Quantification of gas and solid emissions during Strombolian explosions using simultaneous sulphur dioxide and infrared camera observations, *J. Volcanol. Geotherm. Res.*, *300*, 167–174, doi:10.1016/j.jvolgeores.2014.10.003.

Besicovitch, A. S. (1929). On linear sets of points of fractional dimension. *Mathematische Annalen*, *101*(1), 161–193. https://doi.org/10.1007/BF01454831.

Blackburn, E. A., L. Wilson, and R. S. J. Sparks (1976), Mechanisms and dynamics of strombolian activity, *J. Geol. Soc.*, *132*(4), 429–440, doi:10.1144/gsjgs.132.4.0429.

Bogusławski, L., and C. O. Popiel (1979), Flow structure of the free round turbulent jet in the initial region, *J. Fluid Mech.*, *90*(3), 531–539, doi:10.1017/S0022112079002378.

Bonadonna, C., M. Pistolesi, R. Cioni, W. Degruyter, M. Elissondo, and V. Baumann (2015), Dynamics of wind-affected volcanic plumes: The example of the 2011 Cordón Caulle eruption, Chile, *J. Geophys. Res. Solid Earth*, *120*(4), 2014JB011478, doi:10.1002/2014JB011478.

Burton, M., P. Allard, F. Muré, and A. L. Spina (2007), Magmatic Gas Composition Reveals the Source Depth of Slug-Driven Strombolian Explosive Activity, *Science*, *317*(5835), 227–230, doi:10.1126/science.1141900.

Capponi, A., J. Taddeucci, P. Scarlato, and D. M. Palladino (2016), Recycled ejecta modulating Strombolian explosions, *Bull. Volcanol.*, *78*(2), 13, doi:10.1007/s00445-016-1001-z.

Catrakis, H. J., and Dimotakis, P. E. (1998). Shape Complexity in Turbulence. *Physical Review Letters*, *80*(5), 968–971. https://doi.org/10.1103/PhysRevLett.80.968.

Cerminara, M., Ongaro, T. E., Valade, S., and Harris, A. J. (2014). Ash plume properties retrieved from infrared images: a forward and inverse modeling approach. *ArXiv Preprint ArXiv:1405.0883*.

Chojnicki, K., A. Clarke, J. Phillips, and R. Adrian (2015b), The evolution of volcanic plume morphology in short-lived eruptions, *Geology*, *43*(8), 707–710.

Chojnicki, K. N., A. B. Clarke, R. J. Adrian, and J. C. Phillips (2014), The flow structure of jets from transient sources and implications for modeling short-duration explosive volcanic eruptions, *Geochem. Geophys. Geosystems*, *15*(12), 4831–4845, doi:10.1002/2014gc005471.

Chojnicki, K. N., A. B. Clarke, J. C. Phillips, and R. J. Adrian (2015a), Rise dynamics of unsteady laboratory jets with implications for volcanic plumes, *Earth Planet. Sci. Lett.*, *412*(0), 186–196, doi:10.1016/j.epsl.2014.11.046.

Chouet, B., N. Hamisevicz, and T. R. McGetchin (1974), Photoballistics of volcanic jet activity at Stromboli, Italy, *J. Geophys. Res.*, *79*(32), 4961–4976, doi:10.1029/JB079i032p04961.

Cigala, V., U. Kueppers, J. J. Peña Fernández, J. Taddeucci, J. Sesterhenn, and D. B. Dingwell (2017), The dynamics of volcanic jets: Temporal evolution of particles exit velocity from shock-tube experiments, *J. Geophys. Res. Solid Earth*, 2017JB014149, doi:10.1002/2017JB014149.

Cioni, R., M. Pistolesi, and M. Rosi (2015), Plinian and Subplinian Eruptions, in *The Encyclopedia of Volcanoes*.

Clarke, A. B., B. Voight, A. Neri, and G. Macedonio (2002), Transient dynamics of vulcanian explosions and column collapse, *Nature*, *415*(6874), 897–901, doi:10.1038/415897a.

Clarke, A. B., T. E. Ongaro, and A. Belousov (2015), Vulcanian Eruptions, in *The Encyclopedia of Volcanoes*.

Costa, A., Suzuki, Y. J., Cerminara, M., Devenish, B. J., Ongaro, T. E., Herzog, M., … Bonadonna, C. (2016). Results of the eruptive column model inter-comparison study. *Journal of Volcanology and Geothermal Research*, *326*, 2–25. https://doi.org/10.1016/j.jvolgeores.2016.01.017.

De Angelis, S. D., O. d. Lamb, A. Lamur, A. j. Hornby, F. w. von Aulock, G. Chigna, Y. Lavallée, and A. Rietbrock (2016), Characterization of moderate ash-and-gas explosions at Santiaguito volcano, Guatemala, from infrasound waveform inversion and thermal infrared measurements, *Geophys. Res. Lett.*, 2016GL069098, doi:10.1002/2016GL069098.

Del Bello, E., E. W. Llewellin, J. Taddeucci, P. Scarlato, and S. J. Lane (2012), An analytical model for gas overpressure in slug-driven explosions: Insights into Strombolian volcanic eruptions, *J. Geophys. Res. Solid Earth*, *117*(B2), B02206, doi:10.1029/2011JB008747.

Delle Donne, D., and M. Ripepe (2012), High-frame rate thermal imagery of Strombolian explosions: Implications for explosive and infrasonic source dynamics, *J. Geophys. Res. Solid Earth*, *117*(B9), B09206, doi:10.1029/2011JB008987.

Dimotakis, P. E., and Catrakis, H. J. (1999). Turbulence, Fractals and Mixing. In *Mixing: Chaos and Turbulence* (Springer Science & Business Media, pp. 59–143). H Chate, E Willermaux, JM Chomaz.

Dimotakis, P. E., Miake-Lye, R. C., and Papantoniou, D. A. (1983). Structure and dynamics of round turbulent jets. *Physics of Fluids*, *26*(11), 3185–3192.

Dürig, T., M. T. Gudmundsson, S. Karmann, B. Zimanowski, P. Dellino, M. Rietze, and R. Büttner (2015a), Mass eruption rates in pulsating eruptions estimated from video analysis of the gas thrust-buoyancy transition—a case study of the 2010 eruption of Eyjafjallajökull, Iceland, *Earth Planets Space*, *67*(1), 1–17, doi:10.1186/s40623-015-0351-7.

Dürig, T., M. T. Gudmundsson, and P. Dellino (2015b), Reconstruction of the geometry of volcanic vents by trajectory tracking of fast ejecta - the case of the Eyjafjallajökull 2010 eruption (Iceland), *Earth Planets Space*, *67*(1), 64, doi:10.1186/s40623-015-0243-x.

Francalanci, L., P. Manetti, and A. Peccerillo (1989), Volcanological and magmatological evolution of Stromboli volcano (Aeolian Islands): The roles of fractional crystallization, magma mixing, crustal contamination and source heterogeneity, *Bull. Volcanol.*, *51*(5), 355–378, doi:10.1007/BF01056897.

Freund, J. B., S. K. Lele, and P. Moin (2000), Numerical Simulation of a Mach 1.92 Turbulent Jet and Its Sound Field, *AIAA J.*, *38*(11), 2023–2031, doi:10.2514/2.889.

Gaudin, D., J. Taddeucci, P. Scarlato, M. Moroni, C. Freda, M. Gaeta, and D. M. Palladino (2014), Pyroclast Tracking Velocimetry illuminates bomb ejection and explosion dynamics at Stromboli (Italy) and Yasur (Vanuatu) volcanoes, *J. Geophys. Res. Solid Earth*, *119*(7), 2014JB011096, doi:10.1002/2014JB011096.

Gaudin, D., Moroni, M., Taddeucci, J., Scarlato, P., and Shindler, L. (2014). Pyroclast Tracking Velocimetry: A particle tracking velocimetry-based tool for the study of Strombolian explosive eruptions. *Journal of Geophysical Research: Solid Earth*, *119*(7), 2014JB011095. https://doi.org/10.1002/2014JB011095.

Gaudin, D., Taddeucci, J., Scarlato, P., Bello, E., Ricci, T., Orr, T., ... and Bucci, A. (2017). Integrating puffing and explosions in a general scheme for Strombolian-style activity. *Journal of Geophysical Research: Solid Earth*, *122*(3), 1860-1875.

Global Volcanism Program, 2012. Report on Fuego (Guatemala). In: Sennert, S K (ed.), Weekly Volcanic Activity Report, 11 January-17 January 2012. Smithsonian Institution and US Geological Survey.

Harris, A., and M. Ripepe (2007), Synergy of multiple geophysical approaches to unravel explosive eruption conduit and source dynamics – A case study from Stromboli, *Chem. Erde - Geochem.*, *67*(1), 1–35, doi:10.1016/j.chemer.2007.01.003.

Harris, A. J. L., M. Ripepe, and E. A. Hughes (2012), Detailed analysis of particle launch velocities, size distributions and gas densities during normal explosions at Stromboli, *J. Volcanol. Geotherm. Res.*, *231–232*(0), 109–131, doi:10.1016/j.jvolgeores.2012.02.012.

Harris, A. J. L., D. Delle Donne, J. Dehn, M. Ripepe, and A. K. Worden (2013), Volcanic plume and bomb field masses from thermal infrared camera imagery, *Earth Planet. Sci. Lett.*, *365*, 77–85, doi:10.1016/j.epsl.2013.01.004.

Harris, A. (2013b). Thermal remote sensing of active volcanoes: a user's manual. Cambridge University Press.

Hausdorff, F. (1918). Dimension und äußeres Maß. *Mathematische Annalen*, *79*(1–2), 157–179. https://doi.org/10.1007/BF01457179.

Hussein, H. J., S. P. Capp, and W. K. George (1994), Velocity measurements in a high-Reynolds-number, momentum-conserving, axisymmetric, turbulent jet, *J. Fluid Mech.*, *258*, 31–75, doi:10.1017/S002211209400323X.

Iguchi, M. (2016), Method for Real-Time Evaluation of Discharge Rate of Volcanic Ash : Case Study on Intermittent Eruptions at the Sakurajima Volcano, Japan (Special Issue on Integrated Study on Mitigation of Multimodal Disasters Caused by Ejection of Volcanic Products), *J. Disaster Res.*, *11*(1), 4–14.

Iguchi, M., H. Yakiwara, T. Tameguri, M. Hendrasto, and J. Hirabayashi (2008), Mechanism of explosive eruption revealed by geophysical observations at the Sakurajima, Suwanosejima and Semeru volcanoes, *J. Volcanol. Geotherm. Res.*, *178*(1), 1–9, doi:10.1016/j.jvolgeores.2007.10.010.

Iguchi, M., T. Tameguri, Y. Ohta, S. Ueki, and S. Nakao (2013), Characteristics of Volcanic Activity at Sakurajima Volcano's Showa Crater During the Period 2006 to 2011, Bull. Volcanol. Soc. Japan, 58(1), 115-135

Iqbal, M. O., and F. O. Thomas (2007), Coherent structure in a turbulent jet via a vector implementation of the proper orthogonal decomposition, *J. Fluid Mech.*, *571*, 281–326, doi:10.1017/S0022112006003351.

Ishihara, K. (1985), Dynamical analysis of volcanic explosion, *J. Geodyn.*, *3*(3–4), 327–349, doi:10.1016/0264-3707(85)90041-9.

Japan Meteorological Agency (2016), 平成 28 年（2016 年）の桜島の火山活動 Volcanic activity of Sakurajima in Heisei 28 (2016), [http://www.data.jma.go.jp/svd/vois/data/tokyo/STOCK/monthly_v-act_doc/fukuoka/2016y/506_16y.pdf]

Johnson, J. B., A. J. L. Harris, S. T. M. Sahetapy-Engel, R. Wolf, and W. I. Rose (2004b), Explosion dynamics of pyroclastic eruptions at Santiaguito Volcano, *Geophys. Res. Lett.*, *31*(6), L06610, doi:10.1029/2003GL019079.

Johnson, J. B., R. C. Aster, and P. R. Kyle (2004a), Volcanic eruptions observed with infrasound, *Geophys. Res. Lett.*, *31*(14), L14604, doi:10.1029/2004GL020020.

Kim, K., D. Fee, A. Yokoo, and J. M. Lees (2015), Acoustic source inversion to estimate volume flux from volcanic explosions, *Geophys. Res. Lett.*, *42*(13), 2015GL064466, doi:10.1002/2015GL064466.

Kinoshita, K. (1996), Observation of flow and dispersion of volcanic clouds from Mt. Sakurajima, *Atmos. Environ.*, *30*(16), 2831–2837, doi:10.1016/1352-2310(95)00401-7.

Kitamura, S., and I. Sumita (2011), Experiments on a turbulent plume: Shape analyses, *J. Geophys. Res. Solid Earth 1978–2012*, *116*(B3).

Kolmogorov, A. N. (1941). The Local Structure of Turbulence in Incompressible Viscous Fluid for Very Large Reynolds Numbers. *Proceedings: Mathematical and Physical Sciences*, *434*(1890), 9–13.

Kolmogorov, A. N. (1962). A refinement of previous hypotheses concerning the local structure of turbulence in a viscous incompressible fluid at high Reynolds number. *Journal of Fluid Mechanics*, *13*(1), 82–85. https://doi.org/10.1017/S0022112062000518.

Lane-Serff, G. F. (1993). Investigation of the fractal structure of jets and plumes. *Journal of Fluid Mechanics*, *249*, 521–534. https://doi.org/10.1017/S0022112093001272.

Leduc, L., L. Gurioli, A. Harris, L. Colò, and E. F. Rose-Koga (2015), Types and mechanisms of strombolian explosions: characterization of a gas-dominated explosion at Stromboli, *Bull. Volcanol.*, *77*(1), 1–15, doi:10.1007/s00445-014-0888-5.

Lele, S. K. (1992). Compact finite difference schemes with spectral-like resolution. *Journal of Computational Physics*, *103*(1), 16–42. https://doi.org/10.1016/0021-9991(92)90324-R.

Liebovitch, L. S., and Toth, T. (1989). A fast algorithm to determine fractal dimensions by box counting. *Physics Letters A*, *141*(8), 386–390. https://doi.org/10.1016/0375-9601(89)90854-2.

Lovejoy, S. (1982). Area-perimeter relation for rain and cloud areas. *Science (New York, N.Y.)*, *216*(4542), 185–187. https://doi.org/10.1126/science.216.4542.185.

Lovejoy, S., and Mandelbrot, B. B. (1985). Fractal properties of rain, and a fractal model. *Tellus A*, *37A*(3), 209–232. https://doi.org/10.1111/j.1600-0870.1985.tb00423.x.

Lyons, J. J., and G. P. Waite (2011), Dynamics of explosive volcanism at Fuego volcano imaged with very long period seismicity, *J. Geophys. Res. Solid Earth*, *116*(B9), B09303, doi:10.1029/2011JB008521.

Lyons, J. J., G. P. Waite, W. I. Rose, and G. Chigna (2010), Patterns in open vent, strombolian behavior at Fuego volcano, Guatemala, 2005–2007, *Bull. Volcanol.*, *72*(1), 1, doi:10.1007/s00445-009-0305-7.

Mandelbrot, B. (1982). *The fractal geometry of nature*.

Marchetti, E., M. Ripepe, A. J. L. Harris, and D. Delle Donne (2009), Tracing the differences between Vulcanian and Strombolian explosions using infrasonic and thermal radiation energy, *Earth Planet. Sci. Lett.*, *279*(3–4), 273–281, doi:10.1016/j.epsl.2009.01.004.

Mastin, L. G. (2007), A user-friendly one-dimensional model for wet volcanic plumes, *Geochem. Geophys. Geosystems*, *8*(3), Q03014, doi:10.1029/2006GC001455.

Mastin, L. G., Guffanti, M., Servranckx, R., Webley, P., Barsotti, S., Dean, K., … Waythomas, C. F. (2009). A multidisciplinary effort to assign realistic source parameters to models of

volcanic ash-cloud transport and dispersion during eruptions. *Journal of Volcanology and Geothermal Research*, *186*(1–2), 10–21. https://doi.org/10.1016/j.jvolgeores.2009.01.008.

Mastin, L. G. (2014). Testing the accuracy of a 1-D volcanic plume model in estimating mass eruption rate. *Journal of Geophysical Research: Atmospheres*, *119*(5), 2013JD020604. https://doi.org/10.1002/2013JD020604.

Morton, B., G. Taylor, and J. Turner (1956), Turbulent gravitational convection from maintained and instantaneous sources, vol. 234, pp. 1–23, The Royal Society.

Morton, B. (1959). Forced plumes. *Journal of Fluid Mechanics*, *5*(01), 151–163.

Neri, A., T. Esposti Ongaro, G. Macedonio, and D. Gidaspow (2003), Multiparticle simulation of collapsing volcanic columns and pyroclastic flow, *J. Geophys. Res. Solid Earth*, *108*(B4), 2202, doi:10.1029/2001JB000508.

Panchapakesan, N. R., and J. L. Lumley (1993), Turbulence measurements in axisymmetric jets of air and helium. Part 1. Air jet, *J. Fluid Mech.*, *246*, 197–223, doi:10.1017/S0022112093000096.

Patrick, M., A. L. Harris, M. Ripepe, J. Dehn, D. Rothery, and S. Calvari (2007), Strombolian explosive styles and source conditions: insights from thermal (FLIR) video, *Bull. Volcanol.*, *69*(7), 769–784, doi:10.1007/s00445-006-0107-0.

Patrick, M. R. (2007), Dynamics of Strombolian ash plumes from thermal video: Motion, morphology, and air entrainment, *J. Geophys. Res. Solid Earth*, *112*(B6), B06202, doi:10.1029/2006jb004387.

Peña Fernández, J. J., and J. Sesterhenn (2017), Compressible starting jet: pinch-off and vortex ring–trailing jet interaction, *J. Fluid Mech.*, *817*, 560–589, doi:10.1017/jfm.2017.128.

Pioli, L., M. Pistolesi, and M. Rosi (2014), Transient explosions at open-vent volcanoes: The case of Stromboli (Italy), *Geology*, *42*(10), 863–866, doi:10.1130/G35844.1.

Pioli, L., E. Erlund, E. Johnson, K. Cashman, P. Wallace, M. Rosi, and H. Delgado Granados (2008), Explosive dynamics of violent Strombolian eruptions: The eruption of Parícutin Volcano 1943–1952 (Mexico), *Earth Planet. Sci. Lett.*, *271*(1–4), 359–368, doi:10.1016/j.epsl.2008.04.026.

Prasad, R. R., and Sreenivasan, K. R. (1989). Scalar interfaces in digital images of turbulent flows. *Experiments in Fluids*, *7*(4), 259–264. https://doi.org/10.1007/BF00198005.

Prasad, R. R., and Sreenivasan, K. R. (1990). The measurement and interpretation of fractal dimensions of the scalar interface in turbulent flows. *Physics of Fluids A: Fluid Dynamics*, *2*(5), 792–807. https://doi.org/10.1063/1.857733.

Quinn, W. R. (2006), Upstream nozzle shaping effects on near field flow in round turbulent free jets, *Eur. J. Mech. - BFluids*, *25*(3), 279–301, doi:10.1016/j.euromechflu.2005.10.002.

Richardson, L. F. (1922). *Weather prediction by numerical process*. Cambridge, The University press. Retrieved from http://archive.org/details/weatherpredictio00richrich.

Ripepe, M., M. Rossi, and G. Saccorotti (1993), Image processing of explosive activity at Stromboli, , *54*, 335–351.

Ripepe, M., C. Bonadonna, A. Folch, D. Delle Donne, G. Lacanna, E. Marchetti, and A. Höskuldsson (2013), Ash-plume dynamics and eruption source parameters by infrasound and thermal imagery: The 2010 Eyjafjallajökull eruption, *Earth Planet. Sci. Lett.*, *366*, 112–121, doi:10.1016/j.epsl.2013.02.005.

Rosi, M., M. Pistolesi, A. Bertagnini, P. Landi, M. Pompilio, and A. D. Roberto (2013), Chapter 14 Stromboli volcano, Aeolian Islands (Italy): present eruptive activity and hazards, *Geol. Soc. Lond. Mem.*, *37*(1), 473–490, doi:10.1144/M37.14.

Rys, F. S., and Waldvogel, A. (1986). Fractal shape of hail clouds. *Physical Review Letters*, *56*(7), 784–787. https://doi.org/10.1103/PhysRevLett.56.784.

Sahetapy-Engel, S. T., and A. J. L. Harris (2009), Thermal-image-derived dynamics of vertical ash plumes at Santiaguito volcano, Guatemala, *Bull. Volcanol.*, *71*(7), 827–830, doi:10.1007/s00445-009-0284-8.

Sawyer, G. M., and M. R. Burton (2006), Effects of a volcanic plume on thermal imaging data, *Geophys. Res. Lett.*, *33*(14).

Scharff, L., M. Hort, and N. R. Varley (2015), Pulsed Vulcanian explosions: A characterization of eruption dynamics using Doppler radar, *Geology*, *43*(11), 995–998, doi:10.1130/G36705.1.

Spampinato, L., Calvari, S., Oppenheimer, C., and Boschi, E. (2011). Volcano surveillance using infrared cameras. Earth-Science Reviews, 106(1), 63-91.

Sparks, R. S. J., M. Bursik, S. N. Carey, J. S. Gilbert, L. S. Glaze, H. Sigurdsson, and A. W. Woods (1997), *Volcanic plumes*, John Wiley.

Sreenivasan, K. R. (1991). Fractals and Multifractals in Fluid Turbulence. *Annual Review of Fluid Mechanics*, *23*(1), 539–604. https://doi.org/10.1146/annurev.fl.23.010191.002543.

Sreenivasan, K. R., and Meneveau, C. (1986). The fractal facets of turbulence. *Journal of Fluid Mechanics*, *173*, 357–386. https://doi.org/10.1017/S0022112086001209.

Sreenivasan, K. R., Ramshankar, R., and Meneveau, C. (1989). Mixing, Entrainment and Fractal Dimensions of Surfaces in Turbulent Flows. *Proceedings of the Royal Society of London A: Mathematical, Physical and Engineering Sciences*, *421*(1860), 79–108. https://doi.org/10.1098/rspa.1989.0004.

Sun, D., S. Roth, and M. J. Black (2010), Secrets of optical flow estimation and their principles, in *2010 IEEE Computer Society Conference on Computer Vision and Pattern Recognition*, pp. 2432–2439.

Sun, D., S. Roth, and M. J. Black (2014), A Quantitative Analysis of Current Practices in Optical Flow Estimation and the Principles Behind Them, *Int. J. Comput. Vis.*, *106*(2), 115–137, doi:10.1007/s11263-013-0644-x.

Suwa, H., Y. J. Suzuki, and A. Yokoo (2014), Estimation of exit velocity of volcanic plume from analysis of vortex structures, *Earth Planet. Sci. Lett.*, *385*, 154–161, doi:10.1016/j.epsl.2013.10.032.

Taddeucci, J., P. Scarlato, A. Capponi, E. Del Bello, C. Cimarelli, D. M. Palladino, and U. Kueppers (2012), High-speed imaging of Strombolian explosions: The ejection velocity of pyroclasts, *Geophys. Res. Lett.*, *39*(2), L02301, doi:10.1029/2011gl050404.

Taddeucci, J., Palladino, D. M., Sottili, G., Bernini, D., Andronico, D., and Cristaldi, A. (2013). Linked frequency and intensity of persistent volcanic activity at Stromboli (Italy). *Geophysical Research Letters*, *40*(13), 3384–3388. https://doi.org/10.1002/grl.50652.

Taddeucci, J., M. Edmonds, B. Houghton, M. R. James, and S. Vergniolle (2015), Hawaiian and Strombolian eruptions, in *The Encyclopedia of Volcanoes*.

Turner, J. S. (1962), The "starting plume" in neutral surroundings, *J. Fluid Mech.*, *13*(3), 356–368, doi:10.1017/S0022112062000762.

Turner, J. S. (1969), Buoyant Plumes and Thermals, *Annu. Rev. Fluid Mech.*, *1*(1), 29–44, doi:10.1146/annurev.fl.01.010169.000333.

Turner, J. S. (1979), *Buoyancy Effects in Fluids*, Cambridge University Press.

Valade, S., A. Harris, and M. Cerminara (2014), Plume Ascent Tracker: Interactive Matlab software for analysis of ascending plumes in image data, *Comput. Geosci.*, *66*, 132–144.

Webb, E. B., N. R. Varley, D. M. Pyle, and T. A. Mather (2014), Thermal imaging and analysis of short-lived Vulcanian explosions at Volcán de Colima, Mexico, *J. Volcanol. Geotherm. Res.*, *278–279*, 132–145, doi:10.1016/j.jvolgeores.2014.03.013.

Wilson, L., R. S. J. Sparks, T. C. Huang, and N. D. Watkins (1978), The control of volcanic column heights by eruption energetics and dynamics, *J. Geophys. Res. Solid Earth*, *83*(B4), 1829–1836, doi:10.1029/JB083iB04p01829.

Woods, A. W. (1988), The fluid dynamics and thermodynamics of eruption columns, *Bull. Volcanol.*, *50*(3), 169–193, doi:10.1007/BF01079681.

Xu, G., and R. Antonia (2002), Effect of different initial conditions on a turbulent round free jet, *Exp. Fluids*, *33*(5), 677–683, doi:10.1007/s00348-002-0523-7.

Yamamoto, H., I. M. Watson, J. C. Phillips, and G. J. Bluth (2008), Rise dynamics and relative ash distribution in vulcanian eruption plumes at Santiaguito Volcano, Guatemala, revealed using an ultraviolet imaging camera, *Geophys. Res. Lett.*, *35*(8), L08314, doi:10.1029/2007GL032008.

Yuan, A. T. E., S. R. McNutt, and D. H. Harlow (1984), Seismicity and eruptive activity at Fuego Volcano, Guatemala: February 1975 –January 1977, *J. Volcanol. Geotherm. Res.*, *21*(3), 277–296, doi:10.1016/0377-0273(84)90026-X.

Zanon, V., M. Neri, and E. Pecora (2009), Interpretation of data from the monitoring thermal camera of Stromboli volcano (Aeolian Islands, Italy), *Geol. Mag.*, *146*(4), 591–601, doi:10.1017/S0016756809005937.